UNIVERSITAT DE BARCELONA

Final Degree Project

Biomedical Engineering Degree

"Development of hydrogel cavities of tuneable stiffness for the growth of epithelial crypts"

Barcelona, 23th January 2024

Author: Victòria Sanllehí i Barceló

Director/s: Jordi Comelles Pujadas

Tutor: Jordi Comelles Pujadas

Abstract

Depending on their function, the epithelial cell monolayers that line the inner surfaces of organs adopt a variety of three-dimensional shapes. Traditional studies *in vitro* have been using mainly flat cell culture dishes, overseeing the impact of these *in vivo* shapes in tissue function. Recent research has begun to address this issue, by trying to mimic the 3D structures found in tissues. However, those novel culture platforms still have some limitations, especially in cases where the architecture must correspond with the original tissue's stiffness. Tissues have a quite low physiological rigidity, and most of the microfabrication techniques used nowadays need quite firm materials to achieve the desired 3D structures without issue. A type of structure difficult to fabricate using soft materials are invaginations, which can be found *in vivo* in kidneys, lungs, and the small intestine. Low rigidity substrates are typically characterized by high deformability and lack of structural support, which can result in unprecise final features due to distortions of the material during the microfabricating process.

In this project, 3D cavities have been fabricated into polyacrylamide (PA), a material which allows the tuneability of its rigidity by changing the proportion of acrylamides during the synthesis of the prepolymer solution. Replica moulding has been employed to acquire these structures. The invaginations successfully recreated key aspects of the *in vivo* environment, both with their shape and stiffness, and multiple copies were created easily, enabling precise characterization. Finally, after the assessment of the mechanical properties and the architectural features of the microcavities, the functionalization of the samples was successful, confirming the suitability of the resulting scaffold as a model to study epithelial growth, morphology, and conformity in these inward bended structures.

Keywords: microfabrication, 3D cell cultures, hydrogels, cavities, stiffness, epithelial tissues, polyacrylamide, replica moulding.

Acknowledgments

I would like to express my deepest gratitude to all those who have supported me throughout the journey of completing this project.

First and foremost, Jordi Comelles, my director, has my sincere gratitude. His advice, knowledge and priceless insights during the process were extremely helpful for the elaboration of this project. I specially thank his constructive feedback, as well as his guidance every step of the way.

In addition, I would like to express my gratitude to Dr. Elena Martinez, for allowing me to work on this project in her group and use the IBEC facilities, and also to all the members of the Biomimetics systems for cell engineering team, for their help and advice during the elaboration of the project.

Finally, I am immensely grateful to my friends and family for their unfailing support and believe in me. Their encouraging and motivating words have consistently provided me with strength during moments of discouragement or fatigue.

List of figures

Figure 1. Schematic illustrating developmental motifs that result in tissue folding and invagination [10] 14
Figure 2. Schematics illustrating typical cell shapes observed in epithelial tissues [10] 15
Figure 3. Schematic of the anatomy and cellular composition in mammalian lungs (mouse and human) [13] 16
Figure 4. Histologic features of chronic bronchitis, stained with haematoxylin – eosin dye, x200 magnification [14] 16
Figure 5. Renal corpuscle schematic (left) [15] and renal tubule system schematic (right) [17] 17
Figure 6. Histological section of the kidney dyed with haematoxylin – eosin dye, x400 magnification (left) [18], and thick glomerular capillary basement membrane, stained with lead citrate and uranyl acetate, x4800 magnification (right) [19] 18
Figure 7. Schematic of the structure and cell layers of the intestine (left) [23], and histological section of the intestine dyed with haematoxylin – eosin dye, x100 magnification (right) [24] 19
Figure 8. Schematic representation of a small piece of intestinal epithelial tissue mounted in the Ussing chamber [31] 20
Figure 9. Schematic illustration of a Transwell system [32] 21
Figure 10. Intestinal organoid morphology. Schematic of a mature intestinal organoid (left) and brightfield image of a mature (day 5) mouse intestinal organoid (right) [33] 21
Figure 11. Intestine-on-a-chip [35] 22
Figure 12. Estimated hydrogel market size from 2021 to 2032 [45] 25
Figure 13. Hydrogel Market Growth Rate by Regions from 2022 to 2027 [47] 26
Figure 14. General scheme of the steps of this project 28
Figure 15. General workflow of the replica-moulding process 33
Figure 16. Scheme of the master 33
Figure 17. Scheme of a single region of the master 34
Figure 18. Scheme of the PDMS thin mould acquisition 35
Figure 19. Scheme of the PA polymerization with thin PDMS moulds 37
Figure 20. Schematic depicting the Sulfo-SANPAH activation and the protein functionalization 37
Figure 21. SU-8 master with PDMS on top 41
Figure 22. PDMS1 on top of glass coverslip with spin coated PDMS on top 43
Figure 23. PDMS2 on top of 22x22 cover glass 44
Figure 24. Sample 1 medium-big posts (from the 300 µm master's posts, after PDMS1) profile, with the mentioned small peak circled in red 45
Figure 25. Sample 4 biggest cavities (from the 400 µm master's posts), with the mentioned small peak circled in red 45
Figure 26. Sample 4 smallest cavities (from the 100 µm master's posts), with the profile of the top-left structure 46
Figure 27. Sample 2 medium-big posts (from the 300 µm master's posts, after PDMS1), with the mentioned black regions of non-detection 46
Figure 28. Considered top and base diameters of posts (Sample 2 biggest diameter posts) 47
Figure 29. Considered top and base diameters of posts (Sample 1 medium-big diameter cavities) 48

Figure 30. 35 mm glass bottom dish with 20 mm coverslip with micro-well marked in red [75] 49
Figure 31. 35 mm petri dishes with PA hydrogels in micro-wells, covered with PBS. The small petri dishes are inside plates for easier transportation 50
Figure 32. Normalized swelling measurements of hydrogels during the first 3 days after fabrication 51
Figure 33. Top and base areas measurements with Fiji software, x20 magnification 52
Figure 34. Cross-sections of PA4 big cavities, showing their top (left) and bottom (right) 52
Figure 35. Base diameter bar graphs for the 4 different sizes of cavities 53
Figure 36. Top diameter bar graphs for the 4 different sizes of cavities 54
Figure 37. Depth bar graphs for the 4 different sizes of cavities 55
Figure 38. Force-displacement curves for the 4 different hydrogels' stiffnesses 56
Figure 39. Montage of the functionalized walls and base of one of the PA1 hydrogels obtained with confocal microscopy 57
Figure 40.. Montage of the functionalized base and plane of one of the PA4 hydrogels obtained with epifluorescence microscopy 58
Figure 41. Force-displacement curves for the 4 different hydrogels' stiffnesses after functionalization 59
Figure 42. Work breakdown Structure (WBS) of the current project 61
Figure 43. PERT Diagram 67
Figure 44. GANTT Diagram 68

List of tables

Table 1. Photolithography, replica moulding and 3D bioprinting compared as potential microfabrication processes of this project 30
Table 2. PDMS, PEG and PA comparison for microfabrication processes 31
Table 3. Polyacrylamide hydrogels composition for each stiffness 36
Table 4. Protocol followed for the fabrication of the second PDMS moulds 43
Table 5. Percentage of difference (decrease) of top and base diameters (considered as the ones shown in Figure 29), and height between the PDMS1 and PDMS2 moulds by size 48
Table 6. Measured (mean and standard deviation) and theoretical Young's Moduli of the hydrogels 56
Table 7. Measured (mean and standard deviation) and theoretical Young's Modulus of the hydrogels 58
Table 8. Percentage of difference between previous and post-functionalization hydrogels 59
Table 9. Ordered tasks required to perform the project, with precedencies and timings 65
Table 10. SWOT analysis of the project 69
Table 11. Direct costs of the project 71
Table 12. Approximation of the total cost of the project 73

List of equations

Equation 1. Circular area formula 47
Equation 2. Percentage of difference between cavity (PDMS1) and post (PDMS2) 48
Equation 3. Acquisition of the volumes needed of each chemical 49
Equation 4. Formula used to calculate the z-scores 51
Equation 5. Relationship between the applied force and the Young's modulus 56
Equation 6. PERT-Beta distribution [78] 65

Glossary of abbreviations

2D	Two-dimensional
3D	Three-dimensional
PA	Polyacrylamide
IBEC	Institute for Bioengineering of Catalonia
UB	University of Barcelona
UPC	Universitat Politècnica de Catalunya
PCB	Parc Científic de Barcelona
TFG	Final Degree Project
PERT	Program Evaluation and Review Technique
CPM	Critical Path Method
WBS	Work Breakdown Structure
AT1	Alveolar Type I cells
AT2	Alveolar Type II cells
OcCs	Organs-on-chip
ECM	Extracellular Matrix
PEG	Poly(Ethylene Glycol)
USD	United States Dollar
CAGR	Compound Annual Growth Rate
UV	Ultraviolet
PDMS	Poly(dimethylsiloxane)
OH	Hydroxide
TEMED	Tetramethylethylenediamine
RT	Room Temperature
O/N	Overnight
Sulfo-SANPAH	Sulfosuccinimidyl-6-(4'-azido-2'-nitrophenylamino)hexanoate
NHS	N-Hydroxysuccinimide
PBS	Phosphate Buffered Saline
AFM	Atomic Force Microscopy
Teflon	Trichloro(1H,1H,2H,2H-perfluoroctyl)silane
Silane	(3-Aminopropyl)trimethoxysilane 97%
RPM	Revolutions per minute
APS	Ammonium Persulfate
EU	European Union
NTP	Prevention Technical Notes
ISO	International Organization for Standardization
GLP	Good Laboratory Practices

Table of contents

Abstract 3

Acknowledgments 4

List of figures 5

List of tables 7

List of equations 7

Glossary of abbreviations 8

1. Introduction 11

1.1. Motivation, aim and scope of the project 11

1.2. Objectives 12

1.3. Methodology and structure 12

2. Background 14

2.1. General concepts 14

2.1.1. Structure and histology of the lung 15

2.1.2. Structure and histology of the kidney 16

2.1.3. Structure and histology of the small intestine 18

2.2. State of the art 19

2.2.1. First 3D cultures of intestinal tissue 20

2.2.2. Possible 3D culture models for this project 21

2.2.3. 3D culture model used in this project 22

2.2.4. Fabrication techniques to obtain 3D microstructures 22

2.3. State of the situation 23

3. Market analysis 24

3.1. Hydrogel market trends 24

3.2. Hydrogel market restraint 25

3.3. Hydrogel market analysis 25

3.4. Major market players 25

3.5. Principal interested sectors 26

4. Concept Engineering 28

4.1. Fabrication method of the scaffolds and materials 28

4.1.1. Comparison of microfabrication techniques 28

4.1.2. Comparison of materials 30

4.1.3. Chosen option 32

4.1.4. Replica-moulding process 32

4.2. Functionalization of the sample 37

4.3. Characterization of the shapes of the cavities 37

4.3.1. Optical microscope 38

4.3.2. Profilometer 38

4.3.3. Interferometer *38*
4.3.4. Confocal microscope *38*
4.3.5. Optical epifluorescence microscope *39*
4.4. Characterization of the mechanical properties of the samples 39
5. Detailed engineering 40
5.1. Fabrication of cavities on thin PDMS (replica-moulding) 41
5.1.1. First PDMS mould (PDMS1) *41*
5.1.2. Second PDMS moulds (PDMS2) *42*
5.1.3. Comparison cavities - posts 1st and 2nd moulds *43*
5.2. Fabrication of the cavities on PA 49
5.2.1. Preparation of PA solutions *49*
5.2.2. Silanization of the microwells/coverslips where the PA was to be placed *49*
5.2.3. Fabrication of the PA moulds *50*
5.3. Swelling measurements 50
5.4. Comparison of cavities of different rigidities after maximum swelling 51
5.4.1. Comparison of the base diameters *53*
5.4.2. Comparison of the top diameters *54*
5.4.3. Comparison of the depths *55*
5.5. Stiffness characterization (AFM) pre-functionalization 55
5.6. Functionalization and checking of the coating 57
5.7. Stiffness characterization (AFM) post-functionalization 58
6. Execution Schedule 60
6.1. Work Breakdown Structure (WBS) 60
6.2. PERT-CPM Diagram 65
6.3. GANTT Diagram 68
7. Technical viability: SWOT analysis 69
8. Economic viability 71
9. Regulations and Legal aspects 74
10. Conclusions 76
10.1. Future work 77
Bibliography 78
Annexes 85
Annex 1. Plasma cleaner protocol used 85
Annex 2. Profilometer measurement parameters 85

1. Introduction

This first introductory section lays forth the project's goal and the inspiration behind its creation. The scope and aims of the project, as well as the methodology used, and the report's structure are also included.

1.1. Motivation, aim and scope of the project

The monolayer of epithelial cells that coats the internal surfaces of organs adopts a variety of conformations in three dimensions, depending on its function. For instance, intestinal epithelia line three-dimensional structures in the form of evaginations, called 'villi', and invaginations, called 'crypts'; lung epithelia line a series of branched spherical cavities; and kidney epithelia also line a series of invaginations or cavities. All these different shapes are optimized to maximize the efficiency of the tissue when performing its function.

Traditional studies *in vitro* have been using mainly flat 2D cell culture dishes, ignoring these 3D *in vivo* shapes. A major problem in the development of new drugs is that promising preclinical activity, studied using 2D cell cultures, often does not transmit to the clinical situation when the drug is given to the patient [1, 2]. It has been thought that drugs that perform well in *in vitro* assays may not do as well with patients because of this discrepancy between the *in vitro* and *in vivo* settings. To try to minimize this correlation mismatch between the preclinical and clinical situations, one of the many techniques that have been developed is the introduction of *in vitro* systems that have the three-dimensional complexity of *in vivo* systems.

2D cell models can be used to effectively predict *in vivo* drug responses for many targets and pathways and are still very useful in drug discovery. However, they oversee the impact of the *in vivo* shapes in tissue function, and they suffer disadvantages associated with the loss of tissue-specific architecture, mechanical and biochemical cues, and cell-to-cell and cell-to-matrix interactions [3]. This makes them relatively poor models to predict drug responses for certain diseases, such as cancer. For example, HCT-116 cells cultured in 3D structures have been found to be, with respect to the ones cultured in 2D structures, more resistant to certain standard cytotoxic anticancer drugs, such as melphalan, fluorouracil (5-FU), oxaliplatin, and irinotecan [4]. This type of chemoresistance has also been observed *in vivo*, where most cancer drugs in use today show low to modest activity in the major solid tumours [5, 6].

Recent studies have started to address this lack of complexity in *in vitro* cultures by introducing three dimensional architectures that resemble the ones found *in vivo* [3]. However, those novel culture platforms still have some limitations, specifically when architecture needs to match the mechanical properties (for example, the stiffness) of the native tissue.

While the evagination (or villus) morphogenesis has been extensively studied, the mechanism behind the formation of the mentioned invaginations is not well understood. In the case of intestinal crypts, they have been demonstrated to be initiated by apical constriction of the intravillus tissue

[7]. However, further research is needed to fully understand the mechanisms of these cavities' formation and development.

The fabrication of cavities or 3D features in soft substrates can be challenging due to several factors related to the mechanical properties of soft materials. Soft substrates, which are typically characterized by low stiffness and high deformability, present unique challenges in terms of processing and fabrication. Some of the reasons why this fabrication can be difficult are [8]:

- Tendency of soft materials to deform and distort easily under the influence of external forces or during the fabrication process. This deformation can lead to imprecise or unintended cavity shapes, making it challenging to achieve the desired features.
- Lack of the structural support and rigidity found in harder materials, which can make it difficult to maintain the structural integrity of the substrate during fabrication processes.
- Material adhesion to tools or moulds, causing challenges in demoulding or separating the substrate from the fabrication tool, which can result in unprecise features.
- Limited compatibility with standard processes, which are optimized for harder materials and may not be well-suited for soft substrates.

The aim of this project is to develop three dimensional cavities with dimensions and mechanical properties similar to the ones encountered *in vivo*, and characterize them. These cavities will be formed in polyacrylamide (PA) hydrogels, which allow to reach physiological stiffness.

1.2. Objectives

As stated above, the project's primary goal is to acquire 3D cavities of controllable size and stiffness. In order to do that, a number of objectives have been established:

I. Develop an effective protocol for the fabrication of the microcavities to acquire PA replicas with the features imprinted on them.
II. Evaluate the structure and dimensions of the resulting cavities.
III. Assess the mechanical properties of the hydrogels.
IV. Functionalize the walls of the microcavities with a proper coating with functionally active proteins.
V. Re-assess the mechanical properties of the hydrogels after the functionalization.

1.3. Methodology and structure

This project has been developed from June 2023 to January 2024, with a previous period of preparation from June to July 2023. In this previous period of preparation, a familiarization with all the techniques, materials and instruments needed to achieve the aim of the project was completed. Then, the bibliographic research needed to understand the topic of the project was done. This previous theoretical study can be found in section 2, which offers the main concepts that involve this project, as well as the state of the technology in which this field is found, and the situation where the project is framed in.

This project was done at the Institute of Bioengineering of Catalonia (IBEC), more specifically in the 'Biomimetics Systems for Cell Engineering' group. The IBEC is a centre of interdisciplinary research with its headquarters in Barcelona, dedicated to the research at the frontier between engineering and sciences, with the aim to create new knowledge, integrating fields like nanomedicine, biophysics, biotechnology, tissue engineering and the applications of information technology in the area of health [9].

The institution was created in 2005 by the department of Innovation, Universities and Business and the department of Health of the 'Generalitat de Catalunya', the 'Universitat de Barcelona' (UB) and the 'Universitat Politècnica de Catalunya' (UPC). Nowadays it has 22 research groups with 336 researchers, and it is located at the 'Parc Científic de Barcelona' (PCB).

During the first semester of the fourth year of my degree, I have completed this project, to present it in January. The agreement of the internship in IBEC to complete the Final Degree Project (TFG) had a durability of maximum 30 weeks, so I had to complete the whole project before this time.

It can be divided into 4 parts. In the first place, the fabrication of the necessary moulds to obtain the final polyacrylamide (PA) one. Then, the characterization of the shapes obtained in the polyacrylamide, and the assessment of the mechanical properties of the hydrogel. Next, the functionalization of the structures, followed finally by a new assessment of their mechanical properties.

In section 3, a market analysis is presented, and in section 4, a study of all the possible solutions is performed. This section also includes a summary of the final procedure used. To organize the project and take the time to perform each task into account, a PERT and GANTT diagram are shown in section 6, as well as an WBS and an analysis of precedencies. Sections 7 and 8 expose the technical and economic viability of the project, and section 9, the regulations and legal aspects surrounding it. The combination of these 4 last sections determines if this whole project is attainable. The details of the way each task of the project has been carried out are exposed in section 5, as well as the calculations for the characterization of the cavities, with the corresponding results and discussions. The conclusions of the project have been discussed in section 10, where the future work has also been commented on. Finally, a bibliographic section has been added where all the sources of information are displayed.

2. Background

It is essential to give a thorough description of the theoretical underpinning supporting this project before beginning the market study. That is, learning about the conformation of these cavities *in vivo*, by studying the structure and histology of organs that have them, such as lungs, kidneys, and the small intestine. To appropriately contextualise this work, it is also important to research the current state of the art of 3D models, as well as the techniques that exist to obtain 3D microstructures, and the state of the situation of the project.

2.1. General concepts

Tissues are collections of cells, and a tissue's function is closely related to its structure. For effective oxygen exchange, for instance, lung alveoli and the pulmonary vasculature must be in close proximity to one another throughout the lung. Similar to this, for the kidneys to eliminate waste and extra fluid from the body, the renal vasculature and kidney ducts need to be adjacent to each other. Regarding intestinal crypts, these invaginations are often used to increase surface area [10]. Many of these structures are either formed by apical constriction of the cells in the centre of the future fold, or by buckling of a tissue experiencing compressive forces, as it can be seen in Figure 1.

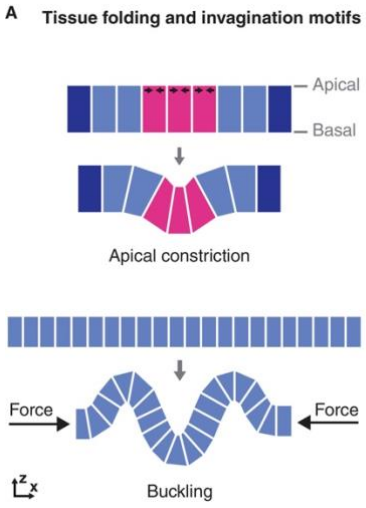

Figure 1. Schematic illustrating developmental motifs that result in tissue folding and invagination [10]

Epithelial cells typically form monolayers that line organs and thereby create barriers between compartments. The remarkable ability of these type of cells to change shape based on where they are in a tissue has implications for how they operate. For example, looking at the organs mentioned above, squamous epithelia are present in lung alveoli to enable gas exchange, as thin cell layers allow rapid diffusion. On the other hand, cuboidal epithelia are often found in ducts of glands like the kidney, where they perform functions related to absorption and secretion. As for the small intestine, columnar epithelia are responsible for taking up nutrients and transporting them across the intestine's lining. Since this process relies on active transport rather than diffusion, the larger distances provided by a columnar geometry can be overcome. Moreover, columnar epithelia are less brittle and offer a mechanically durable barrier due to their greater thickness when compared

to squamous and cuboidal epithelia. Pseudostratified epithelia are found, for example, in the lung trachea and bronchi. These cell shapes described above are all illustrated in Figure 2.

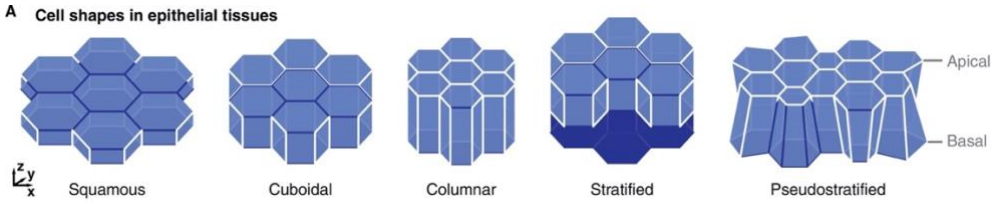

Figure 2. Schematics illustrating typical cell shapes observed in epithelial tissues [10]

To better understand epithelial invaginations, the structure and histology of the three organs mentioned above (lung, kidney, and small intestine) have been researched and explained in sections 2.1.1, 2.1.2 and 2.1.3.

2.1.1. Structure and histology of the lung

The lungs are a pair of primary organs of respiration, present in the thoracic cavity beside the mediastinum. The respiratory system consists of the conduction portion (from the nose to the terminal bronchiole) and the respiratory portion (from the bronchiole to the alveoli). The alveoli are the structural and functional units of the respiratory system, and it is where the significant exchange of gases takes place [11].

Specialized respiratory epithelium comprises the entire respiratory tree, and these cells collaborate to warm, moisturize and remove air entering the lung. As mentioned above, most of the respiratory epithelium is formed by ciliated pseudostratified epithelium. The five main types of cells found in these regions are ciliated, goblet, brush and neuroendocrine cells. These first ciliated cells are the most abundant, and they control the actions of the mucociliary escalator[1]. On the other hand, goblet cells are filled with mucin granules at their apical surface with the nucleus remaining towards the basilar layer. These cells provide mucus that traps inhaled particles, and they are progressively replaced by club cells as the respiratory tree gets smaller. As for the basal cells, they provide the attachment layer of the ciliated and goblet cells, and they maintain the ability to potentiate into these two kinds of epithelial cells. Brush or tuft cells are identified by their short microvilli covered apical layer, but no function has been officially assigned to them. Finally, the bronchial mucosa also contains a small cluster of neuroendocrine cells, also known as Kulchitsky cells. They have neurosecretory type granules that can secrete several factors, such as serotonin or calcitonin.

As for the alveolar epithelium, 90 to 95% of it is formed by flat, squamous epithelia that resemble plate-like structures. These cells, also called alveolar type 1 cells (AT1), have a fragile membrane that allows for easier gas permeability between the alveoli and the blood vessels. As for the

[1] Primary defence mechanism of the lungs that removes debris. The cilia move inhaled particles toward the pharynx to swallow or cough out.

remaining 5 to 10%, alveolar type II cells (AT2) are also found in lungs, and they are responsible for the secretion of pulmonary surfactant[2].

In the proximal airway, the invagination of epithelium forms submucosal glands, which are characterized by a variable proportion of mainly ciliated and goblet cells [12]. All the structures and cell layers mentioned above can be seen in Figures 3 and 4, where Figure 3 shows a schematic, whereas Figure 4 shows a real image of the structures of the lung obtained with optical microscopy. In Figure 4, A represents a section of the bronchiole wall, with the arrow marking the basement membrane, and B shows the bronchial wall with squamous metaplasia with the arrow head, and hyperplasia of the subepithelial gland with the arrow. These are histologic features of chronic bronchitis, which are not relevant for this study, but the image shows clearly the invaginations found in lungs.

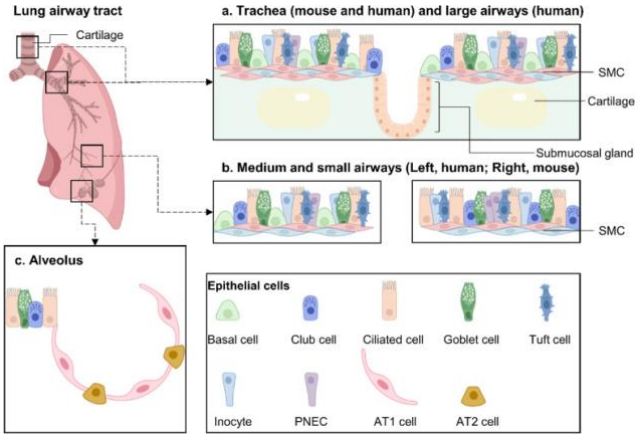

Figure 3. Schematic of the anatomy and cellular composition in mammalian lungs (mouse and human) [13]

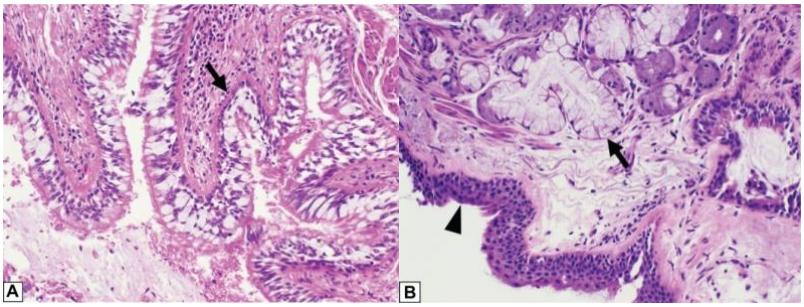

Figure 4. Histologic features of chronic bronchitis, stained with haematoxylin – eosin dye, x200 magnification [14]

2.1.2. Structure and histology of the kidney

The kidneys are two organs with several essential homeostatic functions, such as waste removal, fluid/electrolyte balance, metabolic blood acid-base balance, as well as producing/modifying hormones for blood pressure, calcium/potassium homeostasis, and red blood cell production. The functional unit of this organ is the nephron, which consists of the renal corpuscle (filtration unit, with

[2] The surfactant is necessary to maintain an open airway. It lowers the surface tension and prevents the alveoli from collapsing upon themselves during exhalation.

the glomerulus and the surrounding glomerular or Bowman's capsule) and the tubules (reabsorption and excretion) [15].

The renal corpuscle consists of several histological structures, such as the glomerulus capillaries, the intraglomerular mesangial cells, the Bowman's capsule, the glomerular basement membrane, and the juxtaglomerular apparatus. All of these structures appear schematically in the left image of Figure 5, and they are described hereunder.

The glomerulus capillaries from a central tuft of looped capillaries located in the centre of the renal corpuscle. They deliver blood and create a large surface area for renal filtration. The intraglomerular mesangial cells physically support these capillaries. As for the Bowman's capsule, it consists of the inner visceral layer, which encircles the glomerular capillaries, and the outer parietal layer, which is a single layer of simple squamous epithelium. The inner visceral layer is comprised of specialized epithelial cells named podocytes. These cells are very large and serve both as support of glomerular capillaries and are part of the glomerular filtration barrier. Then, the glomerular basement membrane is a fused membrane of the podocytes, and it also offers some support to the glomerular capillaries. Finally, the juxtaglomerular apparatus is an important group of structures located at the entry of the capillaries in the glomerulus, which are specialized sensory structures with feedback mechanisms to regulate glomerular blood flow and filtration rate.

The renal tubule system is the part of the nephron which processes glomerular ultrafiltrate into urine by reabsorbing necessary molecules and secreting waste substances [16]. It consists of the proximal tubule, the nephron loop (or loop of Henle) and the distal tubule. The proximal tubule is the first part of the tubular system, and it is composed of simple cuboidal epithelium rich in microvilli, which's morphology is adapted to its function of absorption and secretion. As for the nephron loop, it is the U-shaped bend of the nephron. It is composed of simple squamous epithelium, and its function is to adjust the filtrate's salt and water levels. Finally, the distal tubule has similar morphology to the proximal one, but it shows less well-developed microvilli, as reabsorption and secretion in this section is performed to a lesser degree than in the proximal tubule. A scheme of these tubules can be seen in the right image of Figure 5.

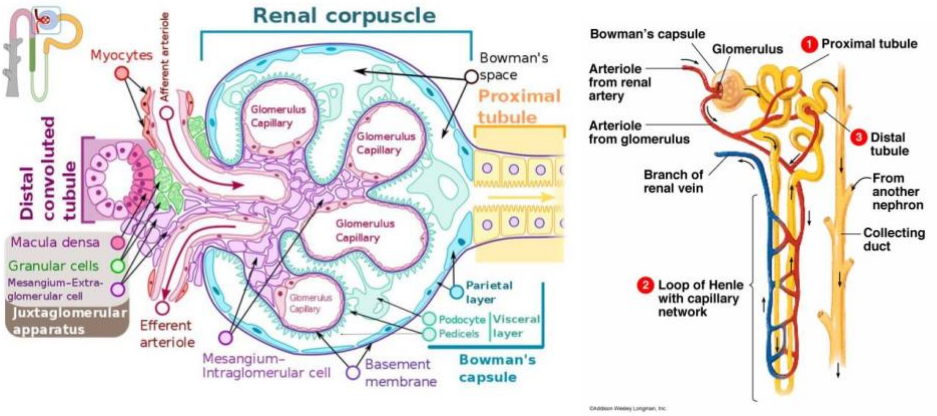

Figure 5. Renal corpuscle schematic (left) [15] and renal tubule system schematic (right) [17]

Figure 6 shows real images of the structure of the kidneys obtained with optical and electron microscopy. The left image shows an optical microscopy image of the general cortex of the kidney, where 'glom' is the glomerulus, 'p' the proximal tubules, and 'd' the distal tubules. A more magnified image on the left shows a glomerular capillary basement membrane, obtained with electron microscopy. These figures show the invaginations that can be found in kidneys.

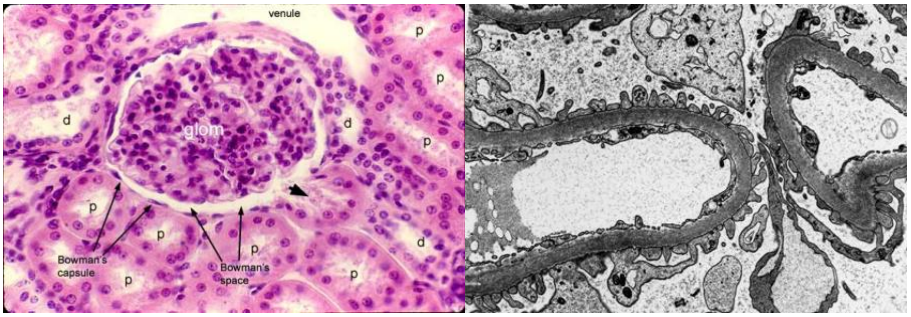

Figure 6. Histological section of the kidney dyed with haematoxylin – eosin dye, x400 magnification (left) [18], and thick glomerular capillary basement membrane, stained with lead citrate and uranyl acetate, x4800 magnification (right) [19]

2.1.3. Structure and histology of the small intestine

The small intestine is the organ that goes from the pylorus of the stomach to the union of the caecum with the ascendent portion of the colon (where the large intestine starts). Its average length is of 6 to 7 meters, and it is divided into the duodenum, the jejunum, and the ileum [20]. The histology of any of these subdivisions is composed by four structures: the mucosa, the submucosa, the muscular and the serosa.

The mucosa is constituted by a monolayer of epithelial cells, the lamina propria, and the muscular of the mucosa. The epithelium is projected to the intestinal surface forming, as mentioned above, the 'villi'. In between these protrusions, there are simple tubular glands that penetrate in the lamina propria until almost entering in contact with the muscular of the mucosa, called crypts or 'Lieberkühn glands'.

The submucosa is the way through which the capillaries, greater calibre blood and lymphatic vessels cross, which drain and give nutrients to the mucosa and external musculature. Blood and lymphatic vessels cross this external muscular to reach the submucosa. Finally, the serosa is the mesothelium that covers the organ. It is a strip of loose connective tissue that contains blood vessels and nerves.

The main cells present at the villus are the ones called 'cells of absorption', which are tall and columnar, with the nucleus at their base. The apical surface (edge facing the lumen of the organ) of these cells is composed by microvillus and glycocalyx, which act like a barrier against the microorganisms and exogenous substances. This edge also contains enzymes that intervene in the final digestive processes.

Regarding the crypts, these structures contain stem cells of four types of cells present in the small intestine: absorption, caliciform, Paneth and endocrine cells. Their differentiation and maturation lasts for about 5 to 6 days, while they travel from the depths of the crypts to the tips of the villus, where they are released at the lumen. The Paneth cells are the only ones that stay at the crypts, and their function is to provide niche factors to the intestinal stem cell compartment, regulating the composition of the microbiome through the production and secretion of antimicrobial peptides, performing phagocytosis and efferocytosis, taking up heavy metals, and preserving barrier integrity [21].

The lamina propria is formed by intertwined packs and other fibres, like fibroblasts, plasmatic cells, smooth muscular cells, and collagen and elastic fibres. On the other hand, the muscular of the mucosa is composed by smooth muscular tissue and elastic fibres, with two different muscle strips placed perpendicular to each other: the internal one (arranged circularly) and the external one (arranged longitudinally) [22].

All the structures and cell layers mentioned above can be seen in Figure 7, where left image shows a schematic, whereas the right one shows a real image of the structure of the intestine obtained with optical microscopy. In this second image, the different parts mentioned above are marked with numbers, which correspond to:

1. The Paneth cells.
2. The intestinal glands or Lieberkühn crypts.
3. The lamina propria.
4. The epithelium coating.
5. The intestinal villus.
6. And the muscular of the mucosa.

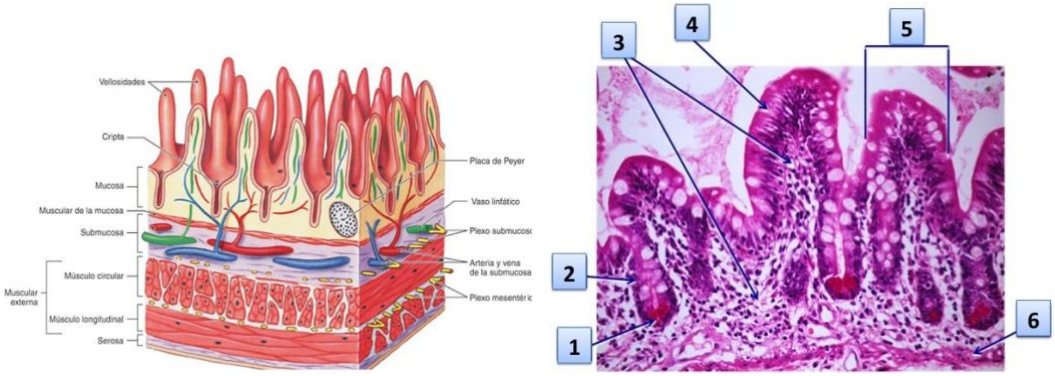

Figure 7. Schematic of the structure and cell layers of the intestine (left) [23], and histological section of the intestine dyed with haematoxylin – eosin dye, x100 magnification (right) [24]

2.2. State of the art

Technology related to *in vitro* cell-based cultures has experimented significant advances in the last decades. In traditional drug screening methods, intestinal tissues and organs were directly harvested from animals, and cell culture studies were carried out in two-dimensional (2D) culture dishes. This caused that lots of drugs that passed the animal testing showed inadequate therapeutic effects and even toxicity to humans. Due to the species differences between animals

and humans, animal toxicity testing fails to predict toxicity in almost 50% of drugs in the pipeline between Phase I trials and early post-market withdrawals [25].

On the other hand, these 2D structures do not accurately replicate the complex three-dimensional (3D) architectures found *in vivo*. Recent advances have attempted to address this limitation by introducing 3D culture platforms that more closely mimic *in vivo* architectures. In this section, the most common *in vitro* intestinal tissue models are described.

2.2.1. First 3D cultures of intestinal tissue

One of the first intestinal models *in vitro* were the intestinal rings and intestinal segments, which were proposed by Agar *et al.* in 1954. These structures are constructed by a part of fresh intestine that is washed thoroughly and cultured in a high oxygenated buffer [26]. They are easy to operate and have a wide variety of sources. However, as intestinal cells lack the normal physiological environment (regarding pH or temperature), the tissues in both models survive hardly more than 2 hours, and they have more attached microorganisms.

Another model is the everted intestine sac, which is commonly used for exploring mechanisms of drug metabolism and drug absorption, and for the investigation of the role of intestinal enzymes and transporters during drug transport through the intestine [27, 28]. It was proposed in 1954 by Wilson and Wiseman [29], and to construct it, one end of the everted intestine segment is tied, and the other is connected to tubing that flows a buffer, forming a sac. The viability of the cells in this model also only keeps up to 2 hours, and the absorption process in this *ex vivo* intestine model consumes much more time than that in the living intestine, since the compound has to cross the muscle layers, and the fluid is stagnant.

The Ussing chambers were initially developed to measure the transport of ions, nutrients and drugs across various epithelial tissues in 1951 by Ussing and Zerhan [30]. This technique consists in mounting an intestinal segment in an Ussing chamber, where the apical side is exposed to buffer with the compound of interest and the basolateral side is exposed to buffer without the compound of interest. In this system, different parts of the intestine can be used, which is an advantage, but it is laborious, and it has a relatively low efficiency, and short-term survival in culture.

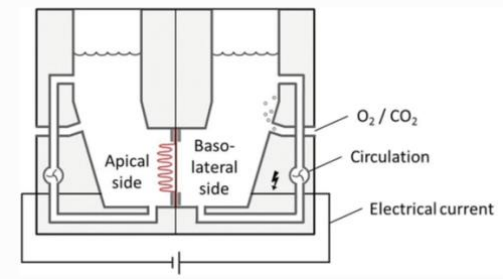

Figure 8. Schematic representation of a small piece of intestinal epithelial tissue mounted in the Ussing chamber [31]

The isolated and perfused intestinal segments were first described by Baker *et al.* in 1968 [30]. For this system, a part of the intestine is isolated, and both ends of the organ are sealed before the tissue is mounted into the perfusion system, where it is perfused with a well-defined buffer. A major

advantage of the system is that the model displays a normal morphology, histology and physiology. However, the difficulty of obtaining sufficient quality and quantity of organs, and the limited duration of the experiments are two major drawbacks.

2.2.2. Possible 3D culture models for this project

Transwells (or Boyden Chambers) consist of two-filled chambers separated by a microporous membrane [30]. They are usually used for cell culture, migration observation and invasion testing, so they are not the optimal models for the goals of this specific project. Nonetheless, this model is easy to operate, with a repeatable protocol at a lower cost, with culture time of up to 3 weeks.

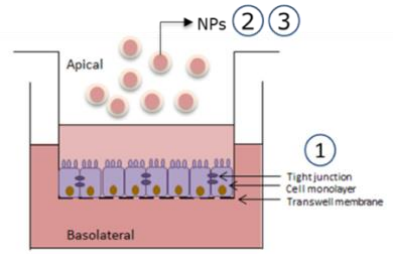

Figure 9. Schematic illustration of a Transwell system [32]

An organoid is a collection of organ-specific cell types that develops from stem cells or organ progenitors and self-organizes through cell sorting and spatially restricted lineage commitment in a manner similar to *in vivo* [3]. Some advantages it presents, in the case of an intestinal organoid, are that it is well organized, with all the cell types found *in vivo*, and its ability to create crypts with complex architectures similar to the ones found in tissues. However, its main drawback is that the lumen is closed, and therefore, not accessible.

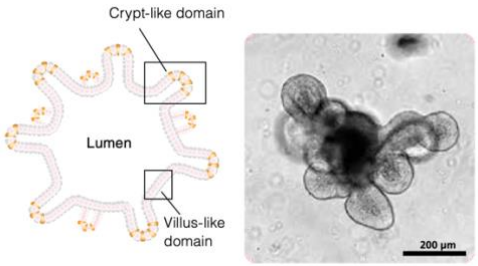

Figure 10. Intestinal organoid morphology. Schematic of a mature intestinal organoid (left) and brightfield image of a mature (day 5) mouse intestinal organoid (right) [33]

Organs-on-chip (OoCs) refer to artificial, miniature models of human organs on a microfluidic cell culture chip. Regarding human intestine-on-a-chip, these microfluidic models have been widely used in disease model construction and drug development. The coculture of epithelial cells with endothelial cells, pathogens, probiotics, immune cells, fibroblasts and tumour cells can recapitulate intestinal microenvironments in different physiological statuses to model intestinal diseases, study disease mechanisms, and explore therapeutic methods [34]. They are usually used for these studies, so they are not the optimal models for the goals of our specific project.

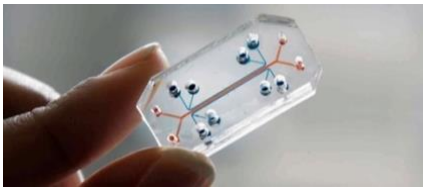

Figure 11. Intestine-on-a-chip [35]

2.2.3. 3D culture model used in this project

This project is based on the synthesis of **hydrogels**. **Scaffolds or hydrogels** are 3D structures made of a large variety of materials with different porosities, permeability, surface chemistries, and mechanical characteristics designed to mimic the microenvironment of specific tissues [3].

These models can be classified into two groups: biological and polymeric (or synthetic). The biological ones mostly use naturally derived extracellular matrix (ECM), such as Matrigel and collagen, to promote appropriate cell attachment and reorganization into 3D structures. Compared with the other type, they provide a more physiologically relevant microenvironment of soluble growth factors, hormones, and other molecules with which cells interact in an *in vivo* environment. However, when working with Matrigel, lot-to-lot variability during manufacturing is very common, and it has a very complex composition, which is often ill-defined, making it difficult to determine exactly which signals are promoting cell function. On the other hand, polymeric scaffolds use synthetic hydrogels or other biocompatible polymeric materials to generate the physical supports for 3D cultures. The use of these materials can minimize the relatively poor reproducibility of biological ECMs between batches and the resulting lack of consistency between cultures, as they are often simply processed and manufactured. They also allow for fine tuning of biochemical and mechanical properties, so they allow the optimization of both mechanical and chemical cues for 3D cultures. Moreover, their high-water content enables the transport of oxygen, nutrients, waste and soluble factors, all of which are important to cell functions. Some examples of hydrogels used for 3D culture include poly(ethylene glycol) (PEG), poly(vinyl alcohol), poly(2-hydroxy ethyl methacrylate), and polyacrylamide (PA). All of these hydrogels allow the fabrication of cavities, but only the stiffness of the polyacrylamide can be reduced to physiological values.

The problematic where the project is framed in is in obtaining models with both the architecture and mechanical characteristics of cavities, and, as there are some hydrogels (such as polyacrylamide) that allow the tuneability of their properties, as well as of their architecture, this was the final model used. The material chosen for the completion of this study is decided in section 4, after a comparison of different materials.

2.2.4. Fabrication techniques to obtain 3D microstructures

There are three main methodologies that allow the fabrication of 3D microstructures. These three options are 3D bioprinting, photopatterning and replica moulding. A more thorough comparison of these three techniques can be seen in section 4.

3D bioprinting refers to the printing of cells, biocompatible materials, and supporting components into complex 3D living tissues with the desired cell/organoid architectures topology, and

functionality using additive manufacturing [3]. Some advantages that they have are that they are custom-made architectures, and that they allow co-culturing and high-throughput production. They can work with hard hydrogels, but some challenges arise with the use of soft materials. It is challenging to obtain crypts with this technique using low rigidity hydrogels due to their inability to retain a desired shape following extrusion [36].

On the other hand, hydrogel photopatterning, by modifying the ends of gels, allow hydrogels such as PEG to be photo crosslinked in the presence of appropriate initiating agents [37]. This type of curing offers spatial control over polymerization. The main issue with this methodology is that it has been well established using hard hydrogels, and not with low-stiffness ones. A recent study has achieved the formation of cavities using this technique with PA hydrogels, whose rigidity can be tuned by changing the proportion of the materials used in fabrication. However, the only successful results they obtained were of gels of more than 100 kPa. As soft tissues have a range of Young's moduli values between 2.5 and 160 kPa, this technique did not allow the study of all the softer tissues found in the body [38].

Finally, the **replica moulding** technique is a process for shaping polymer materials using a micro sized rigid frame or model called a 'mould' [39]. This mould is then filled with a prepolymer, which is cross-linked and the resulting polymer is peeled off of the mould. Using a mould rather than the object itself allows multiple copies to be made without damaging the original.

2.3. State of the situation

Although there have been efforts to introduce more realistic 3D cultures, limitations remain, especially in reproducing the mechanical properties and architecture of native tissues. The state of the art reflects a growing recognition of the importance of reproducing not only cellular morphology, but also mechanical characteristics to fully understand epithelial tissue function, such as the stiffness of native tissues.

The scaffold characteristics, along with the material properties, can regulate cell adhesion, proliferation, activation and differentiation. Although hydrogels represent a simplified architecture and they can be variable across lots, they are highly reproducible models with co-culture ability. On the other hand, the replica moulding technique allows the fabrication of multiple copies, which allows us to study the behaviour of the moulds more thoroughly.

This project is based on the fabrication of three-dimensional cavities with **polyacrylamide synthetic hydrogels with the use of the replica moulding technique**. Their mechanical properties and architectures similar to the ones encountered *in vivo* will be studied and characterized throughout this report.

3. Market analysis

Cell culture technology has been slow to innovate, and progress has been incremental over the past 50 years. 3D scaffolds provide a physical support for the growth of cells in a 3D microenvironment allowing better cell-cell, cell-extracellular matrix (ECM), and intracellular signalling interactions. The properties of these scaffolds can be modified in terms of strength, interconnected porosity, elasticity, biochemistry and bio-functionality to better mimic the native tissue-specific microarchitecture. Hydrogels are a type of scaffolds that are highly hydrated polymer networks, and due to their ability to better mimic the ECM, they are the most widely used scaffolds [40]. Both natural and synthetic hydrogels are being thoroughly studied at this time. For instance, Sheehy *et al.* explored the potential of hydrogels derived from natural biomaterials, such as alginate, fibrin and chitosan, toward chondrogenesis[3] and hypertrophy[4] of Mesenchymal Stem Cells [41]. Regarding synthetic hydrogels, there have also been efforts in making them have greater flexibility and tunability for chemical modifications. An example of this effort is the project carried out by Stüdle *et al.,* in which they used poly(ethylene glycol) (PEG) based bilayered hydrogels toward the development of osteochondral tissue[5] [43]. However, 3D cell cultures usually have a slower rate of cell proliferation and migration compared to 2D cultures, and structural strength for culturing cells is scaffolds-dependent. Moreover, as it has been mentioned before, the now existing soft hydrogels do not allow the correct formation of microcavities with the mechanical stiffness of *in vivo* tissues. Therefore, further work is warranted to manage these characteristics and create a more robust and reliable model.

The hydrogel market size was accounted for USD 26 billion in 2022, and it is estimated to grow at 6.4% CAGR (Compound Annual Growth Rate) to reach USD 48.12 billion by 2032 [44]. This demand is driven by factors such as the expanding aging population, a growing incidence of chronic wounds, and a strong focus on achieving superior healing outcomes. Furthermore, hydrogels, with their moisture-retaining properties, ease of application, and ability to facilitate wound healing are becoming preferred choices in advanced wound care [45].

3.1. Hydrogel market trends

The increasing prevalence of chronic wounds and ulcers is expected to supplement the industry expansion. For instance, according to the International Wound Journal report, global prevalence of chronic wounds is estimated at 1.51 to 2.2 per 1000 population [46], and incidence is expected to rise with ageing populations worldwide. As the number of individuals affected by conditions such as diabetic foot ulcers, pressure ulcers, and venous leg ulcers continues to rise, there is a growing demand for effective wound management solutions. Furthermore, there is an increasing awareness among healthcare professionals about the benefits of hydrogels in managing chronic wounds [45].

[3] Process of development of cartilage.
[4] Increase in the volume of cells.
[5] Tissue found at synovial joint surfaces and composed of both articular cartilage and subchondral bone [42].

Although the major market trends do not involve the fabrication of organ models, any investigation regarding hydrogels can provide more information about their behaviour in different situations, which can potentially result as advantageous for the development of *in vitro* models.

3.2. Hydrogel market restraint

High development and manufacturing costs may hamper the hydrogel market, as the process of researching, developing, and manufacturing medical hydrogel products can be expensive, particularly when advanced formulations, materials and production techniques are involved. The costs incurred in conducting research studies, obtaining regulatory approvals, and scaling up production may pose challenges for market players, especially small size manufacturers. Additionally, the demand for specialized raw materials and equipment further contributes to the overall cost burden. These high costs can limit the accessibility and affordability of hydrogel-based products [45].

3.3. Hydrogel market analysis

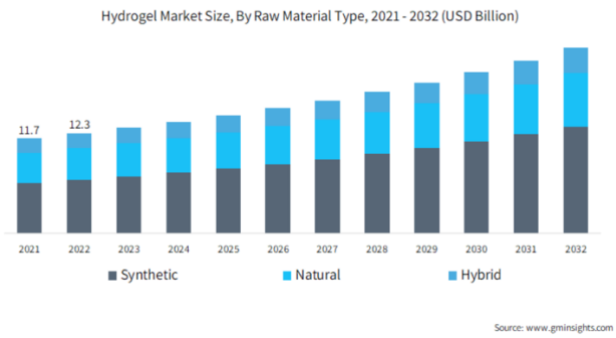

Figure 12. Estimated hydrogel market size from 2021 to 2032 [45]

Depending on the type of material used to fabricate hydrogels, they can be classified into natural and synthetic, as it was mentioned before. There is also another category for hybrid hydrogels, which are a mixture of these two main types. The synthetic segment accounted for 53.4% of the industry share in 2022. This type of hydrogels offers several advantages, including enhanced control over their physical and chemical properties, improved biocompatibility, and tailored functionality to meet specific medical applications. Also, the mechanical strength, adjustable permeability, and controlled drug release capabilities make synthetic hydrogels ideal for a wide range of medical applications. As it can be seen in Figure 12, there is a persistent market increase in hydrogels, with a more significant increase in the synthetic type.

3.4. Major market players

Regarding the hydrogel market share, North America's hydrogel market accounted for 46.6% of share in 2022. Factors such as well-established healthcare infrastructures, increasing aging population and a high prevalence of chronic diseases will drive the regional industry progression. Additionally, North America has the presence of key market players, robust research and development activities, and supportive government initiatives.

The major market players operating in the hydrogel market include Smith and Nephew, 3M Company, Convatec Inc., Integra LifeSciences Corporation, Johnson&Johnson, Cardinal Health, CooperVision. All these companies have a section focused on the research and development of new products that empower healthcare professionals with options to improve patient outcomes. They represent around 30% of the share of this market [47].

In Figure 13, each country is presented with a different shade of blue depending on their growth rate value in the hydrogel market, being those with a darker shade the ones with the highest growth. As it can be seen, Spain still has a low growth rate for this market, but some Spanish companies that have programs of research developing models based on hydrogels are: the Institute for Bioengineering of Catalonia (IBEC), where several groups, such as the 'Biomimetic systems for cell engineering' group, have studies regarding this research path; the 'Depósito de Investigación de la Universidad de Sevilla' or IDUS [48], in which they work with the development of tissue engineering; the 'Laboratorio de Estudios Cristalográficos' of the University of Granada [49], which patented a new supramolecular hydrogel with numerous biotechnological applications; and the 'Bioforge' group of the University of Valladolid [50], which participates in a project with the aim to fabricate hydrogels sensible to diagnostics and therapies in the biomedical field.

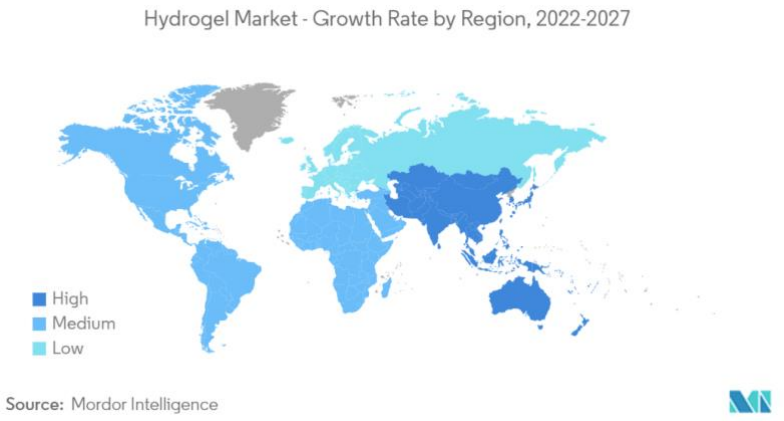

Figure 13. Hydrogel Market Growth Rate by Regions from 2022 to 2027 [47]

3.5. Principal interested sectors

The main uses of 3D models nowadays are for **drug discovery**, **cell therapy** and **tissue engineering** [3]. In this section, a market analysis of these three sectors will be exposed, stating their global market value and some future perspectives that they have.

The global **drug discovery** market size was valued at USD 55.46 billion in 2022, and it is expected to be worth around USD 133.11 billion by 2032, growing at a CAGR of 9.2% from 2023 to 2032 [51]. This market is significantly driven by the rising prevalence of various chronic diseases, rising healthcare expenditure, and patent expiration of certain popular drugs across the globe.

About the **cell therapy** market, its global value in 2022 was estimated at USD 12 billion, and it is expected to hit USD 83.78 billion in 2032, poised to grow at a CAGR of 21.50% during the period from 2023 to 2032 [52]. This is the most significant growth within the three interested sectors, due

to the rising incidents of chronic disorders and infections, as well as the growing cases of diabetes. This therapy is widely used for research purposes nowadays, with a market share value of 62% compared with its clinical use.

Finally, the global **tissue engineering** market size was accounted at USD 11.81 billion in 2022 and it is expected to hit around USD 33.38 billion by 2032, expanding at a CAGR of 11% during the period from 2023 to 2032 [53]. This global market is growing because of developed countries adopting regenerative medicine and tissue engineering technologies. One of the key market drivers is the rising incidence of chronic diseases and road traffic accidents with trauma injuries. In order to restore injured tissues, tissue engineering offers an alternative to mechanical device instruction, surgical reconstruction and transplantation.

The model described in this project is based on synthetic hydrogels, and it could be used for both drug discovery and cell therapy purposes after its validation. The fabrication of hydrogel cavities with dimensions and mechanical properties similar to the ones encountered *in vivo* could be the first step used to create a more complex model that simulates real tissues and, with the use of human cells, be able to test drugs or to place new healthy tissues fabricated *ex vivo* into the body to replace diseased or damaged ones.

4. Concept Engineering

This section aims to expose all the materials and methods used during the completion of this project, showing how it was conceived. Different options and proposals of each step will be presented, and the best one will be chosen. As it was mentioned in the introduction, this study can be divided into 4 parts. A general scheme of the steps followed can be seen in Figure 14.

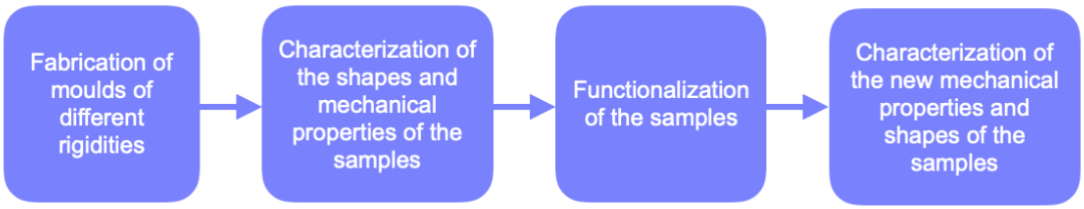

Figure 14. General scheme of the steps of this project

Firstly, the fabrication method of the moulds of different rigidities will be chosen, choosing the final material that we worked with as well. This will be done by comparing different methods and materials that could have been used to achieve our goal. Then, a description of the protein that was seeded on top of the scaffold to functionalize it will be included. Finally, the equipment to assess the viability of the sample before and after the functionalization will be presented. This last step will evaluate both the quality of the shapes and the mechanical properties found on the different samples.

Here we also present a brief description of the final procedure that was used, and in section 5, all the details about the protocols and the results obtained will be shown.

4.1. Fabrication method of the scaffolds and materials

As it has been shown in section 2, the importance of the methodology used for the fabrication of 3D structures in *in vivo* cultures has led to the development of various types of methodologies to do so. However, this project aims to implement only one of these. In order to choose which fabrication method is best suited for this study, a further investigation of the possible solutions has been done. The proposed solution will not only be based on the positive and negative aspects of the methodology itself, but also on the realistic possibility of a fourth-year degree student being able to develop it.

4.1.1. Comparison of microfabrication techniques

The design of the final scaffold must ensure to meet several requirements, including the ability to modify the rigidity of the material used, the capacity to transfer the microstructures into this material, and a simple fabrication procedure that allows the replicability of the experiment. For the fabrication of the scaffolds with different rigidities and the three-dimensional conformations, there are three proposals that achieve the necessary requirements, introduced in section 2.

For the first option, **photolithography** intervened by reaction-diffusion is used for the manufacture of microstructures in **poly(ethyl glycol)-based (PEG)** hydrogels. Photolithography or ultraviolet (UV) lithography is a reliable and fast technique for constructing various patterns of thin film on a substrate with high precision [54]. This process consists of a single step and does not require a mould: by controlling the manufacturing parameters, such as the diffusion and oxygen depletion time scale, the distance to the source of light and the exposure dose, the dimensions and geometry of the microstructures can be well defined. This is the methodology used in the article 'Dynamic photopolymerization produces complex microstructures on hydrogels in a mouldless approach to generate a 3D intestinal tissue model' [55]. This study was performed at IBEC, and it proposed a simple, single-step, and cost-effective strategy for producing models of intestinal epithelium that can be easily integrated into standard cell culture platforms. This fabrication technique, which only requires a UV lamp and inexpensive photomasks, is relatively low cost. A recent study has also shown results of photolithography-obtained cavities on **polyacrylamide (PA)** hydrogels [38]. However, as mentioned before, they only obtained scaffolds of more than 100 kPa, not reaching the lowest stiffnesses found on some tissues. Moreover, this method only works well for the fabrication of evaginations, and not for invaginations.

On the other hand, the second proposal would be to use **flexible polyacrylamide (PA)** hydrogels as final moulds for cell cultures, using **replica moulding** as the technique to microfabricate the cavities into the hydrogels. Replica moulding is one of the most common and low-cost methods for fabricating microstructures for various applications, including tissue engineering, dry adhesives, optics and strain sensors [56]. This option is used in the article 'Microfabrication of poly(acrylamide) hydrogels with independently controlled topography and stiffness' [57], study also done at IBEC, which presented a reliable microfabrication method to obtain well defined topographical structures of micrometre size (from 5 to 10 μm) on soft polyacrylamide hydrogels with tuneable mechanical stiffness (from 3 to 145 kPa) that closely mimic the *in vivo* situation of a cell's ECM. The fact that it only needs simple laboratory equipment to be performed makes it an inexpensive technique, and it allows the formation of both evaginations and invaginations.

The third and final method is **3D bioprinting of hydrogels**. Using additive manufacturing, this technique is the process of printing cells, biocompatible materials, and supporting elements into intricate 3D living tissues with the required structure, functionality, and architecture topologies. Among their benefits are their custom-made architectures, which enable high throughput production and co-culturing [3]. While they can work with rigid hydrogels to create 3D microstructures, using soft materials presents certain difficulties. Because low stiffness hydrogels cannot hold their proper shape after extrusion, it is difficult to create invaginations using this method [36]. Most of the bioprinters used for this technique are quite expensive, making it a costly methodology compared to the previous ones [58]. Due to a need of a certain level of expertise for the successful implementation of 3D bioprinting, this technique might be considered not as simple as the other two.

Table 1. Photolithography, replica moulding and 3D bioprinting compared as potential microfabrication processes of this project
- Green → advantage; Red → drawback
- Plus sign → presence; Negative sign → lack

Properties	Photolithography	Replica moulding	3D bioprinting
Ability to produce 3D microstructures	+++	+++	+++
Ability to produce both evaginations and invaginations	-	+++	+++
Ability to work in soft materials	-	+++	-
Control over feature geometry	+++	+	+++
Velocity of production	+++	-	+
Moulds	-	+	-
Inexpensiveness	+	+++	-
Simplicity	+++	+++	-
Repeatability	+++	+++	+++
Multiple replicas of a single template	-	+++	+

In Table 1, a summary of the advantages and disadvantages of the three fabrication techniques can be seen. To further investigate the optimal procedure to be used in this project, a comparison of various materials was also computed in the next section.

4.1.2. Comparison of materials

Choosing a suitable material is critical to obtain efficient scaffolds, since it affects its performance, monitoring, and the results of the experiments. In general, there are some requirements that must be considered when choosing the scaffold's material. These requirements are:

- Optical transparency, to be able to be inspected using a microscope.
- Tuneable stiffness, to mimic and replicate, to the greatest extent feasible, the mechanical characteristics of *in vivo* tissues.
- Low cost.
- Easy to use.
- Appropriate swelling and stability properties.
- Fairly resistant to deformation and damage.
- Flexibility and elasticity.
- Water permeability.
- Biomimetic properties.
- Non-toxicity to cells (biocompatible), to be capable of conducting future cellular studies on it, to further evaluate its functionality.

The three materials that have being considered are **poly(dimethylsiloxane) (PDMS),** as it is the most used material for 3D cell culture studies nowadays; and **poly(ethyl glycol) (PEG)** and **polyacrylamide (PA),** to further compare the fabrication techniques mentioned above.

Poly(dimethylsiloxane) (PDMS) is an elastomer with excellent optical, electrical and mechanical properties, which makes it well-suited for several engineering applications. Moreover, due to the biocompatibility and inexpensiveness of this soft polymeric material, it is widely used for biomedical purposes [59]. They are extremely versatile and have been applied for the culture of different cell types. Nonetheless, it is not permeable to aqueous solutions, which can lead to local medium heterogeneities and accumulation of cells or residues. Finally, and decisive for the aim of this project, PDMS has poorly tuneable mechanical properties, with supraphysiological high stiffness with elastic modulus values of around 1 MPa [60].

Poly(ethylene glycol)-based hydrogels (PEG) are water-soluble, non-ionic polymeric molecules that are used for various bioengineering applications. Owing to their biocompatibility and facile modifiability, PEG hydrogels have shown great promise in biomedical studies [61]. This PEG derivates can be used to produce 3D microstructures with complex morphologies on them using photolithography, by properly tuning its composition and fabrication parameters. This tuning of the composition by varying molecular weight, allows changes in the stiffness of the hydrogel. This material allows cell adhesion using peptides from the ECM [62]. However, the inflation capacities of PEG-based materials greatly distort the topographical patterns wanted [63].

Finally, **polyacrylamide (PA)** hydrogels offer multiple advantages for developing devices in biological studies. These biocompatible and well-characterized hydrogels have been instrumental in studies that aimed to explore the influence of substrate stiffness on cell morphology [64, 65]. Compared to other gels, it exhibits a greater mechanical strength, enabling an easier handling. Different PA building blocks are commercially available, inexpensive and enable control over the chemical and physical properties of these hydrogels [66]. The physical properties of PA (including its stiffness, porosity and shear modulus) can be controlled and tuned across a wide range, by changing the proportions of its components during synthesis. By adjusting the ratio of acrylamide and bis-acrylamide solutions, the elastic modulus of the hydrogels can be simply modified. Furthermore, these gels can be functionalized with proteins to mimic the composition of the native ECM and enhance their bioactivity [67].

Table 2. PDMS, PEG and PA comparison for microfabrication processes
- Green → advantage; Red → drawback
- Plus sign → presence of the property; Negative sign → lack of the property

Properties	PDMS	PEG	PA
Optical transparency	+++	+++	+++
Tuneable stiffness	+	+++	+++
Inexpensiveness	+++	+	+++
Easy to use	+++	+	+
Swelling and stability	-	+++	+++

Resistance to deformation and damage	+++	-	-
Flexibility and elasticity	+++	+++	+
Water permeability	-	+++	+++
Biomimetic properties	+	+++	+++
Biocompatibility	+++	+	+++

4.1.3. Chosen option

The most profitable and simple option would surely be the first, but, in practice, the large inflation capacities of PEG-based materials greatly distort the topographical patterns wanted after swelling. This prevents the correct development of the microtopography if the elastic modulus is below 250 kPa [57], and as *in vivo* soft tissues usually have an elastic modulus of less than 40 kPa, this would limit the fabrication technique procedure or the tuneability of the scaffolds for the study. Moreover, this technique nowadays only allows the correct formation of evaginations and not invaginations, which are the main issue of this project. On the other hand, the 3D bioprinting technique also presents difficulty when microfabricating in soft materials, which leads us to the use of the **replica-moulding technique** in the end.

Regarding the materials, after seeing that PDMS is the material that presents most disadvantages with respect to the other two, it was concluded that **polyacrylamide** (**PA) hydrogels** were the better option for the project proposals. As it has been mentioned, their stiffness can be easily modified throughout a large range of values depending on their composition, and, as soft tissues present low elastic moduli, it is the optimal option.

4.1.4. Replica-moulding process

This section aims to explain the different procedures implemented to develop the microcavities by replica moulding, the issues that each one presented and the final decisions of the specific protocols. Then, in section 5, further details about the procedures will be shown.

Figure 15 shows the workflow of the replica moulding process: firstly, the SU-8 master is obtained by photolithography; then, PDMS is poured on top of it to obtain the master's contra-replica (referred to as PDMS1 moulds); next, another contra-replica is obtained from the PDMS1 moulds (referred to as PDMS2 moulds); and finally, the thin PDMS2 layer will be used for the fabrication of the final PA moulds with microcavities.

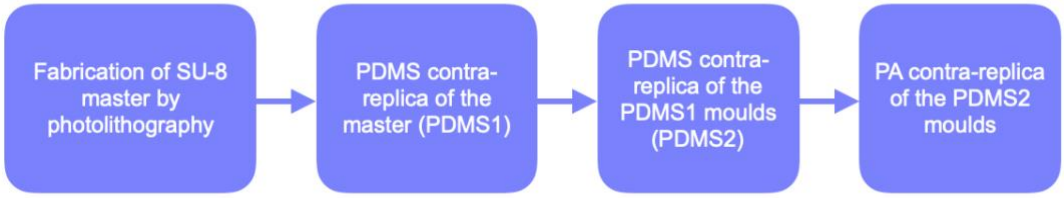

Figure 15. General workflow of the replica-moulding process

4.1.4.1. Geometry and dimensions of the master

For the replica moulding process to begin, a master with hills of diameter and height of sizes similar to the ones found *in vivo* was used. This master had already been prepared for its use in other experiments conducted in the laboratory of the group. It was obtained in the Micro Fabrication unit of IBEC, by photolithography.

This master was made of SU-8. This material is an epoxy-based, negative-tone photoresist consisting of EPON SU-8 resin, solvent and a photoacid generator. Using photolithography, it is able to generate well-defined features ranging from sub-micrometres to micrometres, which have rendered this material as one of the ideal photoresists in microfluidic applications, such as master moulds for poly(dimethylsiloxane) (PDMS) [68]. The posterior silanization of the mask finally allowed the pouring of PDMS on the mould without the material adhering to it.

The master had 56 regions with posts of different sizes of diameter in each of them, as it can be seen in Figure 16. This large number of regions allowed us to create multiple PDMS moulds without having to re-pour PDMS on top of the mask.

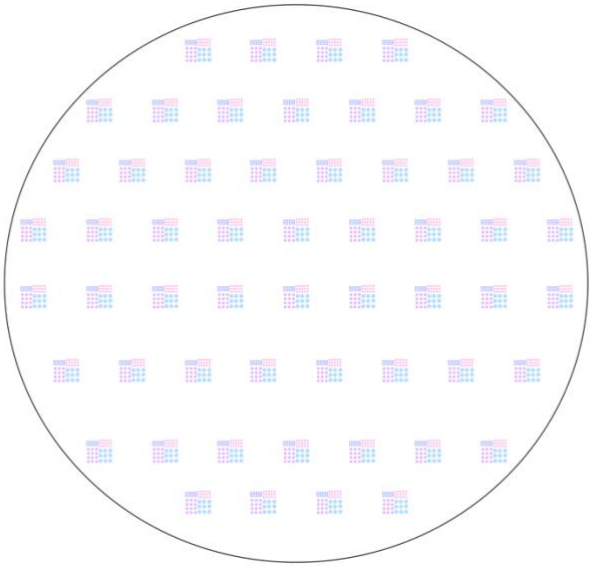

Figure 16. Scheme of the master

Each region, which can be seen more clearly in the scheme of Figure 17, had 21 small posts with a diameter of 100 µm, 15 medium-small posts with a diameter of 200 µm, 12 medium-big posts with a diameter of 300 µm, and 9 big posts with a diameter of 400 µm, organized as it can be seen

on Figure 17, disposed in rectangular shapes inside the square region. All of these posts had a height of around 50 µm. These circular patterns allow to cover the main range of curved geometries found in anatomical structures, such as intestinal crypts, lung alveoli and kidney invaginations.

Having more than one cavity of each size allows us to evaluate different wells of the same size, and also makes it more probable to have at least one well-formed microstructure for each size in every fabrication process.

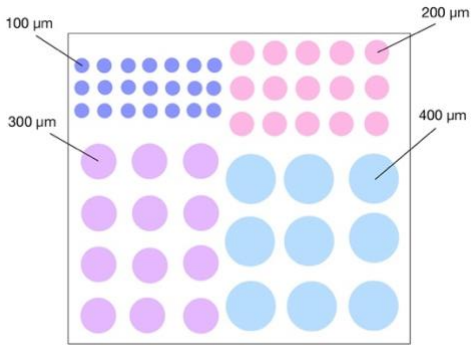

Figure 17. Scheme of a single region of the master

In order to have a softer material with the design of the SU-8 master, it is necessary to first transfer its design into PDMS. This will involve a process of replica and contra-replica with PDMS, explained below.

4.1.4.2. Fabrication of the PDMS moulds

First, we need to obtain the negative mould of the initial structures (therefore, with cavities). To do so, the PDMS mixture is prepared, and then poured on top of the master. Prior to this, Cellotape should be placed around the mask before the pouring, to stick it to the plate, and to make sure that PDMS does not go underneath it, tilting the whole structure. This PDMS is then cured in the oven over night (O/N) at 60 ºC. After this PDMS thick layer is cured, the fabrication of the moulds can begin. The first step of the fabrication is to prepare the primary moulds (PDMS1). To do so, the square structures transferred into the PDMS have to be cut apart from the SU-8 master, making sure not to damage the master with the force made with the scalpel. Then, these PDMS1 moulds will be bonded to a glass microscope slide to ease the subsequent fabrication steps. The back side of the PDMS1 and the microscope glass slide are exposed to O_2 plasma (30 seconds at high power), to create -OH groups in both surfaces which will covalently bind.

Secondly, the surface of the PDMS1 mould must be modified through silanization in order to prevent adhesion. To do so, a O_2 plasma treatment has to be done again on the structures similar to the one performed for the PDMS-glass bonding. Once activated, the silanization process must be completed before the 15 minutes of activation pass. This process consists of the vapor deposition of a self-assembled monolayer of Teflon (Trichloro(1H,1H,2H,2H-perfluoroctyl)silane) on top of the structures. This is done by creating an atmosphere of silane inside a desiccator, which then self-assembles on the sample. The sample is placed in a vacuum desiccator with a drop of the silane (100 µl) next to it. Once vacuum is applied and the atmosphere of silane is created, it is

left for 2 hours in order to allow the formation of the monolayer. Finally, the silanized PDMS1 mould is placed in the oven at 65 ºC or 80 ºC for 2 more hours. As a result, the PDMS1 mould is obtained.

Next, we needed to fabricate a secondary mould (PDMS2) replica of the PDMS1 mould. This mould, which will have posts as the ones of the master SU-8 mould, must be thin, to prevent the inhibition of the hydrogel cross-linking. PDMS can act as an oxygen source, which inhibits the cross-linking of the PA gel. To avoid that, PDMS2 moulds should be 50-100 µm thick. To obtain this secondary thin mould (PDMS2) we spin coated PDMS on top of the silanized structures. To acquire this thickness, a process of 5 seconds at 500 RPM followed by one of 60 seconds at 1000 RPM was used. After this coating, to remove the possible small air bubbles that could have formed inside the cavities, the samples were places in the desiccator for 20 minutes. In the end, the PDMS2 counter moulds were placed in the oven at 65 or 80 ºC O/N for it to cure. A general schematic depicting this whole process can be observed in Figure 18.

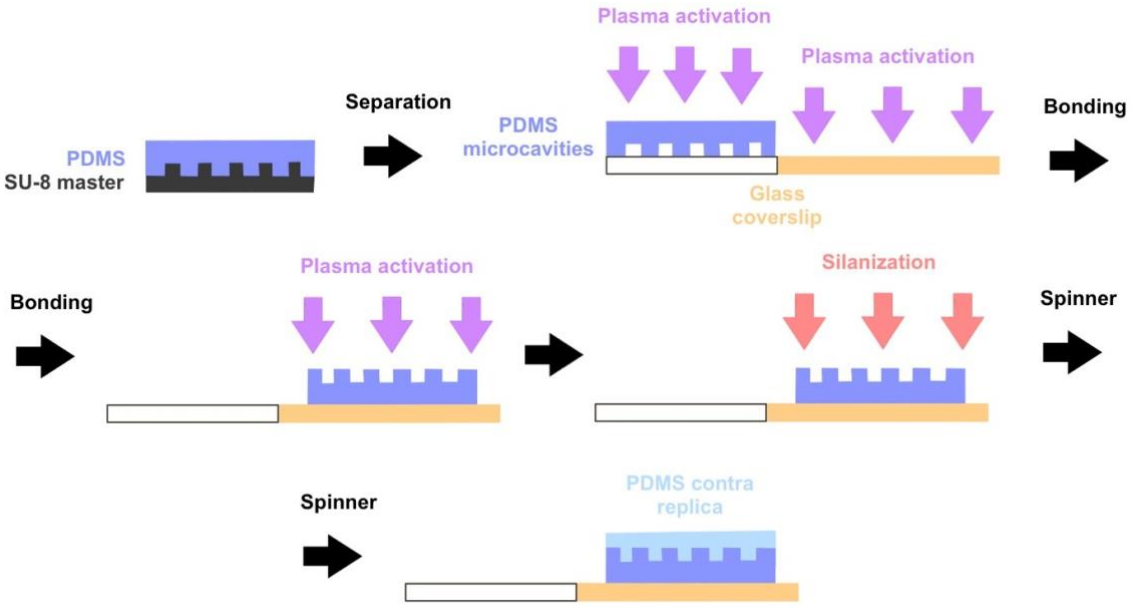

Figure 18. Scheme of the PDMS thin mould acquisition

4.1.4.3. Fabrication of the final PA scaffolds

With the PDMS2 contra replicas, we could proceed with the fabrication of the final polyacrylamide scaffolds. Before the stamping of the structures into the PA hydrogel, we had to choose the rigidities that we wanted to explore. As we want to investigate the behaviour of scaffolds with stiffnesses of biological relevance, similar to the ones found in soft tissues, we chose values from 2.5 to 160 kPa [69]. Four different PA solutions (PA1, PA2, PA3, PA4) were synthesized by varying the concentration of acrylamide and bis-acrylamide of each mixture. These proportions can be seen in Table 3. The PA solutions only had to be produced once, as they can be preserved in the fridge at 4 ºC for long periods of time.

Table 3. Polyacrylamide hydrogels composition for each stiffness

PA solution	PA stiffness (kPa)	Acrylamide (%)	Bisacrylamide (%)
PA1	7	7.5	0.05
PA2	11	7.5	0.075
PA3	23	12	0.150
PA4	172	12	0.600

In this step, the glass in which we later fabricated the PA scaffolds had to be silanized, to ensure the stable attachment of the formed hydrogels. To do so, these coverslips were incubated for 5 minutes with a mixture of 1:1 3-(aminopropyl)trimethoxsylane in Milli-Q water, followed by an incubation with Mili-Q water for 30 minutes on an orbital shaker. Next, the glasses were rinsed thoroughly with Mili-Q water, and then incubated with a solution of 1:50 glutaraldehyde with Mili-Q for another 30 minutes. Finally, the coverslips were rinsed several times with Mili-Q water again, dried with nitrogen gas (N_2), and placed in the vacuum desiccator until they had to be used.

Two thin layers of PDMS (one on top of the other) with a round space in the middle had to be placed on top of the silanized glass, as spacers to contain the PA solutions in it when poured. To obtain them, PDMS was poured on the lid of a large plate and then spined in the spin coater at 500 RPM for 1 minute. Then, we let it cure in the oven O/N at 80ºC. This step was only done once, as the piece of this PDMS layer used in every fabrication process was very little. With this thin layer cured, small squares were cut, a layer was put on top of the other one, making sure that no bubbles formed between them, and with a circular puncher (10 mm in diameter), these round spaces were created and placed on the silanized glasses.

The PDMS2 moulds had to be separated from the PDMS1 moulds to be use as moulds for the PA scaffolds. To do so, a scalpel was used to cut around the structures, and the moulds were placed with the structures facing upwards on a non-silanized small round glass. This process was very dependent on the proper silanization of the PDMS1 moulds, otherwise the two PDMS parts could not be detached.

To produce PA microsctructured hydrogels, the PA solutions were mixed with a solution containing 0.05% (w/v) ammonium persulfate, 0.001% (v/v) of fluorescent beads, and 1% (v/v) tetramethylethylenediamine (TEMED). After this mixture, the next steps had to be completed quickly, as the PA started to polymerize. 75 µl of the prepolymer solutions were poured into the dedicated pools containing the silanized glass coverslips. Immediately after, the PDMS2 mould on the glass was placed on top, to let the microstructures be filled in by capillary force. The hydrogels were then kept at room temperature (RT) for 2 hours to polymerize, covered by a box, to prevent light from damaging the fluorescent beads.

Finally, the polymerized scaffolds were demoulded by carefully removing the flexible PDMS moulds with the help of the small round glasses, and the PDMS circular pool was also removed. The PA microstructures were stored in PBS in the fridge at 4ºC until further use, allowing them to achieve equilibrium swelling. A schematic of this part of the process can be seen in Figure 19.

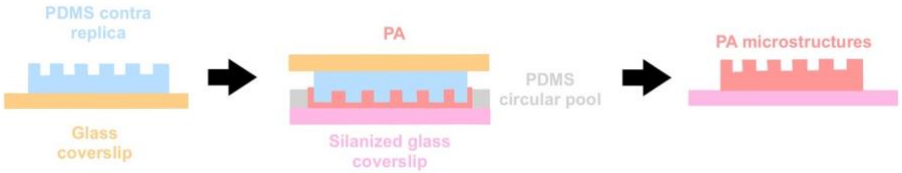

Figure 19. Scheme of the PA polymerization with thin PDMS moulds

4.2. Functionalization of the sample

As the main goal of this scaffold is to then seed cells on top of it, cell adhesion cues have to be provided to the polyacrylamide hydrogels. These cues were implemented by using sulfosuccinimidyl-6-(4'-azido-2'-nitrophenylamino)hexanoate (sulfo-SANPAH), and then by adding the protein of interest.

Sulfo-SANPAH is a reactive that links proteins onto polyacrylamide hydrogels. As a bi-functional crosslinker, sulfo-SANPAH adheres to the PA surface by its photoactivable side and then it contains an NHS ester group for linking with the primary amine groups on proteins [70].

To be able to then check the success of the functionalization in the confocal microscope without having to perform the immunostaining process, we used Streptavidin conjugated with TexasRed fluorophore. It is a protein that is commonly used in the setting up of a fabrication process, and it emits a red fluorescent light. Another protein that could have been used was fibronectin. However, it does not have fluorescent characteristics, so immunostaining would have to be performed. In the end we used the first mentioned protein, Streptavidin, as probe to check the success of the functionalization process.

40 µl of Sulfo-SANPAH were defrosted with 960 µl of Mili-Q, the PBS was removed from the PA scaffolds, Mili-Q was used to rinse the structures carefully, and then 50 µl of the reactive were poured into each hydrogel. Afterwards, we activated it under the UV lamp (Light Source LQ-HXP 120 UV, LEJ) for 5 minutes. After it had turned from pinkish to brownish, we rinsed again with PBS. Then, for the functionalization with the protein, we added 50 µl of 100 µg/mL Streptavidin solution. We left it 1 hour to incubate, and then we rinsed the surface again with PBS, and added 2.5 mL of this buffer on each hydrogel. Finally, it was stored at 4ºC in the fridge. This process can be seen in Figure 20.

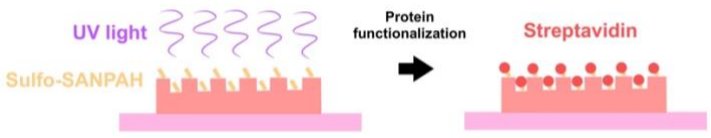

Figure 20. Schematic depicting the Sulfo-SANPAH activation and the protein functionalization

4.3. Characterization of the shapes of the cavities

We aimed at assessing the faithful transfer of the structures along the different steps of the fabrication process, and to rule out the effect of the hydrogel formulation in the preservation of the

shapes. For this characterization, 5 different pieces of equipment where used: the optical microscope, the profilometer, the interferometer, the confocal microscope and the optical epifluorescence microscope. All the information regarding these devices was extracted from the MicroFabSpace services website of IBEC, with reference number [71].

After obtaining the images provided by each of these instruments, they were analysed using the 'FijiJ' software. The results of these analysis are shown in section 5 of this report.

4.3.1. Optical microscope

For the observation of the structures in each step, the optical microscope (Nikon ECLIPSE Ts2) found in the laboratory of the group was used. This conventional optical microscope is made up of two converging lenses (eyepiece and objective), which are arranged in such a way that they generate a highly amplified and virtual image. It was used for the observation of the PDMS cavities and hills, and mainly for the measurement of the diameters of the microwells found on the PA scaffold.

4.3.2. Profilometer

The mechanical profilometer Dektak XT is an instrument used to measure the profile of a surface. It allows the topography of a material to be measured electromechanically, by moving the sample under a diamond tip with a specific contact force, depending on the material being measured. After each acquisition, the surface is analysed with the help of the 'Vision64' software. This equipment allowed to check that both PDMS1 and PDMS2 moulds were well created, each with its corresponding posts or cavities, as well as the characterization of their surface.

4.3.3. Interferometer

The optical profilometer Wyko NT1100 provided us with high resolution 2D or 3D measurements without contact with the sample. It does this by extracting information from light interference. By fusing two or more light sources, this tool creates an interference pattern, which can be measured and analysed, with the help of the 'Vision32' software. This pattern was also used to characterize the surface of the PDMS1 and PDMS2 samples, and to check that they were well created as well.

4.3.4. Confocal microscope

The LSM 800 confocal laser scanning microscope is an instrument equipped with different laser colours that has multiple applications in biology, medicine and the study of materials. It allows images to be obtained from a single confocal plane. The principle on which it is based is to eliminate light coming from out-of-focus planes. It works with samples that reflect light or emit fluorescence, and the images are obtained and analysed with an image software called 'ZEN 2.3'. It also allows for the collection of multiple focal planes in what is called a 'Z-Stack', which provides three-dimensional data of the structures.

With this tool, the shape of the PA hydrogels was examined (with the help of the fluorescent beads that were added during the synthesis of the solution), as well as the functionalization with the fluorescent streptavidin. The diameter and area of both the base and the top of the structures was measured, as well as its depth. These measurements were done after 2 hours, 24 hours, 48 hours and 72 hours of fabrication, to see how they developed and swelled for each stiffness.

4.3.5. Optical epifluorescence microscope

The Leica DiM8 microscope is an inverted light microscope, intended as a general instrument for routine examinations of biological specimens [72]. It was used with phase contrast and fluorescence illumination to measure the sizes and heights of the cavities in the functionalized PA hydrogel using Z-Stack. As it does not give images that are as good as the ones provided by the confocal microscope, it was mainly used to have more quantity of measurements, to be able to perform a more throughput examination of the scaffolds.

4.4. Characterization of the mechanical properties of the samples

Finally, to characterize the mechanical properties of the samples, Atomic Force Microscopy (AFM) was used. It is a tool to probe samples at the nanometric scale. Among its numerous capabilities, the instrument can be operated as a nano-indenter to gather information about the mechanical properties of the sample. In this operating mode, the deformation of the cantilever is displayed as a function of the indentation depth of the tip into the sample. Fitting this curve with different theoretical models permits us to estimate the Young's modulus of the scaffold at the indentation spot [73].

AFM measurements were performed both before and after the functionalization with the protein, to assess the stiffness of the different PA hydrogels. Moreover, it was used to see if this stiffness varied within samples that were produced from the same prepolymer solution, but some were functionalized, and the other were not.

5. Detailed engineering

In order to carry out the project and actually put the theory into practice, a series of steps had to be taken. In this section, each step of these processes will be explained further, giving more details about the techniques and protocols that were followed during the development of the microcavities. Moreover, the calculations done for the characterization of the micro-structures will also be described here, with the corresponding results and discussions.

As it has been repeated throughout this manuscript, 2D cell cultures ignore the three-dimensional shapes that are found *in vivo*, overseeing its impact in tissue function. Although novel 3D culture platforms are already being implemented into recent studies, they still do not always match the mechanical properties of the native tissues. The *in vitro* model designed in this project aims to simulate the properties, structure and functions of the *in vivo* cavities, which are structures that can be found in numerous tissues.

As we already had a mask with the cavities of dimensions similar to the ones found *in vivo*, the first step of the process was to replicate this design into a PDMS sheet. This flexible PDMS moulds, which had cavities in them, were used to create thinner PDMS secondary moulds, using the spin coater. These secondary PDMS moulds with posts were then used to replicate the cavities into softer PA hydrogels. The solutions of PA used were of different stiffnesses, resembling those within the range of the mechanical properties found *in vivo*.

Once the PA samples simulating the 3D cavities were produced, they were characterized, to evaluate their similarity with the *in vivo* tissue. Confocal microscopy was the main characterization technique used to evaluate these structures, as they had fluorescent beads in them. They were also measured using wide-field optical microscopy, both with bright and fluorescent lights. Then, the mechanical properties of this models were assessed using AFM.

Finally, to see how proteins behaved on top of these structures, a functionalization with Streptavidin was performed. This functionalization gives a clue about how the epithelial cells would adhere to the cavities. The success of this step was also addressed by confocal microscopy, and the stiffness of the chemically activated scaffolds was measured again with AFM.

Therefore, these three processes mentioned above:

1. The fabrication of the cavities on PDMS,
2. The fabrication of the cavities on PA,
3. And the functionalization of the cavities,

Will allow the full development of the hydrogel cavities of tuneable stiffness for the growth of epithelial crypts. The evaluations and assays performed to evaluate the goodness of the model will be discussed in the following section.

5.1. Fabrication of cavities on thin PDMS (replica-moulding)

5.1.1. First PDMS mould (PDMS1)

In order to have a softer material with the design of the SU-8 mould, it is necessary to first transfer the design of the mould into a PDMS structure, leaving us with the counter mould of the initial structures: first, we prepare the PDMS mixture, and then we pour it on top of the master. This structure (Figure 21) is then cured in the oven for 12 h at 65 ºC.

The preparation of PDMS is done at a 10:1 ratio of PDMS precursor (SYLGARD™ 184 Silicone Elastomer Base) and crosslinker (SYLGARD™ 184 Silicone Elastomer Curing Agent), mixed with a Pasteur pipette trying not to create bubbles of air. The role of the curing agent is to crosslink the polymer to obtain an elastomer. Right after mixing pre-polymer and crosslinker, to eliminate the bubbles completely, the uncured PDMS was left degassing for 45 minutes to an hour. Finally, the solution was then poured on the master, covering all the surface.

Once the PDMS has cured, the design engraved on the mould will have been successfully transferred into the PDMS structure, and we will have obtained the first mould for the creation of the final PA moulds.

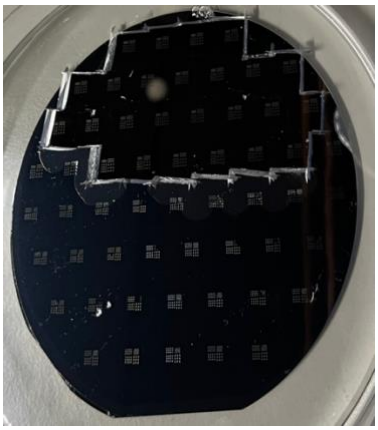

Figure 21. SU-8 master with PDMS on top

5.1.1.1. Plasma cleaner: Covalent bonding of PDMS1 with glass coverslip

The following step is to adhere covalently the PDMS structures with glass coverslips, leaving the structures looking upwards, and then creating a monolayer of silane on top of the microcavities. This whole step is performed in the MicroFabSpace, with the use of the Plasma Cleaner by the manufacturer Harrick, model PCD-002-CE. This equipment generates an O_2 plasma at low pressures and high frequency voltages for processes as plasma bonding of PDMS with glass or PDMS with PDMS, removal of organic contamination from surfaces, or modification/enhancement of physical and/or chemical characteristics of surfaces, required in further processes.

Firstly, the previously prepared PDMS square structures were cut using a scalpel. It is very important to not perform too much force, as it could then damage the SU-8 master bellow the

PDMS. Afterwards, these squares were placed upside down on top of top of the white region of the glass coverslips. These glasses were then set inside the Plasma chamber, after carefully cleaning it with a wipe. The chamber was closed, and the instructions of the protocol found in Annex 1 were followed.

To take out the samples, the door of the chamber had to be slowly opened, regaining little by little the pressure from the environment. Finally, the PDMS structures were placed upright on the glass, to create the covalent bonds between them.

5.1.1.2. Plasma cleaner: Silanization

The silanization of a surface's main goal is to obtain hydrophobic silanized surfaces, that allowed the non-union of the secondary PDMS, that was to be placed on top of them. This silanization process consists of two stages: first the surface cleaning, and then the surface functionalization. These two steps have to be performed with less than 15 minutes of separation for the surface cleaning to be still active for the silanization process.

The objective of the cleaning state is to eliminate organic and inorganic residues and expose the hydroxyl groups of the molecular structure of the PDMS at the surface, obtaining an activated surface that subsequently allows the silanization reaction. This first step was performed at the Plasma cleaner, following the same protocol as before (Annex 1).

Once the residue-free surfaces are obtained, the surface was functionalized with Teflon. This silanization needed for the easy separation of the structures is achieved by vapor-phase deposition of the silane. The process consists of placing a coverslip (round glass) with a Teflon solution (Trichloro(1H,1H,2H,2H-perfluoroctyl)silane) of around 200 µL on top, putting it with the samples inside the desiccator, closing the equipment, and making vacuum inside of it. Thus, an atmosphere of silane is created, and then it is distributed evenly throughout the sample, binding to the exposed hydroxyl groups and reaching functionalization. This was left on vacuum for 2 hours, and then in the oven at 65 or 80 ºC for 2 more hours, to order the self-assembled silane monolayer.

5.1.2. Second PDMS moulds (PDMS2)

As explained in the previous section, for the patterning of the final PA moulds, thin PDMS moulds with the counter mould (posts) of the final desired structures (cavities) are needed. This samples need to be thin in order to minimize the source of oxygen from the PDMS as much as possible. To achieve this slim layer, the spin coater is used. This equipment allows the spreading of the substrate to the edges of the sample by centrifugal force, spinning at a high speed and leaving a thin film. A coating of PDMS (previously fabricated and desiccated totally for the removal of air bubbles, following the same process as before) is placed on top of the first PDMS silanized mould, making sure to cover all the structures, and the following protocol is followed:

Table 4. Protocol followed for the fabrication of the second PDMS moulds

Steps	Time (seconds)	Rotational speed (RPM)	Centripetal Acceleration (RPM/sec)
1	5	500	112
2	60	1000	336

These parameters allowed us to acquire the desired thickness (50 – 100 µm). Then, to remove the possible bubbles that could have formed between these two moulds, the samples were placed in the desiccator for around 20 minutes, and finally in the oven O/N at 85 ºC. In some fabrication processes, the second mould of PDMS was left to cure at ambient temperature in the desiccator, but it was seen that the thin moulds were much less resistant and broke more easily. Therefore, after this was noted, this PDMS2 was left to cure in the oven after staying in the desiccator for 20 minutes. Finally, the secondary mould was demoulded using a scalpel and tweezers, and placed on top of a small round glass coverslip with the design looking up, ready to be used for PA patterning.

It should be mentioned that two different spin coaters were used for the completion of this project, as the first one broke and it had to be replaced. For this second spinner, the parameters of the protocol used for the fabrication of the secondary moulds were the same, but this equipment did not have the option to modify the centripetal acceleration. Nevertheless, it was seen that this did not affect the fabrication process.

Figure 22. PDMS1 on top of glass coverslip with spin coated PDMS on top

5.1.3. Comparison cavities - posts 1st and 2nd moulds

Some of the PDMS2 thin layers were placed in 22x22 cover glasses, as it can be seen in Figure 23. The number at the top-left corner of both this small glass coverslips (seen in Figure 23) and on the big ones carrying the PDMS1 mould (seen in Figure 22) was written to know the correspondence of PDMS1 with PDMS2.

After this was done, both moulds were transported to the MicroFab Unit (CleanRoom) of IBEC, and their dimensionalities were measured with the profilometer and the interferometer. These

measurements were done to be able to compare and evaluate the transmission of the structures from one mould to the other.

Figure 23. PDMS2 on top of 22x22 cover glass

5.1.3.1. Profilometer

For the measurements with the profilometer, the stylus tip was placed next to the structure that we wanted to analyse. This was done with the camera next to the stylus tip, whose magnified image appeared on the screen through the Vision64 software, and with the help of the X-Y macro-positioning levers, that moved the stage where the glass coverslips with the hydrogels were placed. Afterwards, a series of measurement parameters were set, determining the trace of the stylus, which can be seen in Annex 2.

Then, with the set up completed, the stylus was brought down ('Tower Down'), while the exact desired position was achieved by moving the X-Y micro-positioning knobs and looking at the images from the camera. Next, the acquisition of data was done ('Single Acquisition') with the insulating box closed, resulting in a mm (x-axis movement of the stylus) vs µm (y-axis movement of the stylus) graph. If the obtained profile was tilted, this was corrected by choosing two points that we knew needed to be at the same height, and clicking on the 'Level – Two Point Lineal' option from the 'Data Analysis' menu.

Moreover, if the profile had a rough pattern, this roughness could be filtered out with the option 'Filtered roughness'. In the end, the files were saved using a Cleanroom's pen drive, and the stylus was rose to its initial position ('Tower Home').

It must be mentioned that, as the stylus came into contact with the sample, if it did not weight much, the force made by the tip could drag the sample with it. This did not happen with the PDMS1 moulds, as the coverslip that they were placed in weighted enough, but it did happen with the PDMS2 moulds. To solve this, the sample was stuck to the stage using cello-tape around the glass. This helped the sample to stay in place while the stylus scanned it.

It should also be considered that the measurement of posts or cavities with this equipment caused the beginning or end of this structures to be somewhat unclear. In the example of a sample with posts, when the stylus arrived at the start of the structure, it went up, but a small peak could be seen in the measured profile when the stylus reached the top (as it can be seen in Figure 24). Similarly, when a sample with cavities was measured, this small peak appeared but after the stylus had scanned the base of the cavity, in the final moment of moving back to the initial plane (seen in

Figure 25). These peaks were due to the stylus adapting to the shape of the sample, as it passed from going up the post to scanning its top part, or from going up the wall of the cavity to scanning the plane of the sample. Therefore, when doing the measurements of these types of images, this peak was taken into account as part of the top diameter for posts, and not for cavities.

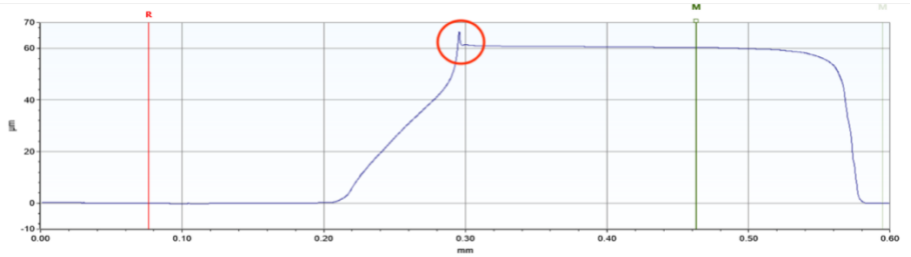

Figure 24. Sample 1 medium-big posts (from the 300 µm master's posts, after PDMS1) profile, with the mentioned small peak circled in red

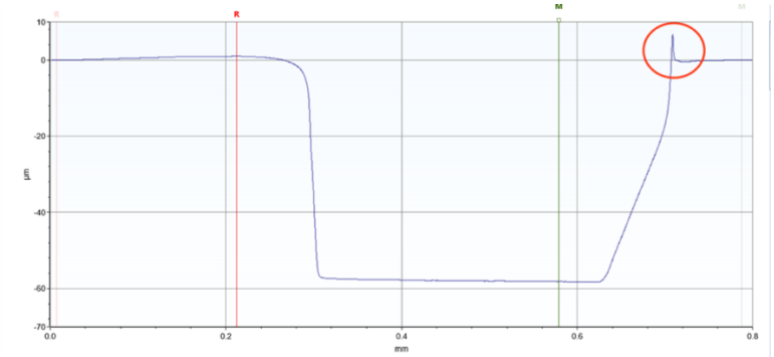

Figure 25. Sample 4 biggest cavities (from the 400 µm master's posts), with the mentioned small peak circled in red

5.1.3.2. Interferometer

Regarding the interferometer measurements, we first placed the sample on the stage, after making sure that it was not tilted using the level, and we opened the Vision32 software. Then we clicked on the 'Illumination Intensity' window and, after finding the sample's structures, they were focused by using the Focus knob, and illuminated by turning the Intensity control knob. By playing with these two parameters, we looked for interferences, finding the maximum intensity of light without saturating the image. Once they were found, we tried to make them as wide as possible using the X and Y tilt knobs.

After this was done, the measurements could be taken. Once we obtained a good measurement similar to the ideal two-coloured measurement (one colour for the bottom of the sample and another one for the top), we could analyse the measures of the structure with the '2D analysis' option. This option allowed us to have a µm (x-axis of the sample) vs. µm (y-axis of the sample) graph with the profile of the structure of interest.

It is important to note that the PDMS is very hard to analyse with this technique, as it does not reflect light. This lack of reflection makes it very hard for us to find interferences, and even when they are found, it is quite difficult for the equipment to detect all the points of the image, creating

some black spots where the point's value was not found, as it can be seen in Figure 27. Nevertheless, when these interferences were found, the final images were quite accurate, leaving us with some clear round shapes of blue or red colour (depending on if the structures where cavities (blue, seen in Figure 26) or posts (red, seen in Figure 27)), and the measurements could be done trouble-free.

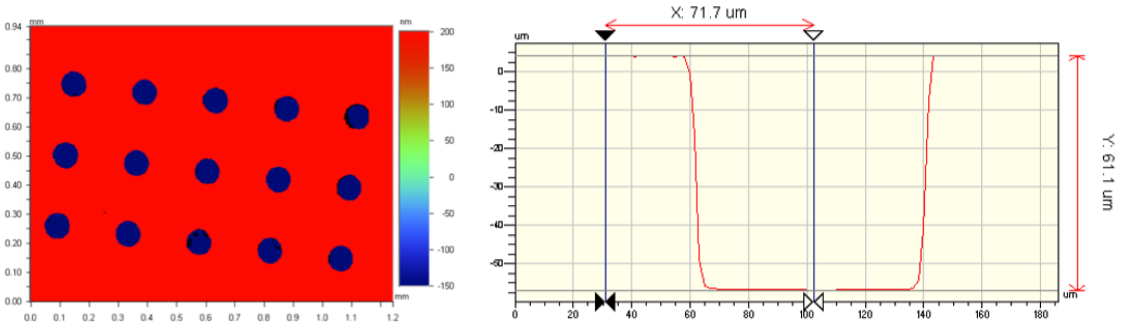

Figure 26. Sample 4 smallest cavities (from the 100 µm master's posts), with the profile of the top-left structure

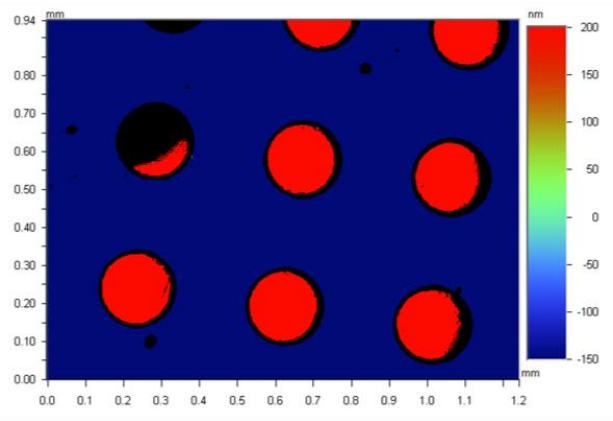

Figure 27. Sample 2 medium-big posts (from the 300 µm master's posts, after PDMS1), with the mentioned black regions of non-detection

5.1.3.3. Comparison PDMS1 – PDMS2

For the comparison of these moulds, the first option was to use the measurements of both the profilometer and the interferometer. The values obtained for every specific size of the sample were averaged between samples, and then compared with the counter-structures of the counter-mould with the same size. After performing these calculations, it was seen that the results made no sense, as the counter-moulds appeared to have bigger dimensions than the initial moulds, which is impossible.

Then, we thought that maybe the parameters obtained from the profilometer did not have the same dimensions as the ones from the interferometer. Therefore, the averages from the profilometer measurements and the ones from the interferometer were done and compared separately, leaving us with reasonable results.

Each graph from both the interferometer and profilometer was analysed similarly using the Fiji software:

1. Firstly, the scaling of the image was set in the software, by using the axis seen in the graphs, with the option 'Set Scale'.
2. Then, as we only wanted to measure lengths of the graph, the measurements were set only to present the perimeter of the drawn line, with the option 'Set Measurement'.
3. Finally, all the recorded measurements were added to an Excel file, where the final calculations were performed.

The structures measured for all the graphs were the diameter of the base, the area of the base, the diameter of the top, the area of the top and the depth. For the areas, as we know that the structures are circular, we calculated it with the circular area formula (Equation 1). We divided the diameters by two to obtain the radius, we raised it to the power of two, and then multiplied this value by π.

$$A = \pi r^2$$

Equation 1. Circular area formula

For the interferometer images, the area could be directly obtained from the coloured picture with Fiji software, by drawing a circle around the structure and adding the area to the measurements set, for it to be shown with the results. However, in this case, it was quicker to use the formula, as we only needed to measure the diameters (top and base) of the structures with the line feature of the software.

The top and base of the posts were considered as the tip and the bottom respectively, whereas the top and the base of the cavities were considered as the bottom and the tip of the structure, as it can be seen in Figures 28 and 29.

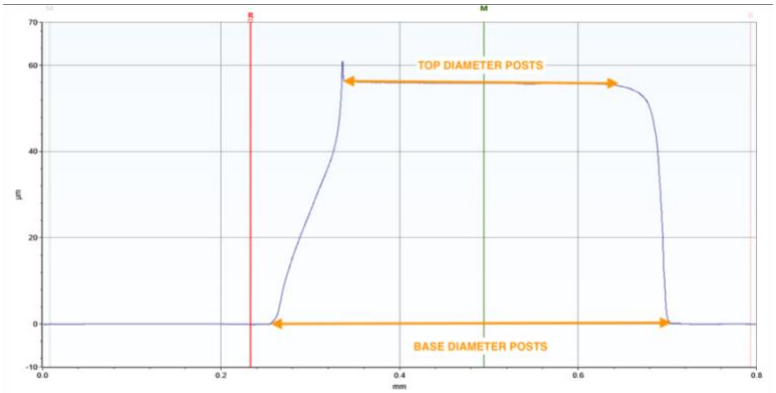

Figure 28. Considered top and base diameters of posts (Sample 2 biggest diameter posts)

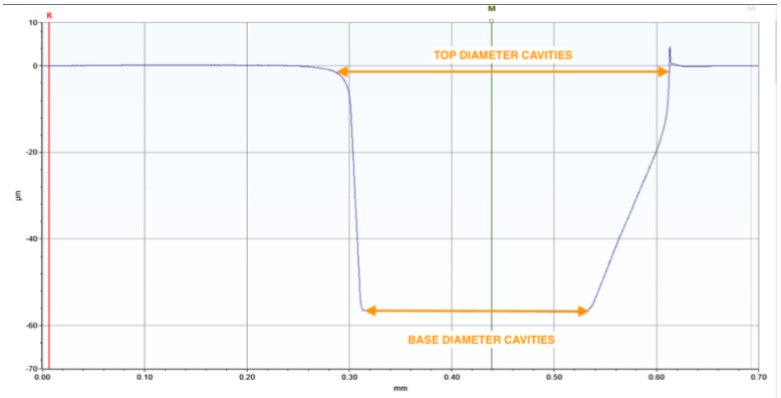

Figure 29. Considered top and base diameters of posts (Sample 1 medium-big diameter cavities)

Therefore, the comparisons that had to be made for each size were:

- The top diameter of the posts with the base diameter of the cavities.
- The base diameter of the posts with the top diameter of the cavities.
- The heights of the structures.

Finally, the percentage of difference between the PDMS1 and PDMS2 was calculated with Equation 2 for all three comparison pairs presented above.

$$\%\ Difference = 100 - \left(\frac{PDMS2\ value * 100}{PDMS1\ value}\right)$$

Equation 2. Percentage of difference between cavity (PDMS1) and post (PDMS2)

Table 5. Percentage of difference (decrease) of top and base diameters (considered as the ones shown in Figure 29), and height between the PDMS1 and PDMS2 moulds by size

Size	% difference height	% difference top diameter	% difference base diameter
Small	7.16	22.45	21.04
Medium-small	11.79	4.65	2.43
Medium-big	3.32	16.66	7.09
Big	0.76	10.26	2.69

Looking at the results obtained in Table 5, it can be confirmed that there is a loss of dimension of the structures from the PDMS1 to the PDMS2 moulds. This loss is more significant for the smallest-sized cavities rather than for the biggest-sized ones. Nevertheless, as this loss means a reduction on the dimensionality of the structures, it could be seen as advantageous for this project's purpose, because we would have smaller posts than the ones from the SU-8 mould, allowing us to fabricate even smaller structures. Knowing that the smallest-sized post of the master was of 100 µm, but also considering that some of the invagination structures found *in vivo* have diameters smaller than this one [74], we could use this apparent loss to our advantage.

5.2. Fabrication of the cavities on PA

5.2.1. Preparation of PA solutions

As it was seen in Table 3 from section 4, the four different PA solutions were obtained with different percentages of acrylamide and bisacrylamide solutions, resulting in stiffnesses of 172, 23, 11 and 7 kPa. As we wanted 5 mL of each solution, the volumes of the two chemicals were calculated first with the corresponding percentages from Table 3, following the formula from Equation 3.

$$V_{11} = \frac{c_{21}V_{21}}{c_{11}}$$

Equation 3. Acquisition of the volumes needed of each chemical

In this equation, c_{21} was the concentration we wanted of the chemical, V_{21} were the 5 mL of volume that we wanted to obtain, and c_{11} was the concentration of the chemical in its original state (40% for acrylamide and 2% for bisacrylamide). Then, 0.5 mL of PBS (x10) were added, and the rest of the mL needed to achieve the 5 mL solution were completed with Mili-Q water.

5.2.2. Silanization of the microwells/coverslips where the PA was to be placed

For the correct observation of the PA moulds with confocal microscopy, they had to be placed into 35 mm petri dishes with a 20 mm microwells in the centre. For the PA to adhere to the petri dish, the microwell surface had to be silanized. This silanization was done with a protocol that employed firstly (3-Aminopropyl) trimethoxysilane 97% (silane) and glutaric dialdehyde 25 wt. % in Mili-Q H_2O (glutardialdehyde solution). Firstly, 400 µl of silane:Mili-Q at 1:1 proportion were added to the microwell and incubated for 5 minutes. Afterwards, the rest of the petri dish's bottom surface was covered with Mili-Q, and it was incubated 30 minutes with shaking at 15 or 20 RPM at RT. It then was rinsed with Mili-Q, the bottom surface was covered again with glutardialdehyde solution:Mili-Q at 1:50 concentration, and incubated again for 30 minutes more. After this time, it was rinsed with Mili-Q and dried with nitrogen gas (N_2). Finally, the petri dishes were stored in the desiccator until the next day, when the PA hydrogels could finally be fabricated.

For the assessment of the stiffnesses of the PA hydrogels, they had to be fabricated on top of 20x20 mm glass coverslips, because the 35 mm dishes did not allow the correct measurements with the AFM equipment. We obtained these coverslips by carefully detaching them from 35 mm glass bottom dishes with 20 mm micro-wells, which can be seen in Figure 30.

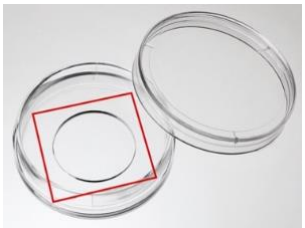

Figure 30. 35 mm glass bottom dish with 20 mm coverslip with micro-well marked in red [75]

5.2.3. Fabrication of the PA moulds

For the final fabrication of the hydrogels, 297 µl of the solution of PA were placed in an Eppendorf tube, and it was degassed for 10-20 minutes. While this was being done, the two thin PDMS layers with a round space in the middle were placed on top of the silanized glasses, to retain the PA mixture in that round region. Then, for the hydrogels to have fluorescence, a 1/1000 proportion of fluorescent beads were poured into the PA solution (0.3 µl), and they were homogeneously dispersed using the Eppendorf Vortex mixer for 2 to 5 seconds. Afterwards, 3 µl of 10 % ammonium persulfate (APS) dissolved in Mili-Q and 0.9 µl of N,N,N',N'-tetramethylethylenediamine (TEMED) were added as initiators of polymerization. Quickly after this addition, 75 µl of the prepolymer mixture were poured into the round PDMS pools, and the PDMS2 thin mould was placed on top with the help of the small round glass at its bottom. The hydrogels were then left to polymerize at RT for 2 to 4 hours, covered all the time with a box, so that the fluorescent beads were not damaged by light. Finally, the top coverslips with the mould were peeled off carefully, the PDMS pool was removed, and the PA hydrogel was covered in PBS and kept in the fridge to swell.

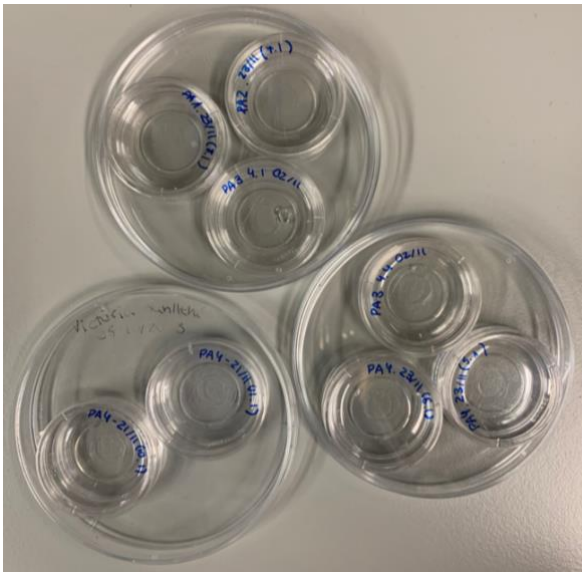

Figure 31. 35 mm petri dishes with PA hydrogels in micro-wells, covered with PBS. The small petri dishes are inside plates for easier transportation

5.3. Swelling measurements

Polymeric materials such as hydrogels have the capacity of absorbing water and holding significant portion of it within their structure without dissolving. One of the most crucial technical aspects of hydrogels is their swelling rate.

To evaluate the behaviour of the hydrogel's swelling throughout the first days of fabrication, the confocal microscope was used to measure the structures 2, 24, 48 and 72 hours after the fabrication process. These images were then analysed to extract the value of the base areas of the structures. Although we chose the same structures for all the hours to evaluate their swelling, the areas measured from one hydrogel to another did not correspond. Therefore, to be able to compare more easily the different behaviour of the hydrogels, the area values were normalized with the Z-

score transformation method. This method measures how many standard deviations above or below the mean a data point is, using Equation 4 [76].

$$z = \frac{data\ point - mean}{st\ dev}$$

Equation 4. Formula used to calculate the z-scores

Figure 32 shows the results obtained. As it can be observed, the softer hydrogels keep on swelling after 24 h of fabrication, while the PA4 and PA3 scaffolds stay essentially steady after an initial swelling. After the 48 h from fabrication, the other two hydrogels also achieve their maximum swelling. Therefore, we could conclude that the maximum swelling of the hydrogels was reached for all of them at day 3 (72 h) from fabrication.

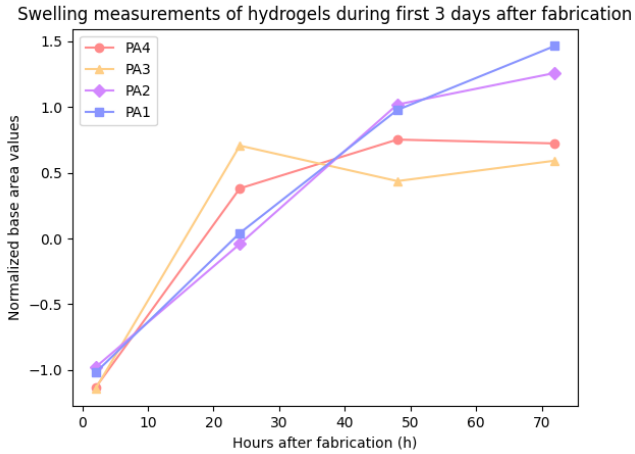

Figure 32. Normalized swelling measurements of hydrogels during the first 3 days after fabrication

5.4. Comparison of cavities of different rigidities after maximum swelling

Knowing that the maximum swelling was obtained after 3 days of fabrication, the measurements of the final cavities were done. All the images from the PA hydrogels after 72 hours of fabrication (obtained with confocal or epifluorescence microscopy) were analysed using the Fiji software. For all of them, an 'Ellipse Fit' was done at the top and at the bottom of the structure, to obtain their areas and their major and minor diameters. An example of this procedure can be seen in Figure 33.

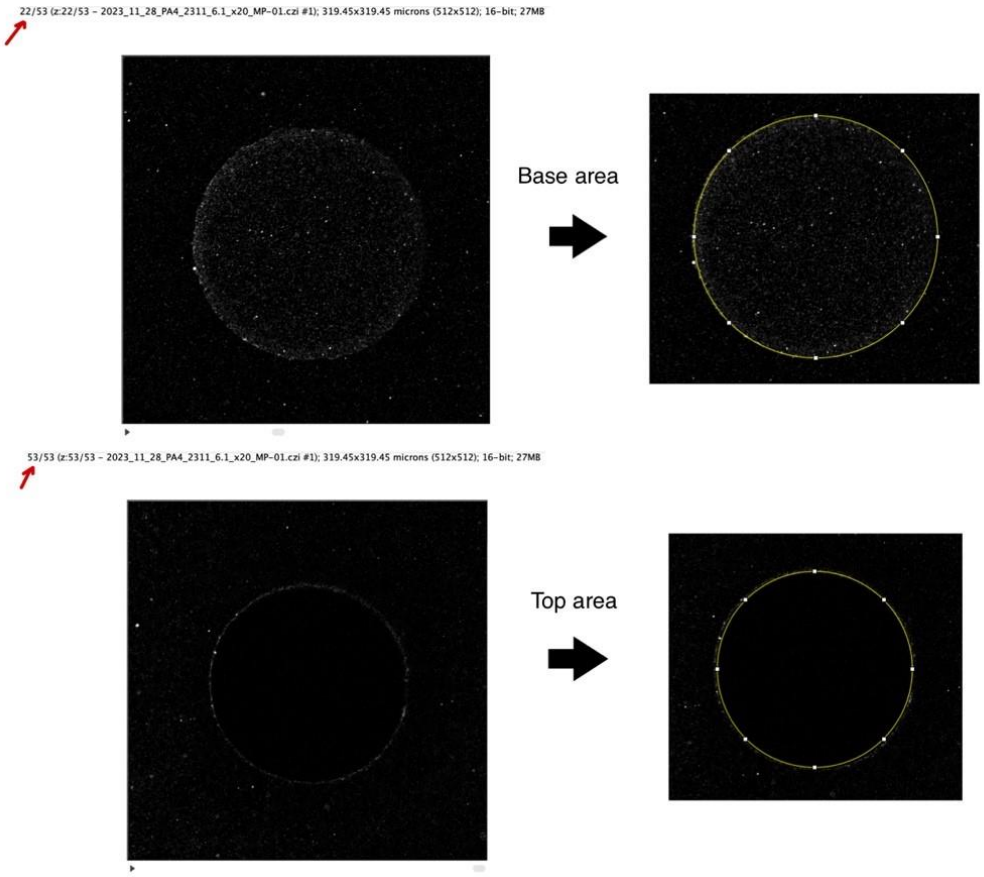

Figure 33. Top and base areas measurements with Fiji software, x20 magnification

As for the depth, we first got the value of the step size of the Z-Stack from the information of the images ('Image > Show Info...'). Then, as we knew which were the top and bottom slices (red arrows in Figure 33), we just had to subtract the numbers corresponding to these slices, and multiply the result by the step size.

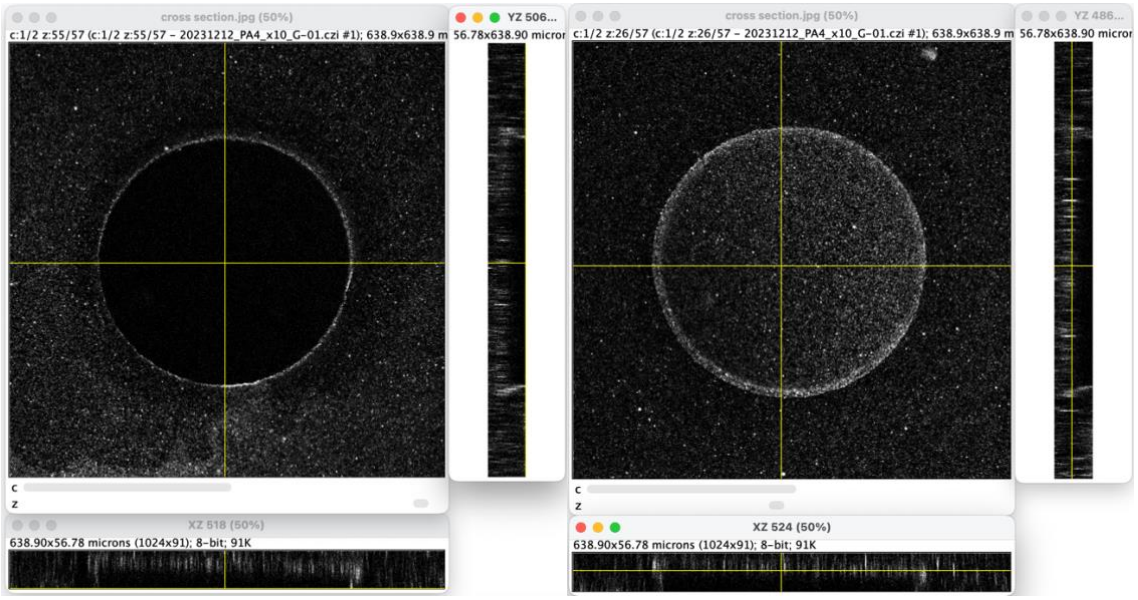

Figure 34. Cross-sections of PA4 big cavities, showing their top (left) and bottom (right)

In Figure 34, the cross-sections of two points of the same cavity are shown. As we can see, at the right side of each image, the YZ cross-section is represented, and at the bottoms, the XZ cross-section. These cross sections show elongated U shapes, corresponding to the cavity structure. It can also be highlighted that in the left image, the top of the cavity is shown, so we do not see the yellow cross at any of the cross sections (it was placed at the upper limit of the Z-Stack). On the other hand, the right side image shows the bottom of the cavity, with the yellow crosses of the cross-sections at the base of the U shape.

After obtaining all the mentioned parameters from all of the images, the average of each one of them was calculated. To examine the base area dimensions, the average of the major and minor diameters was also averaged. Then, the standard deviation of the different variables was calculated, so that we could finally create bar graphs. These kinds of graphs allow us to compare various sets of data among different groups easily, so it was the optimal choice for this comparison of cavities.

5.4.1. Comparison of the base diameters

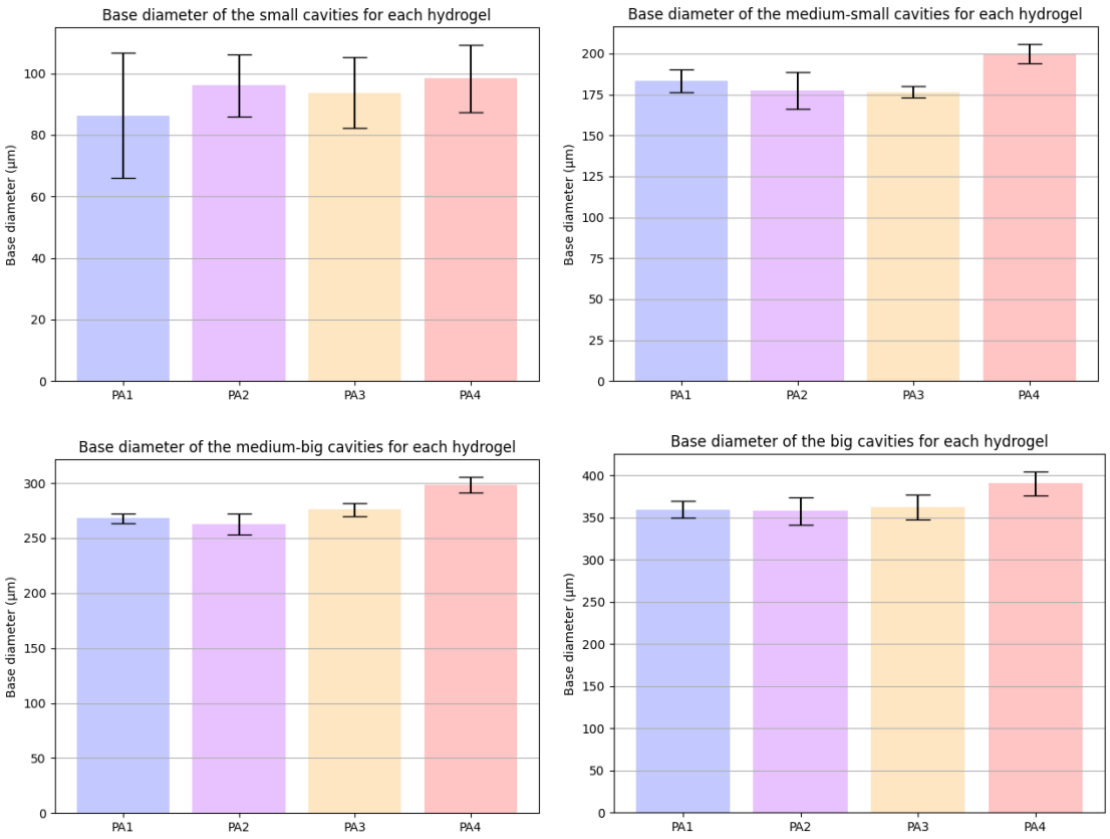

Figure 35. Base diameter bar graphs for the 4 different sizes of cavities

Figure 35 shows the behaviour of the different hydrogel's base surfaces, with values of around 80 to 100 µm for the smallest invaginations, of 175 to 200 µm for the medium-small ones, of 275 to 300 µm for the medium-big ones, and of 360 to 390 µm for the biggest ones. All of these graphs follow a similar pattern, with the lowest base values for the softer hydrogel, and the highest values for the stiffer hydrogels. This means that it is easier for higher stiffness hydrogels to obtain the

exact shape of the base of each size, whereas softer scaffolds, as they are weaker, tend to modify their shape, leaving us with less base diameter.

5.4.2. Comparison of the top diameters

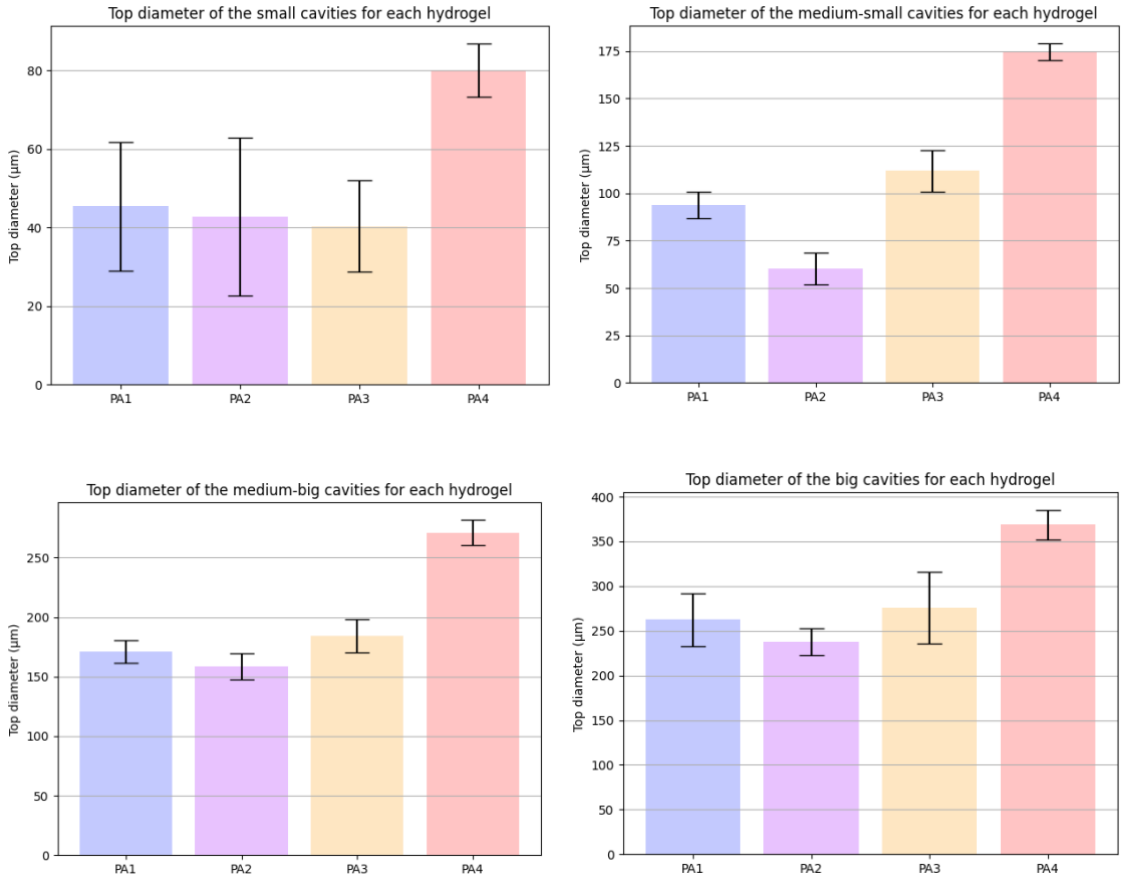

Figure 36. Top diameter bar graphs for the 4 different sizes of cavities

Regarding the top diameters, the smallest cavities have values within a 40 to 80 µm range, the medium-small ones within a 60 and 175 µm range, the medium-big ones within 160 and 270 µm range, and the biggest ones within 240 and 370 µm range. Therefore, we can see that the top diameter has lower size than the bottom one. This shows that the upper part of the cavities swell more than the bottom ones, which results in an approach of the borders at the top of the structure.

All the graphs representing the top diameter for each stiffness (seen in Figure 36) also show a similar conduct between them: approximately, PA1 and PA3 hydrogels show similar values, while PA2 gives lower top diameters, contrary to PA4, which gives much higher values, closer to the base values. This observation indicates that soft hydrogels swell more than stiffer ones.

5.4.3. Comparison of the depths

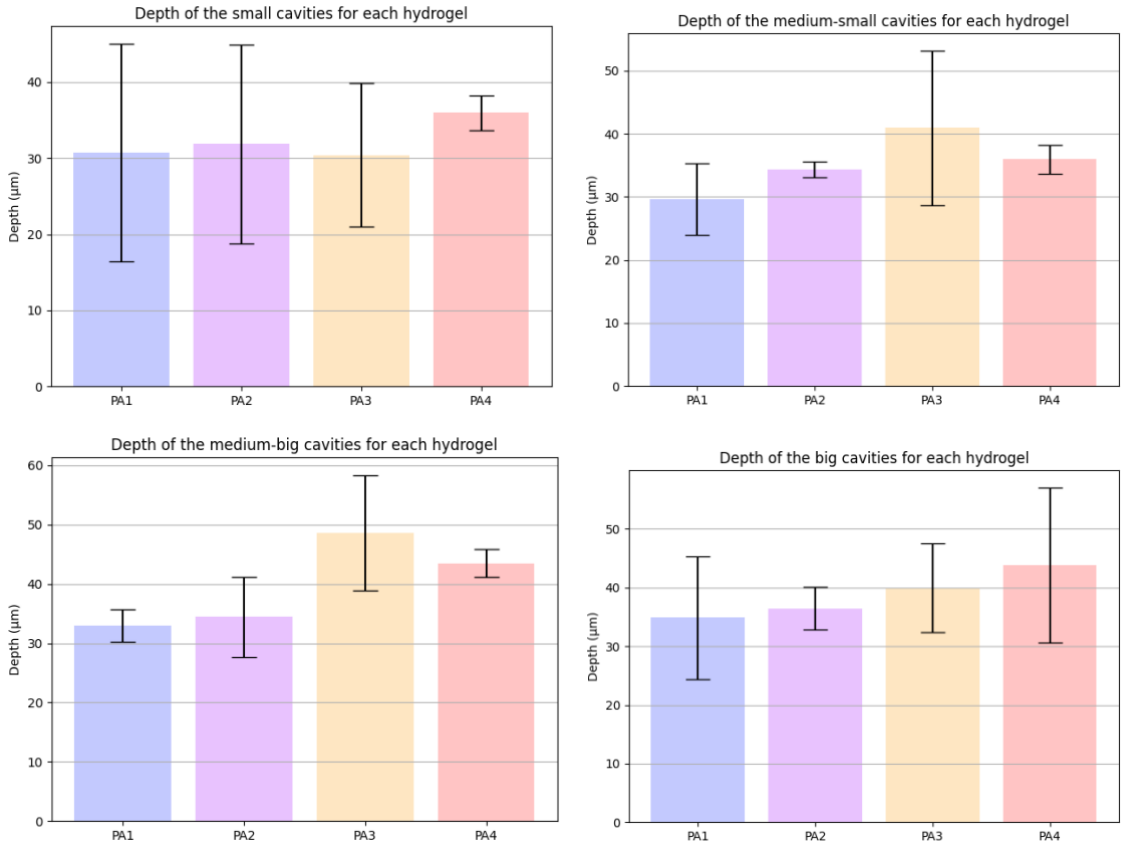

Figure 37. Depth bar graphs for the 4 different sizes of cavities

As for the depths of the cavities, they all are within a range from 30 to 50 µm without any apparent pattern. Depending on the height of the posts that were used as a moulds, the cavities were deeper or shallower.

5.5. Stiffness characterization (AFM) pre-functionalization

AFM is a useful equipment for measuring force vs. distance curves, which provide information about the characteristics of the material's surface, including its stiffness. As one of the main goals of the project was to obtain hydrogels of different stiffnesses with values similar to the ones found *in vivo*, this mechanical property had to be assessed using AFM. This assessment was done to a set of defective hydrogels (which did not have the cavities well formed, but could be used for this purpose instead) after reaching maximum swelling. The experiments were carried out using a NanoWizard® 4 Bioscience AFM (JPK Instruments) mounted on a Nikon Ti inverted microscope. A V-shaped cantilever of 0.08 N/m nominal spring constant and 4-sided pyramidal probe was used.

Through the use of contact mode, the force vs. displacement curves were created, and the JPKSPM Data Processing software was used to analyse these graphs. At least 25 measurements were taken for every hydrogel, but after eliminating the meaningless ones (which had irregular trajectories that did not represent the force vs. distance curves correctly), between 10 to 15 assessments were used to obtain the average Young's Modulus of each scaffold. This value

represents the stiffness of the material, with higher values for stiff materials, and lower values for soft ones. By using the Hertz model to fit the curves, the Young's modulus was found. This model uses Equation 5, where F represents the force applied by the tip of the cantilever, δ the indentation of the tip, E the Young's modulus, R the tip's apex radius, and ν the Poisson's ratio, which is of about 0.5 for soft biological materials [77].

$$F = \frac{4E}{3(1-\nu^2)}\sqrt{R}\delta^{\frac{3}{2}}$$

Equation 5. Relationship between the applied force and the Young's modulus

The mean and standard deviation were calculated from the various values of E for each stiffness, and the resulting stiffnesses were the ones shown in Table 6, with its force-displacement curves exposed in Figure 38.

Table 6. Measured (mean and standard deviation) and theoretical Young's Moduli of the hydrogels

Hydrogel	Measured Young's Modulus (kPa)	Theoretical Young's Modulus (kPa)
PA4	167.11 ± 18.41	172
PA3	23.01 ± 3.01	23
PA2	11.026 ± 0.83	11
PA1	6.89 ± 1.59	7

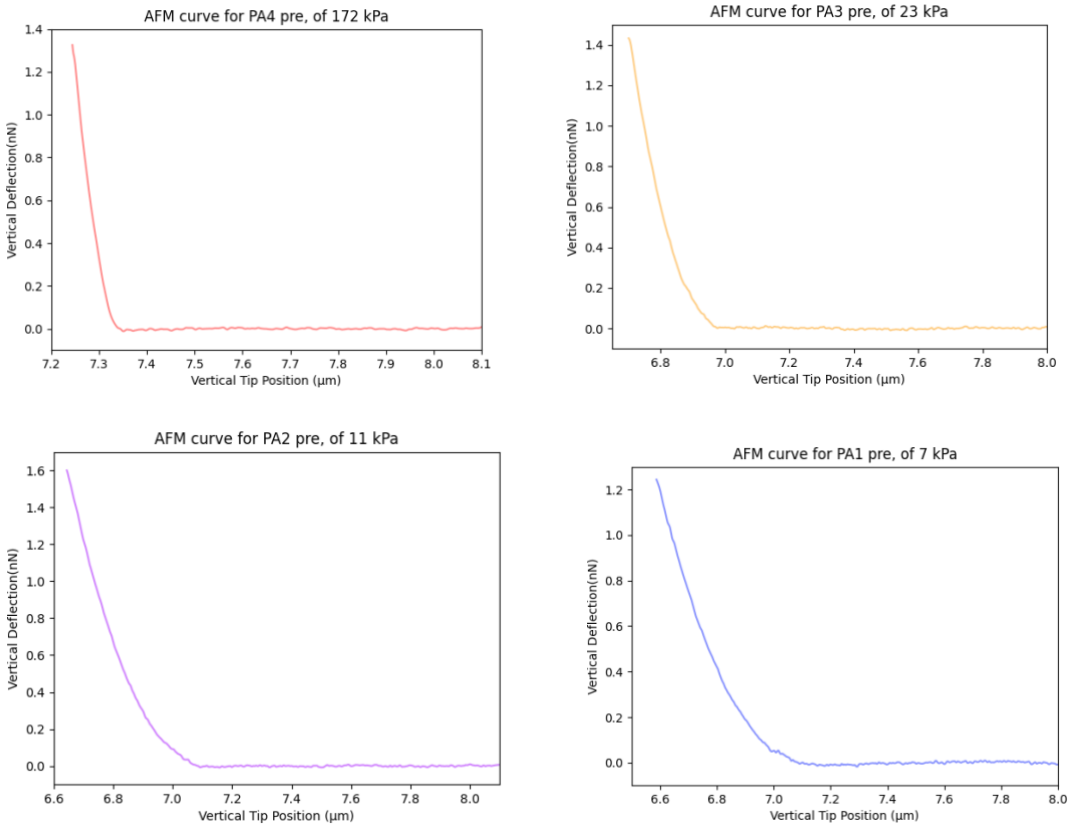

Figure 38. Force-displacement curves for the 4 different hydrogels' stiffnesses

5.6. Functionalization and checking of the coating

For the functionalization of the hydrogels, they had to be adhered to the protein of interest. The protein of interest used was Streptavidin conjugated with a Texas Red fluorophore, so that we could observe its addition to the hydrogel by confocal microscopy without having to do an immunostaining process. To adhere this protein to the PA surface, sulfo-SANPAH had to be used first. This reactive is stored in Eppendorf tubes with 40 µl of the chemical in each of them, in a –80 ºC freezer. After adding 960 µl of Mili-Q, it was left to defrost while the hydrogels were cleaned. For this cleaning, the conservation PBS that they were in had to be aspirated with the vacuum tube, and 5 mL of Mili-Q had to be poured carefully on the hydrogels. Then this water was removed with the vacuum tube, and 50 µl of the sulfo-SANPAH solution were added on each of the hydrogels. For the activation of this reactive, it had to be illuminated with UV light for 5 minutes, until it changed from a pinkish to a brownish colour.

When the surface was activated, the remaining sulfo-SANPAH was removed by adding 5 mL of PBS on each hydrogel, and removing it with the vacuum tube. At the same time, we prepared the Streptavidin solution. 50 µl of PBS were added to the protein solution (100 µg/mL), and 20 µl were poured on top of each of the activated surfaces. This was left for 1 hour at RT to incubate, covered by a box so that the light did not affect the fluorophore conjugated with the protein or the fluorescent beads of the hydrogel. Finally, 5 mL of PBS were poured on the functionalized hydrogels, and they were stored at 4 ºC in the fridge.

To check the success of this functionalization, confocal or epifluorescence microscopies were used. If it had been done correctly, a layer of the protein had to be seen covering the base of the cavities, as it can be seen in Figure 39. Regarding Figure 40, the epifluorescent microscope allowed us to observe the covered bases (top row of images, with centre proteins focused) and the layer of proteins on the upper plane of the hydrogel (last row of images, with periphery proteins focused).

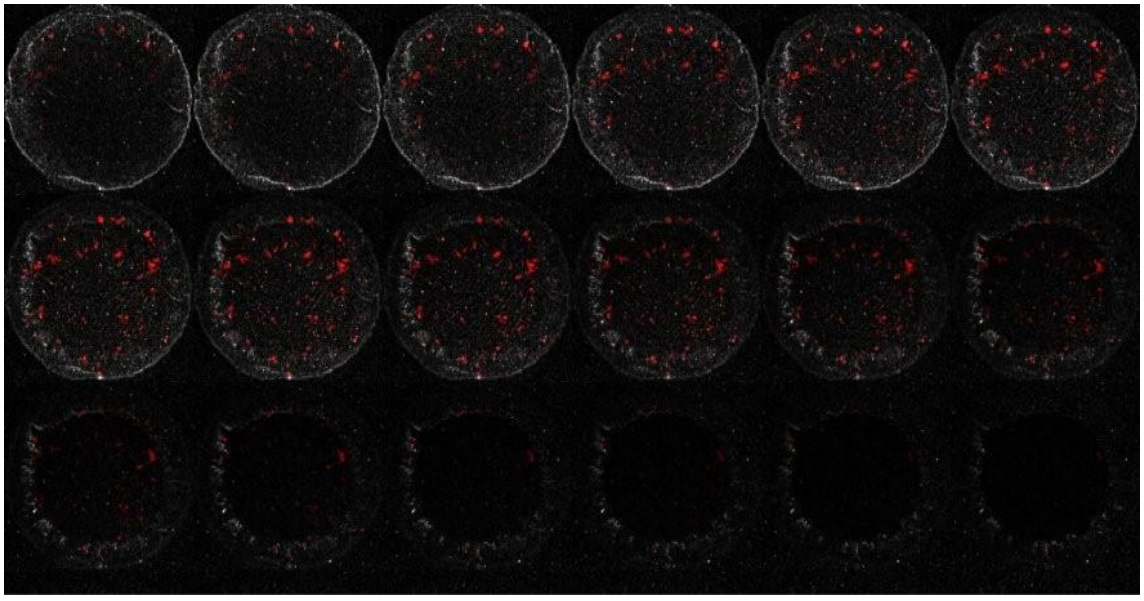

Figure 39. Montage of the functionalized walls and base of one of the PA1 hydrogels obtained with confocal microscopy

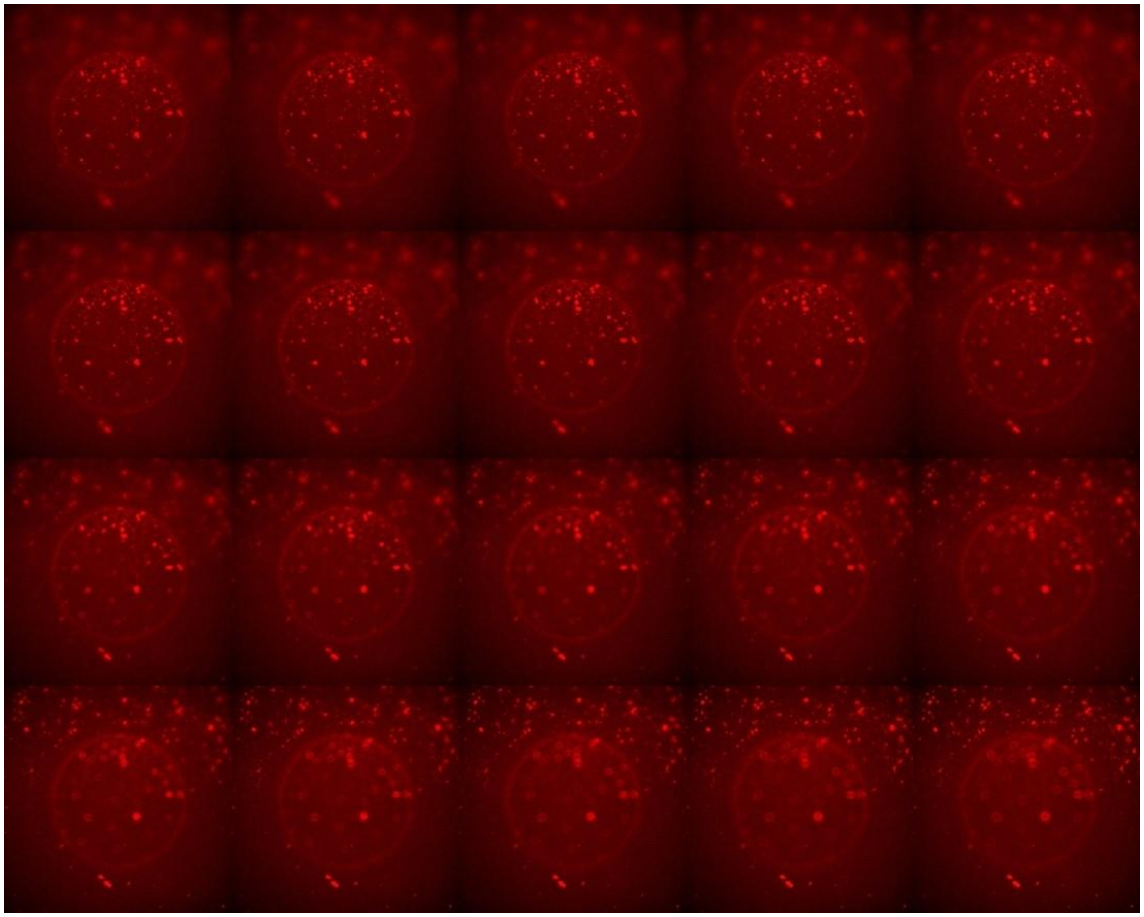

Figure 40.. Montage of the functionalized base and plane of one of the PA4 hydrogels obtained with epifluorescence microscopy

5.7. Stiffness characterization (AFM) post-functionalization

For a final analysis, we wanted to see if the functionalization of the hydrogels resulted in a change of stiffness. Therefore, the AFM measurements were performed again following the same procedure as the one exposed in section 5.5, but with functionalized hydrogels.

The mean and standard deviation were calculated again from the various values of E for each post-functionalization stiffness, and the resulting stiffnesses were the ones shown in Table 7, with its force-displacement curves exposed in Figure 41.

Table 7. Measured (mean and standard deviation) and theoretical Young's Modulus of the hydrogels

Hydrogel	New measured Young's Modulus (kPa)	New theoretical Young's Modulus (kPa)
PA4	90.89 ± 12.01	91
PA3	22.81 ± 1.60	22
PA2	6.60 ± 0.74	6
PA1	2.88 ± 0.40	3

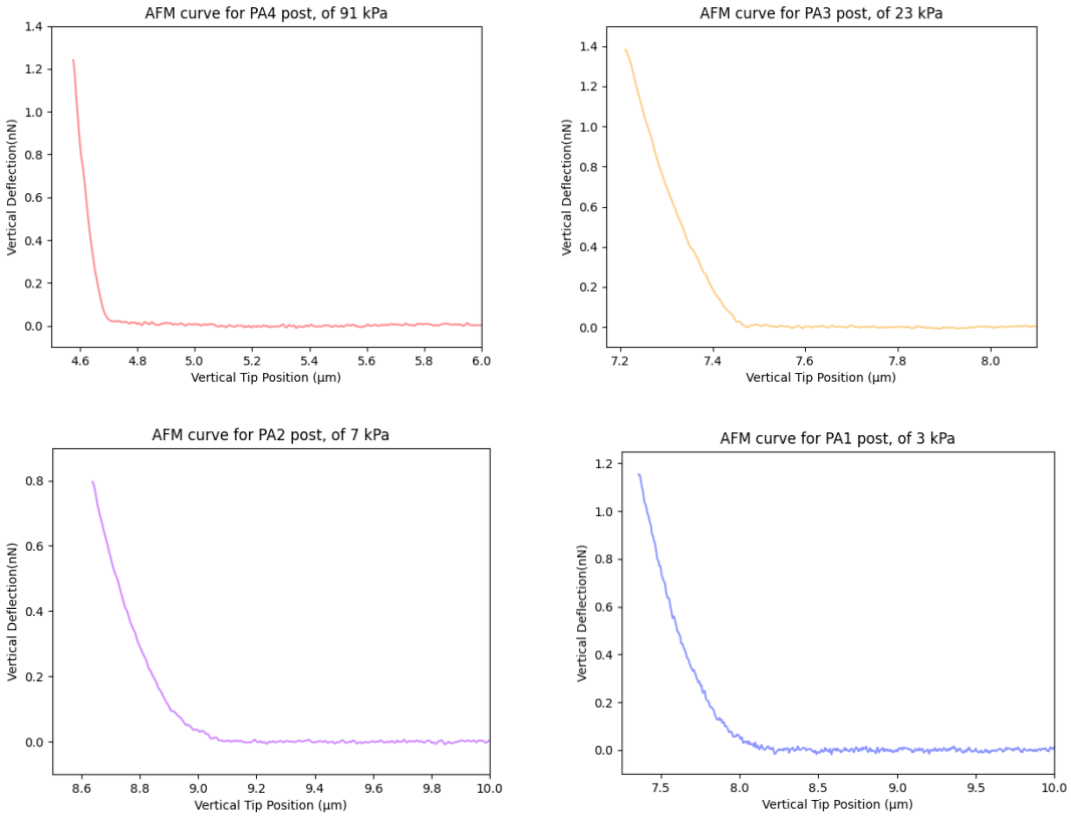

Figure 41. Force-displacement curves for the 4 different hydrogels' stiffnesses after functionalization

Table 8. Percentage of difference between previous and post-functionalization hydrogels

Hydrogel	Previous theoretical E (kPa)	New theoretical E (kPa)	% of difference (%)
PA4	172	91	Decrease of 47.2%
PA3	23	22	Decrease of 0.85%
PA2	11	6	Decrease of 40.2%
PA1	7	3	Decrease of 58.2%

As it can be seen in Table 8, the functionalization of the hydrogels brought with it a decrease in the Young Modulus' value in all cases, meaning that the final chemically coated scaffolds had softer features. This is advantageous for this project, as one of the aims was to create soft scaffolds with stiffnesses of biological relevance, with values in the range of 2.5 to 160 kPa. As all the final stiffnesses are within this range and they all decreased, we can conclude that the functionalization of the scaffolds for the future cellular studies does not suppose a disadvantage for them to be used as *in vivo* models, but rather an advantage.

6. Execution Schedule

The execution of any project requires high levels of organization and planification of the tasks that have to be done, their order, and the time required to carry each one of them out. Having a clear view on what is to be done, and when, is key in working productively and effectively.

This section focuses on the techniques that have been implemented to organise this project, to achieve maximal productivity. The use of different planning tools to define all the activities that had to be done and the time schedule that needed to be accomplished helped us have a temporal view of the project's itinerary.

The three techniques used are a Work Breakdown Structure (WBS), with its corresponding Task Dictionary; a Project Evaluation and Review Technique with its Critical Path Method (PERT-CPM); and finally, a GANTT diagram. Each of these analyses were performed, and their meaning and utility were also exposed.

6.1. Work Breakdown Structure (WBS)

The Work Breakdown Structure (WBS) is based on the breaking of the scope of the study into different, smaller work packages. These correspond to more specific and easier to manage tasks. This hierarchical decomposition of the different tasks that must be carried out allows a clear division of the scope of the project, and offers a visual representation of the amount of work needed to complete each work package.

Figure 42 shows the WBS of the current project. This study is divided into 5 main blocks, based on the management of the project, the fabrication and characterization of the hydrogels before chemically modifying them, their functionalization, and finally the characterization and validation of the final product.

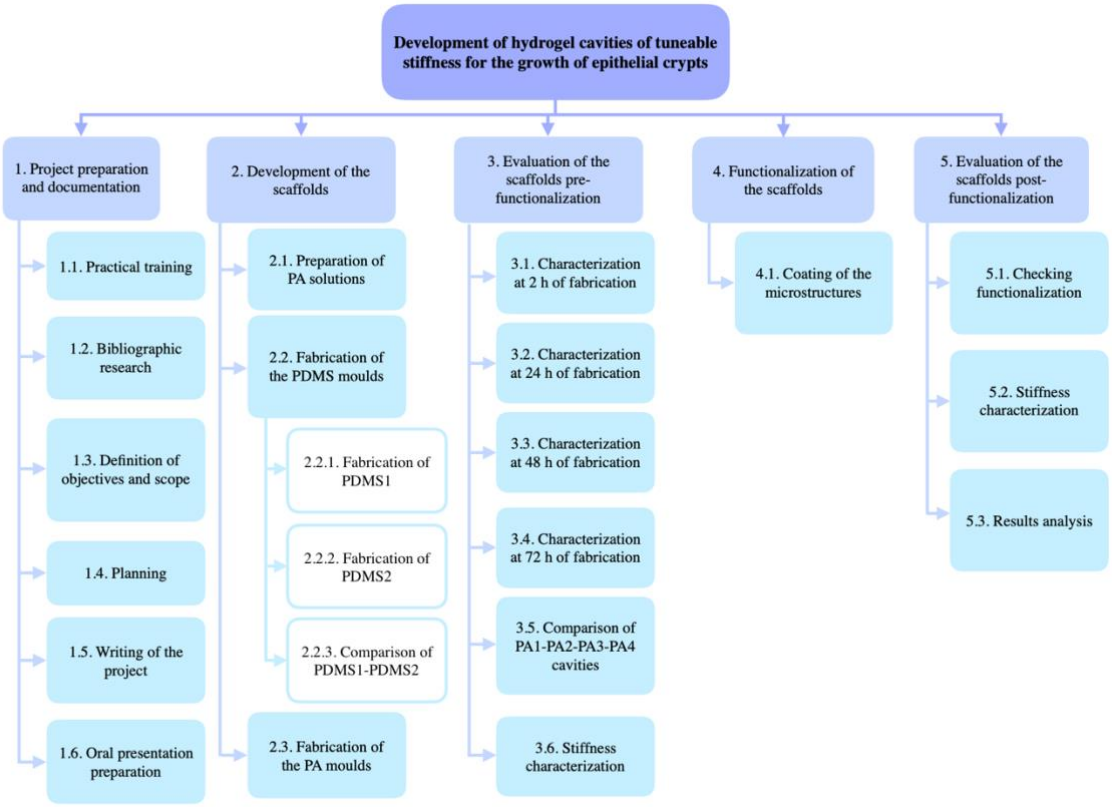

Figure 42. Work breakdown Structure (WBS) of the current project

Each one of these blocks has its subdivided tasks, which, at the same time, are divided into specific activities. These smaller, more specific tasks are showed in the following WBS dictionary, with details of what was done in each of them. Each activity has its own estimated duration time in weeks, as well as the deliverables that had to be obtained from them. It must be noted that this duration time is an estimation, as all the tasks depend on the advances of the experiments and results, as well as on the availability of the equipment needed to perform each one of them.

1. Project preparation and documentation

1.1	Practical training	Duration: 4 weeks
Acquire the basic training to use the facilities and equipment at IBEC required for the project. As for the equipment, two sessions of training needed to be completed for each one that was to be used.		
Deliverable: User Registration Form for the MicroFab and Microscopy facilities.		

1.2	Bibliographic research	Duration: 2 weeks
Studying the state of the art in which the project was developed, as well as analysing the market surrounding the project. Sections 2 and 3 included a general introduction to the tissues found in crypts, the search of different types of 3D models, the limitation posed by crypt formation, and the market surrounding the creation of 3D hydrogels.		
Deliverable: Sections 2 (Background) and 3 (Market analysis).		

1.3	Definition of objectives and scope	Duration: 1 week

Determine the aim of the project, what it intends to solve and how. Present the range of the topic that will be covered.
Deliverable: Section 1 (Introduction).

1.4	Planning	Duration: 1 week
Organizing the whole project to have a clear idea of what we want to do and when. Planning the different experiments and procedures that will be done. Consider the problems that can appear during the process by adjusting the time of each step.		
Deliverable: Project layout.		

1.5	Writing of the project	Duration: 26 weeks
Development of the written project that will be submitted. This process begins with the practical training in July 2023, after the completion of the practical training, and ends in January 2024, with the submission of the Final Degree Project.		
Deliverable: Entire written project.		

1.6	Oral presentation preparation	Duration: 1 week
Preparation of the PowerPoint presentation and organization of the explanation to be done during the oral exposition of the final project.		
Deliverable: PowerPoint of the presentation.		

2. Development of the scaffolds

2.1	Preparation of the PA solutions	Duration: 1 week
Production of the different solutions of PA of different stiffnesses from acrylamide and bis-acrylamide.		
Deliverable: 4 PA solutions in glass tubes.		

These following steps were repeated 9 times throughout the completion of this project, in order to have multiple scaffolds of each stiffness and various fabrication processes. Each time, from 2 to 8 PA hydrogels were created. The durations written on tables 2.2.1, 2.2.2 and 2.3 correspond to the total time spent on each step for all the 9 fabrication processes.

2.2.1	Fabrication of the PDMS1	Duration: 2 weeks
From the SU-8 mould to the binding of the first PDMS moulds into a glass coverslip.		
Deliverable: Thick PDMS structure with the microstructures imprinted.		

2.2.2	Fabrication of the PDMS2	Duration: 2 weeks
From the first PDMS mould, the fabrication of the thin secondary PDMS mould and its placement into a small round glass. Silanization of the glass bottom microwell dishes where the PA hydrogels will be placed.		
Deliverable: Thin PDMS secondary mould on round glass, and silanized microwell dishes.		

2.2.3	Comparison of PDMS1 - PDMS2	Duration: 1 week

Comparison of PDMS1 and PDMS2 to explore their dimensions and structures, to assess that they achieve what we were looking for, and to finally compare them with each other. This will be measured using the profilometer and the interferometer, and then analysed and compared with ImageJ software and Excel.
Deliverable: Table of percentages of difference of depths, top diameters and base diameters for each size.

2.3	Fabrication of the PA moulds	Duration: 1 week
From the mixture of the chemicals to induce the polymerization of the hydrogels to the obtaining of the PA hydrogels.		
Deliverable: PA hydrogels on glass bottom microwell dishes.		

3. Evaluation of the scaffolds pre-functionalization

The characterization of the structures before the chemical modification was done once for every fabrication process, so the durations written on tables 3.1, 3.2, 3.3 and 3.4 correspond to the total time spent on each step for all the 9 fabrication processes.

3.1	Characterization at 2 h of fabrication	Duration: 2 weeks
Assessment of the dimensions of the structures of the different PA hydrogels two hours after the fabrication process. These will be measured with the confocal microscope and then analysed with ImageJ software.		
Deliverable: Confocal images at 2 h of fabrication.		

3.2	Characterization at 24 h of fabrication	Duration: 2 weeks
Assessment of the dimensions of the structures of the different PA hydrogels 24 hours after the fabrication process. These will be measured with the confocal microscope and then analysed with ImageJ software.		
Deliverable: Confocal images at 24 h of fabrication.		

3.3	Characterization at 48 h of fabrication	Duration: 2 weeks
Assessment of the dimensions of the structures of the different PA hydrogels 48 hours after the fabrication process. These will be measured with the confocal microscope and then analysed with ImageJ software.		
Deliverable: Confocal images at 48 h of fabrication.		

3.4	Characterization at 72 h of fabrication	Duration: 2 weeks
Assessment of the dimensions of the structures of the different PA hydrogels 72 hours after the fabrication process. These will be measured with the confocal microscope and then analysed with ImageJ software.		
Deliverable: Confocal images at 72 h of fabrication.		

3.5	Comparison of PA1 - PA2 - PA3 - PA4	Duration: 2 weeks

Compare the areas of the different PA scaffolds at 2, 24, 48 and 72 hours. Evaluate the development of the cavities of each hydrogel with time and compare the development with each scaffold's stiffness (swelling evaluation). This will be done by analysing the data obtained from 3.1, 3.2, 3.3 and 3.4. Comparisons of the dimensions after maximum swelling (72 h) will also be done. The tables and graphs will be created using Excel and Pyhton.
Deliverable: Graph of evolution of the swelling of each PA hydrogel with time. Bar graphs of comparison of the depths of each size of each PA (at 72 h), bar graphs of comparison of the diameter of the cavities at the top part of each PA (at 72 h), and bar graphs of comparison of the diameter of the cavities at the base part of each PA (at 72 h). Summary and small discussion of each of the graphs.

3.6	Stiffness characterization pre	Duration: 1 week
Measurement of the stiffnesses of the PA hydrogels with AFM before their functionalization. The AFM measurement will be evaluated, and the Young's modulus will be extracted using JPK Data Processing™ software. Excel will be used to obtain the mean stiffnesses, and Python to create the graphs.		
Deliverable: Table of the resulting PA stiffnesses pre-functionalization (measured Young's Modulus) and theoretical value of each hydrogel. Vertical Tip Position (µm) vs. Vertical Deflection (nN) graphs of each stiffness, pre-functionalization.		

4. Functionalization of the scaffolds

This functionalization was done twice for two different fabrication processes, so the time shown in table 4.1 corresponds to the total time spent on both functionalization processes.

4.1	Coating of the microstructures	Duration: 1 week
Coating the walls of the microstructures with a fluorescent protein to chemically activate them.		
Deliverable: Coating protocol.		

5. Evaluation of the scaffolds post-functionalization

We checked both functionalization processes, and this time of checking corresponds to the two functionalization tasks.

5.1	Checking functionalization	Duration: 1 week
Confirming and verifying that the coating has been successful, by confocal microscopy.		
Deliverable: Confocal images verifying the coating.		

5.2	Stiffness characterization post	Duration: 1 week
Measurement of the stiffnesses of the PA hydrogels with AFM after their functionalization. The AFM measurement will be evaluated, and the Young's modulus will be extracted using JPK Data Processing™ software. Excel will be used to obtain the mean stiffnesses, and Python to create the graphs.		

Deliverable: Table of the resulting PA stiffnesses post-functionalization (measured Young's Modulus) and theoretical value of each hydrogel. Vertical Tip Position (μm) vs. Vertical Deflection (nN) graphs of each stiffness, post-functionalization.

5.3	Results analysis	Duration: 2 weeks
Comparison of the stiffnesses before and after functionalization, overall analysis of the obtained results and conclusion.		
Deliverable: Table of comparison of hydrogels pre and post functionalization. Report of the results (Section 5) and conclusions (Section 10).		

6.2. PERT-CPM Diagram

In order to coordinate the different tasks that have to be done, and reach the deadline of the project, a PERT-CPM diagram has been made. This diagram allows us to visualize the tasks that must be done.

To estimate a time as close as possible to the reality, we used a probabilistic model that is defined by Equation 6, which considers the duration of each activity to follow a beta distribution.

$$T_{PERT} = \frac{T_O + 4T_m + T_p}{6}$$

Equation 6. PERT-Beta distribution [78]

T_{PERT} is the time that will be considered, T_o the most optimistic time, T_p the most pessimistic, and T_m the normal time we expect the activity to last (the one introduced in the WBS dictionary). Table 9 shows the chronological dependence of each task, and the calculated duration of each one of them.

Table 9. Ordered tasks required to perform the project, with precedencies and timings

ID WBS	ID PERT	ID Previous task	T_o	T_m	T_p	T_{PERT}
1.1	A	-	4	4	5	4
1.2	B	-	1	2	3	2
1.3	C	A, B	1	1	1	1
1.4	D	C	1	1	1	1
1.5	E	A	21	26	27	25
1.6	F	E, J, P, U	1	1	1	1
2.1	G	D	1	1	2	1
2.2.1	H	D	1	2	3	2
2.2.2	I	H	1	2	4	2
2.2.3	J	I	1	1	1	1
2.3	K	G, I	1	1	1	1
3.1	L	K	1	2	3	2
3.2	M	L	1	2	3	2

3.3	N	M	1	2	3	2
3.4	O	N	1	2	3	2
3.5	P	O	1	2	3	2
3.6	Q	N	1	1	2	1
4.1	R	Q	1	1	2	1
5.1	S	R	1	1	2	1
5.2	T	S	1	1	2	1
5.3	U	T	1	2	3	2

From these precedencies, the chronological order of the tasks is set, so that we know which task cannot begin if its precedent has not finished, and which can be done simultaneously. The PERT diagram was generated from Table 9, and the critical path was highlighted in red. To find this critical path, the early and last time were computed. The early time is the minimum time necessary to perform a task, whereas the last time is the latest time in which a task can be done. This highlighted critical path in Figure 43 is the path composed of all the activities that, in case of there being a delay, would modify the final timing of the project. Therefore, it is the longest possible path that affects the total timing of the project. Regarding this study, its critical path is composed by tasks A, E and F. This makes sense, as the project cannot be finished until the writing part is over (E), and this is the process that takes the longest.

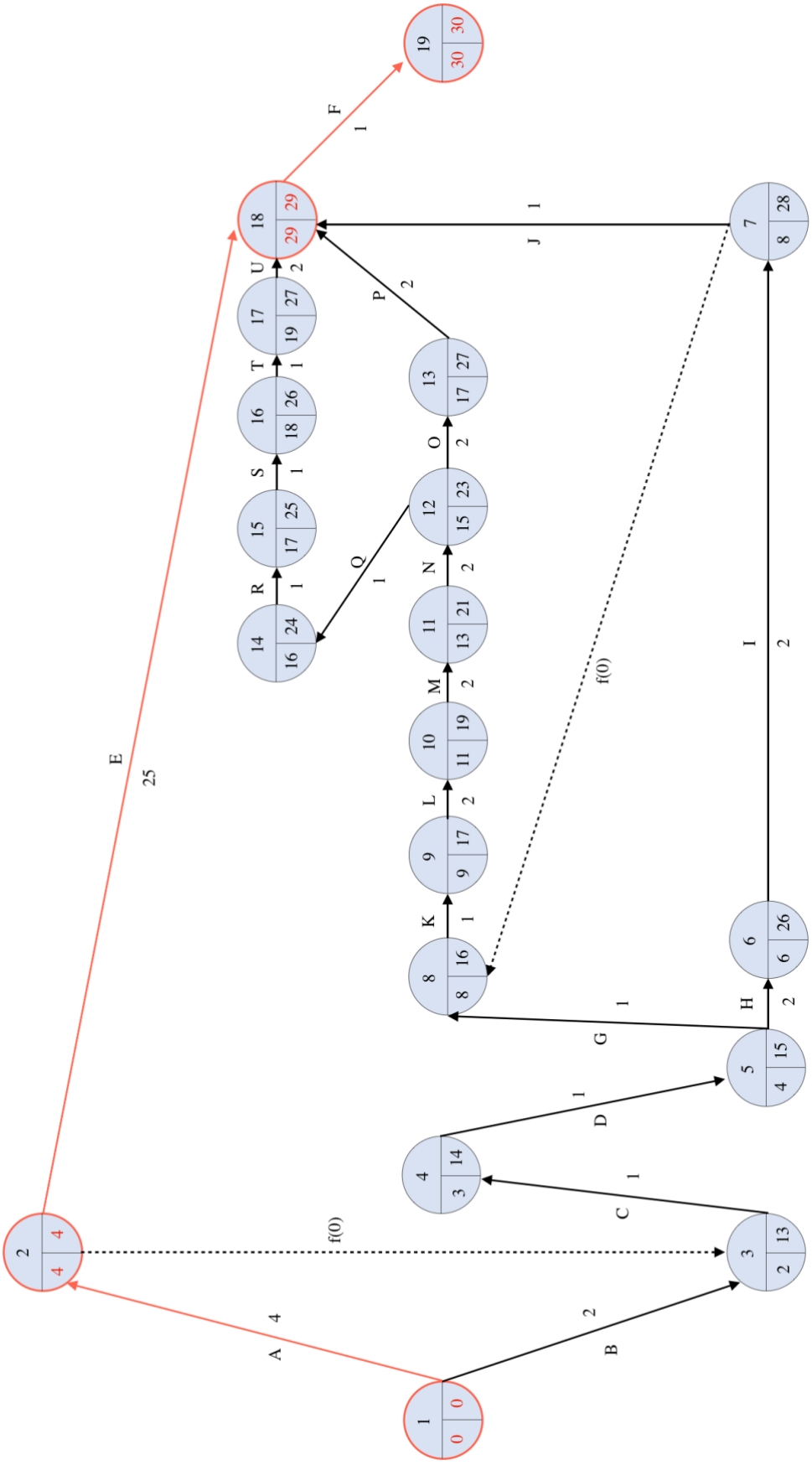

Figure 43. PERT Diagram

6.3. GANTT Diagram

Finally, to visualize the temporal evolution of the project's course, the tasks have been displayed against time in a GANTT diagram, shown in Figure 44. This method facilitates the temporal programming of activities and their monitoring, as well as having a clear view on when each activity begins and ends, how long each task is scheduled to last, which activities overlap with other ones, and to set a start and finish date for the project. The colour red is highlighting the critical path discussed in the previous section.

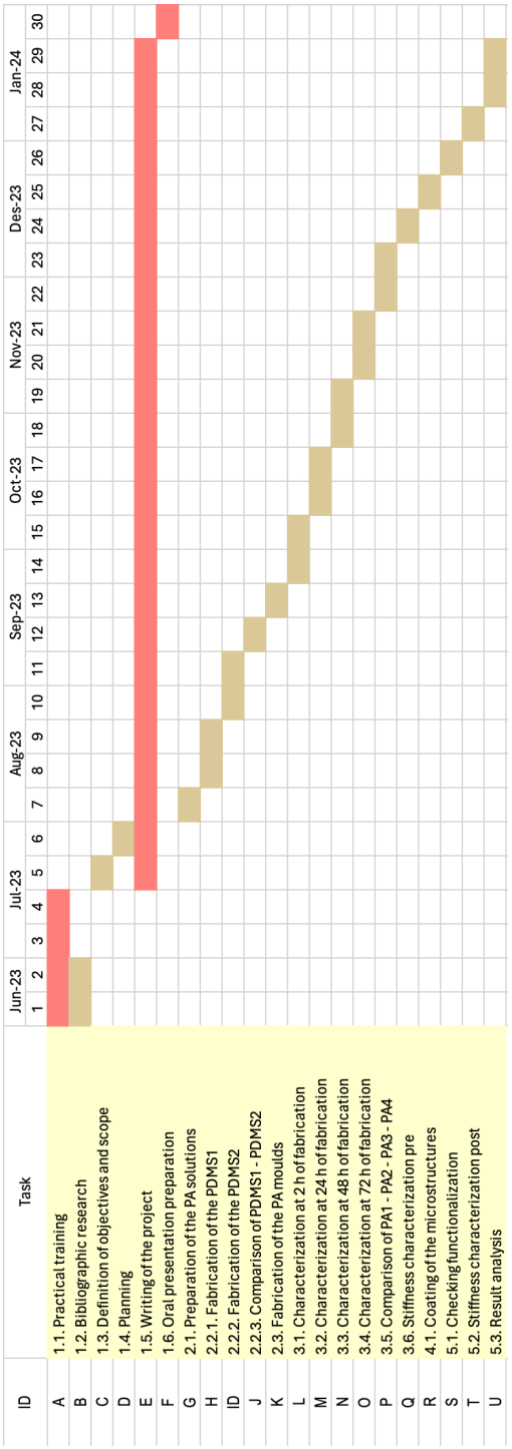

Figure 44. GANTT Diagram

7. Technical viability: SWOT analysis

In this section, an analysis of the strengths, weaknesses, opportunities and threats (SWOT) of the proposed solution is presented. Table 10 summarizes this analysis, to evaluate its technical feasibility.

Table 10. SWOT analysis of the project

	Internal	External
Positive	**Strengths** · High motivation of the author. · Guidance and support of the 'Biomimetics' group, especially of the author's mentor. · Clear definition of the project and its global objectives. · Resources for measurements and characterization. · Easy manufacturing of the cavities. · Considerable number of samples for a throughput analysis of the model. · Repeatability of the fabrication process. · Similarity to the *in vivo* wells, with physiological stiffness. · Biocompatible hydrogel.	**Opportunities** · Scientific advance. · Potential clinical applications. · Increasing research and market on the topic. · Affordable to produce in laboratories. · Alternative to animal testing.
Negative	**Weaknesses** · Limited time. · Lack of experience of the author in the field. · Errors easily made during the fabrication process.	**Threats** · Competence. · Unpredictable results.

An internal analysis of the proposed solution, with its strengths and weaknesses, is portrayed in the first column of Table 10.

Firstly, this final degree project has several strengths that contribute to its success. The author's high motivation towards the project, combined with the guidance and support from the 'Biomimetics' team, especially from the author's mentor, play a crucial role in the development of this project. Moreover, the early and clear definition of the goals made the completion of the project to go smoothly. As the project was conducted at the 'Biomimetics' group's laboratory at IBEC, all the necessary resources and equipment were provided to the author. Furthermore, the easy manufacturing of the microcavities allowed a high throughput analysis, as we had a considerable number of samples, and made it repeatable. In addition, the ability of the hydrogels to tune their stiffness allowed them to have similar properties to the *in vivo* tissues, and its biocompatibility grants the possibility to do cellular studies on them.

Nonetheless, the project presented several weaknesses that ought to be noted. The most significant one is the limited timeframe, which has resulted in not being able to perform cellular studies on top of the scaffolds. Additionally, the author lacked experience in the field of microfabrication, so the process of adaptation was complicated to a certain extent. This lack of experience also caused the author to make some mistakes during manufacturing, which affected the validity of some samples (having hills instead of cavities because of air bubbles when fabricating, failed bonding between the PA and the silanized glass...).

On the other hand, the second column of Table 10 exposes the external opportunities and threats of the project.

In terms of opportunities, the cellular study of the scaffolds produced in this project could contribute to creating more knowledge in the fields of cellular biology and regenerative medicine and, consequently, it could potentially have clinical applications. This exponentially increases the interest in the development of the hydrogels for industrial purposes and incentivized the interest in research. The manufacturing of the hydrogels is economically viable to be performed in any laboratory, and much more ethically responsible, as it does not require animal testing.

Finally, the main risks and threats posed by the project include the existence of other researchers already working on similar studies, which could influence the originality and relevance of the project. Moreover, as the following cellular study is complex, there is a possibility for the results not being consistent or not meeting the established expectations.

8. Economic viability

This project's completion entails a financial outlay. In this section, an analysis of the project's economic features has been done in order to get a sense of this cost and its sources.

As this project was carried out at the Biomimetics systems for cell engineering group's laboratory at IBEC, the equipment, facilities and funds needed for its development were provided by this group and IBEC's Core Facilities unit. Therefore, the cost of using the supplies and equipment is lower, as they were not purchased especially for this project. The hours of use of every equipment were calculated, and the price of the usage of both the equipment and its software has also been taken into account. Nevertheless, the majority of the lab materials utilised, such as glass pipettes and pipette tips, are single-use items that must be disposed of after use. For this reason, the quantity of used units of each of these materials (as well as the reagents) have been taken into account, and their cost has been considered when evaluating the project's cost. In contrast, non-fungible materials that are already provided by IBEC Core Facilities and the Biomimetic Systems for Cell Engineering group (such as microscopes) have not been factored into the project's final budget.

Multiplying the cost of each unit, by the number of units needed for each item, the total approximate price has been computed. Additionally, in terms of human resources, it has been considered that this project is majorly conducted by a biomedical engineering student with a supposed salary of 13 €/h, and supervised by an experienced researcher with a supposed salary of 30 €/h. The amount of time dedicated to the development of the project, considering the time spent at the laboratory and the time dedicated to the research of literature and the writing of the project, sums a total of 360 hours. Moreover, the time spent by the author's mentor for the tutoring of the project has been estimated to be of 50 hours throughout its completion. With these salaries and knowing the number of hours worked, the total cost of human resources has also been calculated.

Table 11. Direct costs of the project
** Provided by Biomimetic Systems for Cell Engineering group or by student license*

Concept: Materials	Provider	Units	Unit price (€/unit)	Total price (€)
50-1000 µl pipette tips	LabClinics	500	0.08	38.41
2-200 µl pipette tips	VWR International	480	0.09	42.64
0.1-10 µl pipette tips	Sigma-Aldrich™	400	0.10	42.08
10 ml serological pipettes	Sigma-Aldrich™	30	1.03	30.90
25 ml serological pipettes	Sigma-Aldrich™	100	0.82	82.00
22 mm x 22 mm cover glasses	Sigma-Aldrich™	40	0.14	5.60
Circular 14 mm diameter cover glass	Marienfeld	40	0.60	23.94
Eppendorf Microtubes 1.5 mL	Sudelab	55	0.014	0.77
Petri Dishes 40 mm TPP	Proquinorte	20	0.20	4.00
Petri Dishes 90 mm	BD Biolab	10	0.084	0.84

Millex Syringe Filter	Millex®	80	0.004	0.33
Nitril Gloves	Santex	250	0.035	8.75
Foot covers	IberoMed	180	0.04	7.22
35 mm petri dish, 20 mm Microwell	MatTek	50	2.28	113.94
35 mm petri dish, 14 mm Microwell	MatTek	8	1.73	13.85
Pasteur pipettes	Fisher Scientific	25	0.071	1.78
10 mL Syringes	Sudelab	50	0.13	6.68
TOTAL MATERIALS COST				**423.73**
Concept: Reagents	**Provider**	**Units**	**Unit price (€/unit)**	**Total price (€)**
Acrylamide (40%)	Bio-Rad	5 mL	0.28	1.39
N,N-Methylene bisacrylamide (2%)	Bio-Rad	3 mL	0.24	0.73
Ammonium persulfate analytical grade (APS)	Serva	10 g	1.20	12.02
N,N,N',N'-Tetramethylethylenediamine (TEMED)	Sigma	50 mL	1.33	66.70
Phosphate Buffered Saline (PBS)	Sigma	1 L	50.00	50.00
SYLGARD® 184 Silicone Elastomer Kit	Dow Corning	1	173.00	173.00
(3-Aminopropyl) trimethoxysilane 97 %	Sigma	60 mL	0.83	49.92
Trichloro(1H,1H,2H,2H-perfluorooctyl) silane	Sigma	10 mL	11.00	110.00
Glutaraldehyde 25 wt. % in H_2O	Sigma	25 mL	1.49	37.25
Sulfo-SANPAH	Life Technologies	5 mg	7.50	37.50
Streptavidin, Texas Red® conjugate	Life Technologies	160 µL	0.40	63.84
TOTAL REAGENTS COST				**602.35**
Concept: Equipment usage	**Provider**	**Units**	**Unit price (€/unit)**	**Total price (€)**
Oven	P Selecta	40 h	4.33	173.2
Plasma Cleaner	Harrick	7 h	7.57	52.99
Optical Microscope	Nikon	24 h	6.24	149.76
Interferometric Microscope	Vecco	5 h	25.66	128.3
Profilometer	Bruker	5 h	25.97	129.85
Spin-Coater	MTI Corporation	12 h	20.98	251.76
Confocal Microscope	ZEISS	27 h	27.30	737.1

TOTAL EQUIPMENT COST			1622.96
Concept: Software	**Units**	**Unit price (€/unit)**	**Total price (€)**
Fiji-Image J	1	0	0
JKPKSM Data Processing	1	0*	0
Microsoft Office 365	1	0*	0
TOTAL SOFTWARE COST			**0**
Concept: Human resources	**Hours**	**Price/hour (€/h)**	**Total price (€)**
Biomedical engineering student	360	13.00	4680.00
Supervisor	50	30.00	1500.00
TOTAL HUMAN RESOURCES COST			**6180.00**

The project's indirect costs – which refer to the use of the Biomimetic Systems for Cell Engineering group's and IBEC's equipment and facilities, like the computers and the electricity – have also been considered. These indirect values have been calculated as 5 percent of the overall expenses of the direct costs. Thus, the project's overall cost is determined by summing the direct and indirect costs:

Table 12. Approximation of the total cost of the project

Type of cost	Concept	Cost (€)
Direct costs	Material resources	423.73
	Laboratory Reagents	602.35
	Equipment use	1622.96
	Software	0
	Human resources	6180
Indirect costs	Structural costs (5%)	441.452
TOTAL COST OF THE PROJECT		**9270.492**

As it can be seen in Table 12, the overall cost of the project is approximately of **9270.492 €** in total.

9. Regulations and Legal aspects

As the project has been wholly developed and executed in Barcelona, the laws and regulations that are in effect are those enforced by the Catalan and Spanish government and, consequently, by the European Union (EU) directives.

Firstly, as the project involves research, it must comply with the ethics in research legislations, which requires that the practice of science is carried out with ethical principles that ensure the advancement of knowledge, the understanding and improvement of human condition and the progress of society. It is focused on the consideration of the ethical aspects of the research, in its nature and purposes, such as the respect of the dignity of the human being, the autonomy of their will, the protection of their data (with privacy and confidentiality), and preservation of the environment [79].

For the health protection of the employees working at IBEC, Law 31/1995, known as the Occupational Risk Prevention Law, establishes regulations to guarantee the safety of workers in their work environments. Its monitoring is crucial to prevent workplace accidents, protect the health of employees and promote safe and healthy working conditions in all activities. This law also seeks collaboration between employers and workers to identify and reduce occupational risks [80]. More specifically, the Royal Decree 664/1997 establishes measures to protect workers against risks related to biological agents in the work environment. It regulates risk assessment, the adoption of preventive measures and the information and training of workers in relation to biosafety [80]. Some Prevention Technical Notes (NTP), such as NTP 479 for minimizing the risks associated with the reactivity of chemical products, NTP 399 for the actuation of the researchers in case of leakages and spills and NTP 359 for the management of hazardous waste in research laboratories in small quantities have also been followed to ensure the security in the laboratory [81]. Moreover, the ISO (International Organization for Standardization) 45001 rule establishes the requirements to implement an occupational health and safety management system. Its primary focus is to provide a framework for organizations to effectively manage occupational risks and continually improve their occupational health and safety performance [82].

Regarding the protection of personal data, the Organic Law 3/2018 on the Protection of Personal Data and Guarantee of Digital Rights, and the Regulation (EU) 2016/679 of the European Parliament and of the Council are abided by IBEC. This first law regulates the processing of personal data and protects the digital rights of citizens. It incorporates specific provisions on privacy and confidentiality, establishing principles such as transparency, limitation of purpose and security in the handling of personal information [80]. This law harmonizes the Spanish legislation with the General Data Protection Regulation of the European Union 2016/679, which is the European regulation that governs the protection of personal data. It establishes key principles for data processing, and it grants individuals expanded rights over their data, such as the right to access, rectification, deletion, and portability [80].

As for the preservation and protection of the environment, the present project has followed the environmental legislations and the appropriate management of residues. For instance, Law

22/2011 of residues and contaminated floors establishes regulations for the correct management of waste, promoting reduction, reuse and recycling. It also imposes measures to prevent or correct soil contamination and protect human health and the environment [80].

If our product were to be introduced to the market, a Good Laboratory Practices (GLP) accreditation would be needed. These are a set of international guidelines that establish the principles and procedures for conducting non-clinical laboratory studies in the field of research and development of chemical and pharmaceutical products. Their main objective is to guarantee the generation of reliable, consistent and high-quality laboratory data. These practices seek to ensure that laboratory studies are carried out with reproducibility, reliability and high quality, to support the safety and effectiveness of chemical and pharmaceutical products before their introduction into the market [83].

10. Conclusions

The elaboration of this project has allowed the development of micrometre-sized cavities in hydrogels of tuneable and controllable stiffness. This model was designed to overcome the shortcomings of the existing 2D cell models by changing the traditional flat culture dishes for 3D conformations. More specifically, as recent research has already begun addressing this lack of complexity *in vitro*, it aimed to reduce the limitations found on these new *in vitro* cultures. Because of supraphysiological stiffnesses of the materials used on these innovative studies, the matching of the rigidity to that of the native tissues cannot be achieved. By using PA hydrogels for the fabrication of this conformations, the final stiffness of our new model has a Young's modulus that is comparable to *in vivo* tissues.

The previous research of the literature surrounding the area of study has given a purpose to this project by shedding light into the necessity of developing models with physiological rigidities, as well as into the difficulty of micro-fabricating cavities in soft materials. After reviewing the state of the art on physiological rigidity models with cavities, it has become clear that more research is needed in this area, in order to create *in vitro* models with similar characteristics as the ones found in tissues, for their application in clinical studies, avoiding animal testing and obtaining more reliable results to improve the safety of the people participating in the clinical trials.

Regarding the development of the model, replica-moulding has showed as a technique that allowed the production of cavities with sizes of physiological interest into PA hydrogels of low rigidity. Moreover, the protocol has shown to be simple, highly reproducible and reliable. With the obtaining of the first PDMS replicas from the SU-8 master and the posterior fabrication of the secondary thin PMDS layers, the PA cavities could be created, by using this last PDMS sheet as a mould for PA polymerization. Moreover, the PA hydrogels' rigidity and their ability to swell have been characterized. By adjusting the concentrations of acrylamide and bis-acrylamide in the PA solutions, we were able to create PA hydrogels with stiffnesses ranging from 6 to 172 kPa. Additionally, it has been demonstrated that softer hydrogels have a higher swelling capacity during the first three days after fabrication than those which are more rigid.

Furthermore, a treatment with Sulfo-SANPAH and Streptavidin has been done on the surfaces of the hydrogels to study the success of the attachment of this protein to the hydrogels. The chemically activated hydrogels' stiffnesses were then assessed with AFM, to guarantee that this treatment maintained the mechanical properties of the materials, which was one of the goals of this project. It has been seen that this chemical coating even improves these mechanical properties, lowering their stiffness, allowing the models to be used for studies of the softest tissues of the body, with Young's Modulus as low as 3 kPa.

After the characterization of the hydrogels with confocal and epifluorescence microscopy, more specifically with the use of Z-stack imaging, it has been proven that the final cavities of the model have dimensions similar to the ones of the initial PDMS1 moulds obtained from the SU-8 master, which were chosen to be relevant for the study of cell conformity and their growth on these invaginations.

To sum up, we have succeeded in creating micrometre-sized cavities with adjustable stiffnesses. The small posts found on the SU-8 master have been successfully transferred to the final PA moulds, creating cavities of dimensions relevant for the study of the behaviour of cell growth on them. These cavities have also been fabricated into hydrogels with rigidities similar to the ones that tissues present *in vivo*, further emphasizing the relevance of the study of the cell growth on them. Moreover, we have proven that the implementation of the protein functionalization of the hydrogels did not make them more rigid, but instead resulted in softer hydrogels, allowing us to mimic the behaviour of tissues with even lower Young's moduli.

10.1. Future work

For a final evaluation of the hydrogel cavities fabricated in this project, epithelial cells such as Caco-2 and/or Madin-Darby canine kidney (MDCK) could be seeded on top of them to assess their growth, morphology and conformity. These cells, after seeding, present a phenotype which, morphologically and functionally, resembles that of the ones found *in vivo* in, for instance, intestinal crypts or kidney invaginations.

Their ability to adhere, spread and form a monolayer on the hydrogels with cavities could be studied. Moreover, the conformity of the epithelial monolayers with the underlying hydrogel's shape could be assessed, to evaluate if the monolayer is formed following the shape of the cavities, as it happens in *in vivo* tissues with these structures. To do so, cells should be seeded on top of the hydrogels and incubated for a period of time, allowing them to grow and adhere to the scaffold, changing their corresponding culture medium once a week, to supply them with new nutrients, necessary for the cells to survive and proliferate. Then, after some time of incubation, these cells could be fixed and immuno-stained in order to study the mentioned aspects with immunofluorescence and confocal microscopy.

Bibliography

[1] J. Gullbo, M. Fryknäs, L. Rickardson, P. Darcy, M. Hägg, M. Wickström, S. Hassan, G. Westman, S. Brnjic, P. Nygren, S. Linder, R. Larsson, 'Phenotype-based drug screening in primary ovarian carcinoma cultures identifies intracellular iron depletion as a promising strategy for cancer treatment', Biochemical Pharmacology, Volume 82, Issue 2, 2011, Pages 139-147, ISSN 0006-2952.

[2] S. Dhar, J. Gullbo, K. Nilsson, P. Nygren, R. Larsson, 'A Nonclonogenic Cytotoxicity Assay Using Primary Cultures of Patient Tumor Cells for Anticancer Drug Screening', SLAS Discovery, Volume 3, Issue 3, 1998, Pages 207-216, ISSN 2472-5552.

[3] Y. Fang, R. M. Eglen, 'Three-Dimensional Cell Cultures in Drug Discovery and Development,' SLAS DISCOVERY: Advancing the Science of Drug Discovery, vol. 22, issue 5, May 2017.

[4] Karlsson H, Fryknäs M, Larsson R, Nygren P. 'Loss of cancer drug activity in colon cancer HCT-116 cells during spheroid formation in a new 3-D spheroid cell culture system'. Exp Cell Res. 2012 Aug 1;318(13):1577-85. doi: 10.1016/j.yexcr.2012.03.026. Epub 2012 Apr 2. PMID: 22487097.

[5] B.A. Chabner, T.G. Roberts Jr., 'Timeline: chemotherapy and the war on cancer', Nat. Rev. Cancer 5 (2005) 65–72.

[6] Sharma, S. *et al*. 'A phase II trial of farnesyl protein transferase inhibitor SCH 66336, given by twice-daily oral administration, in patients with metastatic colorectal cancer refractory to 5-fluorouracil and irinotecan'. Ann. Oncol. 13, 1067–1071 (2002).

[7] Yang, Q., Xue, SL., Chan, C.J. *et al.* 'Cell fate coordinates mechano-osmotic forces in intestinal crypt formation'. *Nat Cell Biol* **23**, 733–744 (2021).

[8] Senjiang Yu, Yadong Sun, Yong Ni, Xiaofei Zhang, and Hong Zhou. 'Controlled Formation of Surface Patterns in Metal Films Deposited on Elasticity-Gradient PDMS Substrates', ACS Applied Materials & Interfaces **2016** 8 (8), 5706-5714.

[9] Institute for Bioengineering of Catalonia. Home page – Institute for Bioengineering of Catalonia. Accessed on July 2023. Retrieved from: https://ibecbarcelona.eu/ca/

[10] Lemke SB, Nelson CM. 'Dynamic changes in epithelial cell packing during tissue morphogenesis'. Curr Biol. 2021 Sep 27;31(18):R1098-R1110. doi: 10.1016/j.cub.2021.07.078. PMID: 34582821; PMCID: PMC8496771.

[11] Khan YS, Lynch DT. 'Histology, Lung'. [Updated 2023 May 1]. In: StatPearls [Internet]. Treasure Island (FL): StatPearls Publishing; 2023 Jan-. Available from: https://www.ncbi.nlm.nih.gov/books/NBK534789/

[12] Ganesan S, Comstock AT, Sajjan US. 'Barrier function of airway tract epithelium. Tissue Barriers'. 2013 Oct 1;1(4):e24997. doi: 10.4161/tisb.24997. Epub 2013 May 30. PMID: 24665407; PMCID: PMC3783221.

[13] Meng X, Cui G, Peng G. 'Lung development and regeneration: newly defined cell types and progenitor status'. Cell Regeneration (London, England). 2023 Apr;12(1):5. DOI: 10.1186/s13619-022-00149-0. PMID: 37009950; PMCID: PMC10068224.

[14] Fischer, Bernard & Pavlisko, Elizabeth & Voynow, Judith. (2011). 'Pathogenic triad in COPD: Oxidative stress, protease-antiprotease imbalance, and inflammation'. International journal of chronic obstructive pulmonary disease. 6. 413-21. 10.2147/COPD.S10770.

[15] Murray IV, Paolini MA. 'Histology, Kidney and Glomerulus'. [Updated 2023 Apr 17]. In: StatPearls [Internet]. Treasure Island (FL): StatPearls Publishing; 2023 Jan-. Available from: https://www.ncbi.nlm.nih.gov/books/NBK554544/

[16] (Hons), E.P.Bs. (2023) '*Kidney histology*', *Kenhub*. Accessed on June 2023. Available at: https://www.kenhub.com/en/library/anatomy/kidney-histology

[17] '*Simple nephron diagram: Basic anatomy and physiology, excretory system, human anatomy and physiology*' (2016) Pinterest. Accessed on June 2023. Available at: https://www.pinterest.com/pin/247698048233756976/

[18] '*Renal corpuscle in renal cortex*', *Histology at SIU*. Accessed on June 2023. Available at: https://histology.siu.edu/crr/RN002b.htm

[19] Mac-Moune Lai, F., Szeto, CC., Choi, P. *et al.* 'Isolate diffuse thickening of glomerular capillary basement membrane: a renal lesion in prediabetes?'. *Mod Pathol* **17**, 1506–1512 (2004).

[20] J. Ferrufino, L. Taxa, G. Angeles, 'Histología normal del intestino delgado,' Revista Médica Herediana, vol. 7, n. 1, January 1996

[21] Wallaeys C, Garcia-Gonzalez N, Libert C. Paneth cells as the cornerstones of intestinal and organismal health: a primer. EMBO Mol Med. 2023 Feb 8;15(2):e16427. doi: 10.15252/emmm.202216427. Epub 2022 Dec 27. PMID: 36573340; PMCID: PMC9906427.

[22] J. Reiriz, 'Sistema Digestivo: Anatomía,' Infermera virtual. Col·legi Oficial Infermeres i Infermers Barcelona, [online document], 2008. Available at: https://www.infermeravirtual.com/files/media/file/98/Sistema%20digestivo.pdf?1358605461

[23] E. Valverde, 'Trabajo fin de grado: Repercusiones de la hipoxia intermitente en intestino delgado. Estudio en un modelo experimental animal.,' Universidad de Valladolid, [online document], 2018-2019. Available at: https://uvadoc.uva.es/bitstream/handle/10324/38302/TFG-M-N1674.pdf?sequence=1

[24] I. García 'SOS Biologia Celular y Tisular.,' Universidad Nacional Autónoma de México, [online document], 2012. Available at: http://sosbiologiacelularytisular.blogspot.com/2012/03/digestivo-intestino_08.html

[25] Van Norman GA. 'Limitations of Animal Studies for Predicting Toxicity in Clinical Trials: Part 2: Potential Alternatives to the Use of Animals in Preclinical Trials'. JACC Basic Transl Sci. 2020 Apr;5(4):387-397. doi: 10.1016/j.jacbts.2020.03.010. Epub 2020 Apr 27. PMID: 32363250; PMCID: PMC7185927.

[26] K.M. Hillgren, A. Kato, R.T. Borchardt, '*In vitro* systems for studying intestinal drug absorption', Med. Res. Rev. 15 (1995) 83–109, https://doi.org/10.1002/med.2610150202

[27] S.A. Acra, 'Methods of investigating intestinal transport', J. Parenter. Enteral Nutr.15 (1991) 93S–98S, https://doi.org/10.1177/014860719101500393S

[28] L. Barthe, M. Bessouet, J.F. Woodley, G. Houin, 'The improved everted gut sac: a simple method to study intestinal P-glycoprotein', Int. J. Pharm. 173 (1998) 255–258, https://doi.org/10.1016/S0378-5173(98)00225-7

[29] B. Carreno-Gómez, J.F. Woodley, A.T. Florence, 'Studies on the uptake of tomato lectin nanoparticles in everted gut sacs', Int. J. Pharm. 183 (1999) 7–11, https://doi.org/10.1016/S0378-5173(99)00050-2

[30] Wang L, Wu J, Chen J, Dou W, Zhao Q, Han J, Liu J, Su W, Li A, Liu P, An Z, Xu C, Sun Y. 'Advances in reconstructing intestinal functionalities *in vitro*: From two/three dimensional-cell culture platforms to human intestine-on-a-chip'. Talanta. 2021 May 1;226:122097. doi: 10.1016/j.talanta.2021.122097. Epub 2021 Jan 20. PMID: 33676654.

[31] Westerhout, J., Wortelboer, H., Verhoeckx, K. (2015). Ussing Chamber. In: Verhoeckx, K., *et al.* 'The Impact of Food Bioactives on Health'. Springer, Cham. https://doi.org/10.1007/978-3-319-16104-4_24

[32] Schematic illustration of a Transwell® System with nanoparticles (NPS) (no date) ESA. Accessed on June 2023. Available at: https://www.esa.int/ESA_Multimedia/Images/2020/02/Schematic_illustration_of_a_Transwell_R_system_with_nanoparticles_NPs

[33] Conder, R., Moccia, J. and Riedel, M. (2015) '*Intestinal Organoid Culture*, *STEMCELL Technologies'*. Accessed on June 2023. Available at: https://www.stemcell.com/intestinal-organoid-culture-lp.html

[34] Dongxue Zhang, Liang Qiao, 'Intestine-on-a-chip for intestinal disease study and pharmacological research', 10.1002/smtd.202301179, 8, 1, (December 2022).

[35] Hale, C. (2022) '*Emulate upgrades intestinal organ-on-a-chip for exploring inflammatory bowel disease'*, *Fierce Biotech*. Accessed June 2023. Available at: https://www.fiercebiotech.com/medtech/emulate-launches-intestinal-organ-chip-exploring-inflammatory-bowel-disease

[36] '*Fresh bioprinting of soft biomaterials'* (2023) *CELLINK*. Accessed June 2023. Available at: https://www.cellink.com/application-notes/fresh-bioprinting-of-soft-biomaterials/

[37] **Lab Chip**, 2010,**10**, 2062-2070. Available at: https://pubs.rsc.org/en/content/articlelanding/2010/lc/c004285d

[38] M. Luciano, M. Versaevel, Y. Kalukula, S. Gabriele, 'Mechanoresponse of Curved Epithelial Monolayers Lining Bowl-Shaped 3D Microwells', Wiley Online Library, 11 October 2023.

[39] Creff J, Malaquin L, Besson A. *In vitro* models of intestinal epithelium: Toward bioengineered systems. Journal of Tissue Engineering. 2021;12. doi: 10.1177/2041731420985202

[40] Y. Pratap, J. Christakiran, N. Bhardwaj, B. B. Mandal, 'Overcoming the Dependence on Animal Models for Osteoarthritis Therapeutics - The Promises and Prospects of *In Vitro* Models', Wiley Online Library, 24 July 2021.

[41] Eamon J. Sheehy, Tariq Mesallati, Tatiana Vinardell, Daniel J. Kelly, 'Engineering cartilage or endochondral bone: A comparison of different naturally derived hydrogels', Acta Biomaterialia, Volume 13, 2015, Pages 245-253, ISSN 1742-7061.

[42] C. Vyas, G. Poologasundarampillai, J. Hoyland, P. Bartolo, '12 - 3D printing of biocomposites for osteochondral tissue engineering', Editor(s): Luigi Ambrosio, In Woodhead Publishing Series in Biomaterials, Biomedical Composites (Second Edition), Woodhead Publishing, 2017, Pages 261 302, ISBN 9780081007525.

[43] Chiara Stüdle, Queralt Vallmajó-Martín, Alexander Haumer, Julien Guerrero, Matteo Centola, Arne Mehrkens, Dirk J. Schaefer, Martin Ehrbar, Andrea Barbero, Ivan Martin, 'Spatially confined induction of endochondral ossification by functionalized hydrogels for ectopic engineering of osteochondral tissues', Biomaterials, Volume 171, 2018, Pages 219-229, ISSN 0142-9612.

[44] 'Hydrogel Market (by Raw Material Type: Synthetic Hydrogels, natural hydrogels, and hybrid hydrogels; by composition: Polyacrylate, polyacrylamide, silicone-modified hydrogels, agar-based, and others; by form: Amorphous hydrogels and semi crystalline hydrogels; by product; by end user) - global industry analysis, size, share, growth, trends, regional outlook, and forecast 2023 – 2032', Precedence Research. Accessed on July 2023. Available at: https://www.precedenceresearch.com/hydrogel-market

[45] '*Hydrogel Market Trends, analysis: Forecast report, 2032*', *Global Market Insights Inc.* Accessed on July 2023. Available at: https://www.gminsights.com/industry-analysis/hydrogel-market?gclid=CjwKCAiA-P-rBhBEEiwAQEXhH0FXoZV7rx-4cyQ22bojBpgGwypHjhw09MtmxMydcjsii0R9y9Fy_hoC2MEQAvD_BwE

[46] Martinengo L, Olsson M, Bajpai R, Soljak M, Upton Z, Schmidtchen A, Car J, Järbrink K. Prevalence of chronic wounds in the general population: systematic review and meta-analysis of observational studies. Ann Epidemiol. 2019 Jan;29:8-15. doi: 10.1016/j.annepidem.2018.10.005. Epub 2018 Nov 12. PMID: 30497932.

[47] '*Mercado de Hidrogel - Tamaño, Informe y Descripción general', Mercado de hidrogel - Tamaño, informe y descripción general*. Accessed on July 2023. Available at: https://www.mordorintelligence.com/es/industry-reports/hydrogel-market

[48] Pérez-Puyana, V.M., Sánchez Cid, P., Jiménez-Rosado, M., Ayala Espinar, R. y Romero García, A. (2021). 'Desarrollo de hidrogeles biopoliméricos a partir de colágeno de cerdo para su uso en Ingeniería de Tejidos'. 25th International Congress on Project Management and Engineering (643-652), Alcoy (Alicante): AEIPRO. Asociación Española de Dirección e Ingeniería de Proyectos.

[49] '*Patentan un Nuevo Hidrogel biocompatible que abre las puertas al desarrollo de fármacos Más Efectivos*', *Secretaría General de la Universidad de Granada*. Accessed on July 2023. Available at: https://secretariageneral.ugr.es/informacion/noticias/patentan-un-nuevo-hidrogel-biocompatible-que-abre-las-puertas-al-desarrollo-de-farmacos-mas-efectivos

[50] DiCYT, A., '*Un Proyecto Europeo Desarrolla Nuevos Hidrogeles para aplicaciones biomédicas'*, *DiCYT*. Accessed on July 2023. Available at: https://www.dicyt.com/noticias/un-proyecto-europeo-desarrolla-nuevos-hidrogeles-para-aplicaciones-biomedicas

[51] '*Drug discovery market (by drug type: Small molecule and large molecule; by end user: Pharmaceutical Companies, CRO, others; by technology: High throughput screening, Pharmacogenomics, combinatorial chemistry, nanotechnology, other technologies) - global industry analysis, size, share, growth, trends, regional outlook, and forecast 2023 – 2032*', *Precedence Research*. Accessed on July 2023. Available at: https://www.precedenceresearch.com/drug-discovery-market

[52] '*Cell therapy market (by use type: Clinical use, research use; by therapy type: Autologous therapies, allogenic therapies; by end user: Hospitals & Clinics, Academic & Research Institutes; by technology) - global industry analysis, size, share, growth, trends, regional outlook, and forecast 2023 – 2032', Precedence Research*. Accessed on July 2023. Available at: https://www.precedenceresearch.com/cell-therapy-market

[53] '*Tissue Engineering Market (By Application: Cord blood & Cell Banking, GI, Gynecology, Cancer, Skin & Integumentary, Dental, Orthopedics, Musculoskeletal, & Spine, Neurology, Urology, Cardiology & Vascular, Others; By Material Type: Synthetic Material, Biologically Derived Material, Others; By End-Use: Regenerative medicine research, Hospitals, Healthcare and medical institutes, Others) - Global Industry Analysis, Size, Share, Growth, Trends, Regional Outlook, and Forecast 2023-2032*', *Precedence Research.* Accessed on July 2023. Available at: https://www.precedenceresearch.com/tissue-engineering-market

[54] Manas Mandal, Krishna Chattopadhyay, Atanu Mitra, Dipankar Halder, 'Micro-supercapacitors based on thin films: Journey so far', Reference Module in Materials Science and Materials Engineering, Elsevier, 2023, ISBN 9780128035818

[55] A. G. Castaño, M. García, N. Torras, G. Altay, J. Comelles, E. Martínez, '*Dynamic photopolymerization produces complex microstructures on hydrogels in a moldless approach to generate a 3D intestinal tissue model*,' *IOP Publishing*, Vol. 11, February 2019.

[56] Jeon J, Choi H, Cho W, Hong J, Youk JH, Wie JJ. '*Height-Tunable Replica Molding Using Viscous Polymeric Resins'*. ACS Macro Lett. 2022 Apr 19;11(4):428-433. doi: 10.1021/acsmacrolett.1c00772. Epub 2022 Mar 14. PMID: 35575341.

[57] J. Comelles, V. Fernández-Majada, N. Berlanga-Navarro, V. Acevedo, K. Paskowska, E. Martínez, '*Microfabrication of poly (acrylamide) hydrogels with* independently controlled topography and stiffness,' IOP Publishing, Vol. 12, March 2020.

[58] Reynolds, J. (2022) 'How much does a 3D printed organ cost', Nikko Industries. Accessed on July 2023. Available at: https://www.nikkoindustries.com/blogs/news/how-much-does-a-3d-printed-organ-cost

[59] Miranda I, Souza A, Sousa P, Ribeiro J, Castanheira EMS, Lima R, Minas G. Properties and Applications of PDMS for Biomedical Engineering: A Review. J Funct Biomater. 2021 Dec 21;13(1):2. doi: 10.3390/jfb13010002. PMID: 35076525; PMCID: PMC8788510.

[60] R. Seghir, S. Arscott. Extended PDMS stiffness range for flexible systems. Sensors and Actuators A: Physical , 2015, 230, pp.33-39. ff10.1016/j.sna.2015.04.011ff. ffhal-02345519f .

[61] Wang Z., Ye Q., Yu S., A. Behnam, 'Poly Ethylene Glycol (PEG)-Based Hydrogels for Drug Delivery in Cancer Therapy: A Comprehensive Review', Advanced Healthcare Materials, 10.1002/adhm.202300105, **12**, 18, (2300105), (2023).

[62] Zhu J. 'Bioactive modification of poly(ethylene glycol) hydrogels for tissue engineering'. Biomaterials. 2010 Jun;31(17):4639-56. doi: 10.1016/j.biomaterials.2010.02.044. Epub 2010 Mar 19. PMID: 20303169; PMCID: PMC2907908.

[63] Yañez-Soto B, Liliensiek SJ, Murphy CJ, Nealey PF. 2013. 'Biochemically and topographically engineered poly(ethylene glycol) diacrylate hydrogels with biomimetic characteristics as substrates for human corneal epithelial cells', J Biomed Mater Res Part A 2013:101A:1184–1194.

[64] Discher DE, Janmey P, Wang YL. 'Tissue cells feel and respond to the stiffness of their substrate'. Science. 2005 Nov 18;310(5751):1139-43. doi: 10.1126/science.1116995. PMID: 16293750.

[65] Rehfeldt F, Engler AJ, Eckhardt A, Ahmed F, Discher DE. 'Cell responses to the mechanochemical microenvironment--implications for regenerative medicine and drug delivery'. Adv Drug Deliv Rev. 2007 Nov 10;59(13):1329-39. doi: 10.1016/j.addr.2007.08.007. Epub 2007 Aug 14. PMID: 17900747; PMCID: PMC4124491.

[66] Tuson HH, Renner LD, Weibel DB. Polyacrylamide hydrogels as substrates for studying bacteria. Chem Commun (Camb). 2012 Feb 1;48(10):1595-7. doi: 10.1039/c1cc14705f. Epub 2011 Oct 31. PMID: 22039586; PMCID: PMC3705218.

[67] P. Nghe, S. Boulineau, S. Gude, P. Recouvreux, J. S. van Zon, S. J. Tans. 'Microfabricated Polyacrylamide Devices for the Controlled Culture of Growing Cells and Developing Organisms'. PLOS ONE. 2013 Nov 24; doi: 10.1371/journal.pone.0075537

[68] Chen Z, Lee JB. Biocompatibility of SU-8 and Its Biomedical Device Applications. Micromachines (Basel). 2021 Jul 4;12(7):794. doi: 10.3390/mi12070794. PMID: 34357204; PMCID: PMC8304786.

[69] Huang, Guoyou & Wang, lin & Wang, Shuqi & Han, Yulong & Wu, Jinhui & Zhang, Q.C. & Xu, Feng & Lu, Tian. (2012). Engineering three-dimensional cell mechanical microenvironment with hydrogels. Biofabrication. 4. 042001. 10.1088/1758-5082/4/4/042001.

[70] Lee S, Stanton AE, Tong X, Yang F. Hydrogels with enhanced protein conjugation efficiency reveal stiffness-induced YAP localization in stem cells depends on biochemical cues. Biomaterials. 2019 May;202:26-34. doi: 10.1016/j.biomaterials.2019.02.021. Epub 2019 Feb 23. PMID: 30826537; PMCID: PMC6447317.

[71] *MicroFabSpace HomePage*, *Institute for Bioengineering of Catalonia*. Accessed on October 2023. Available at: https://ibecbarcelona.eu/ca/services/microfabspace/

[72] Equipment: Leica DMi8 microscope, Wageningen University and Research. Accessed on October 2023. Available at: https://www.wur.nl/en/product/leica-dmi8-microscope.htm

[73] Roduit C, Sekatski S, Dietler G, Catsicas S, Lafont F, Kasas S. Stiffness tomography by atomic force microscopy. Biophys J. 2009 Jul 22;97(2):674-7. doi: 10.1016/j.bpj.2009.05.010. PMID: 19619482; PMCID: PMC2711326.

[74] Onfroy-Roy, L.; Hamel, D.; Foncy, J.; Malaquin, L.; Ferrand, A. Extracellular Matrix Mechanical Properties and Regulation of the Intestinal Stem Cells: When Mechanics Control Fate. Cells *2020, 9,* 2629. https://doi.org/10.3390/cells9122629

[75] *35 mm Glass bottom dish with 20 mm micro-well #1 cover glass*, *Cellvis*. Accessed on December 2023. Available at: https://www.cellvis.com/_35-mm-glass-bottom-dish-with-20-mm-micro-well-number-1-cover-glass_/product_detail.php?product_id=34

[76] *What are z-scores?, Khan Academy.* Accessed on December 2023. Available at: https://www.khanacademy.org/math/statistics-probability/modeling-distributions-of-data/z-scores/a/z-scores-review

[77] T. Glozman, H. Azhari, 'A Method for Characterization of Tissue Elastic Properties Combining Ultrasonic Computed Tomography with Elastography', Journal of Ultrasound in Medicine, Vol. 29, Issue 3, p. 387-398. doi: 10.7863/jum.2010.29.3.387

[78] Hajdu, Miklos & Bokor, Orsolya. (2014). The Effects of Different Activity Distributions on Project Duration in PERT Networks. Procedia - Social and Behavioral Sciences. 119. 766-775. 10.1016/j.sbspro.2014.03.086.

[79] Csic. (n.d.). *Ética en la investigación*. Ética en la investigación | Consejo Superior de Investigaciones Científicas. https://www.csic.es/es/el-csic/etica/etica-en-la-investigacion

[80] *Agencia Estatal Boletín Oficial del Estado*. Página de inicio. https://www.boe.es/buscar/act.php?id=BOE-A-1995-24292

[81] Guía de Seguridad en el Laboratorio - UPCT. https://www.upct.es/contenido/servicios/prevencion/docs/41Guia_laboratorios.pdf

[82] *ISO 45001*. NQA. https://www.nqa.com/es-pe/certification/standards/iso-45001

[83] *Good laboratory practice - bureau for chemical substance - gov.pl website*. Bureau for Chemical Substance. https://www.gov.pl/web/chemical/good-laboratory-practice

Annexes

Annex 1. Plasma cleaner protocol used

1. The vacuum was turned on until a pressure of between 0.2 and 0.3 torr was reached.

2. The valve on the chamber was then turned to the left, to remove the air that stayed in the Oxygen cable, until the 0.2-0.3 torr value was achieved again.

3. Next, the oxygen valve was opened, and we waited for a minute, for the pressure to stabilize to a value of about 0.8 torr.

4. Afterwards, the Plasma was turned on, with the RF level at high. To see if the reaction was taking place, the lights were turned off and, after a few seconds, a slight light appeared from the chamber window, indicating the beginning of the cleanse. A minute later, the device was turned off, as well as the oxygen valve and the vacuum.

5. Finally, the samples could be taken out of the chamber.

Annex 2. Profilometer measurement parameters

- Scan type: the Standard scan was the only type used.
- Range: approximate distance range that we thought that the sample was going to have.
- Profile: if the samples had posts, cavities, or both.
- Stylus type: the 12.5 µm radius stylus was the only type used.
- Stylus force: force with which the stylus scanned the sample. If this force is high, the results of the measurements are more defined, but if it is too high, it could modify the shape of the sample. As we always worked with PDMS samples, this stylus force had to be low, so we chose to work with 1 mg.
- Length: the length of the sample that needed to be measured. When measuring the smallest posts or cavities, this length did not have to be very large, but when measuring the biggest ones, we had to increase it in order to cover the whole structure. This parameter was being changed depending on what we wanted to measure.
- Duration and resolution: these two parameters go hand in hand, because if the duration of the measurement is longer, then the resolution will be better, and if it is shorter, it will have less resolution. We tried to get a resolution of around 0.1 µm/pt for all the measurements.